Universität Hamburg
DER FORSCHUNG | DER LEHRE | DER BILDUNG

Role of Dienelactone Hydrolases (DLHs) in PET Biodegradation and Biofilm Formation by *Maribacter dokdonensis* and *Arenibacter palladensis*

Dissertation

with the aim of achieving the degree of Doctor rerum naturalim (Dr. rer. nat.)

at the Department of Microbiology and Biotechnology

Faculty of Mathematics, Informatics and Natural Sciences,

of the Universität Hamburg

submitted to the Universität Hamburg by

Trinh, Thi Truc Ly

Hamburg, 2025

The following evaluators recommended the admission of the dissertation:

Prof. Dr. Wolfgang R. Streit

PD. Dr. Ines Krohn

Date of Disputation: Dec 5th, 2025

ABSTRACT

Global plastics pollution represents a major environmental challenge, and we have only a very limited knowledge of marine microorganisms involved in possible remediation. Marine Bacteroidota, particularly members of Flavobacteria*,* are known for their ability to hydrolyze a wide range of different algal polymers. More recently, some representatives have been identified to encode PET-active enzymes.

PET degradation is primarily conducted by non-specific and secreted enzymes of esterase class (EC 3.1.1-.). They are either designated as carboxylesterases (EC 3.1.1.1), poly(ethylene terephthalate) hydrolases (EC 3.1.1.101), lipases (EC 3.1.1.3) or cutinases (EC 3.1.1.74). Notably, among the currently known and functional PETases no dienelactone hydolases DLHs (3.1.1.45) are listed.

Dienelactone hydrolases are enzymes that play a central role in the degradation of cyclic esters. In the current study, we show that bacteria affiliated with the Bacteroidota (class Flavobacteria) harbor DLHs acting on PET foil and powder. We report on the isolation of two marine bacterial strains, *Arenibacter palladensis* UHH-Hm9b and *Maribacter dokdonensis* UHH-5R5, forming biofilms on PET foil and releasing µM amounts of terephthalic acid after 5-7 days. Genome sequencing and functional analyses enables the identification of two secreted DLHs, designated PET93 and PET94, involved in PET degradation. While their predicted active sites and substrates binding pockets were identical to previously published PETases, both enzymes differed largely in their structural features from known PETases and represented novel scaffolds. Moreover, they lacked the typical porC-domain that is characteristic of known PETases from Flavobacteria.

For the two recombinant enzymes PET93 and PET94, activity on PET as well as the primary degradation products Bis(2-Hydroxyethyl) terephthalate (BHET) and Mono-(Hydroxyethyl) terephthalate (MHET) was demonstrated. Both enzymes were able to hydrolyze PET foil and powder at low but significant rates. These findings represent the first described DLHs with activity on plastics. This demonstrates that Flavobacteria harbor a greater diversity of PET-active, albeit unspecific, enzymes than previously assumed.

In addition, the PET94 gene is positioned downstream of *Fur-like Transcritiponal regulator*, providing a rationale for testing iron supplementation in this experiment. Indeed, this study demonstrated that BHET degradation was enhanced upon iron supplementation, with up to 9-fold increases in MHET concentration detected by UHPLC. However, transcriptome analysis revealed no expression of PET94 under tested conditions, suggesting iron may modulate PET degradation at the post-transcriptional level, or that the applied concentrations were insufficient to trigger transcriptional activation.

In summary, this study highlights the importance of expanding the currently known biodiversity of PET-hydrolyzing enzymes within marine Bacteroidota phylum. PET93, PET94, and their homologs within this phylum are found in diverse climatic zones worldwide, indicating a potentially important role in the degradation of plastic particles in marine ecosystems.

ZUSAMMENFASSUNG

Die weltweite Plastikverschmutzung stellt eine große Umweltherausforderung dar, und unser Wissen über marine Mikroorganismen, die an möglichen Abbauprozessen beteiligt sind, ist bislang sehr begrenzt. Marine Bacteroidota, insbesondere Vertreter der Flavobakterien, sind für ihre Fähigkeit, ein breites Spektrum unterschiedlicher Algen-Polymere zu hydrolysieren, bekannt. Einige Vertreter wurden kürzlich zudem als Träger PET-aktiver Enzyme identifiziert.

Der Abbau von PET wird überwiegend durch unspezifische, sekretierte Hydrolasen der Esterase-Enzymklasse (EC 3.1.1.-) vermittelt. Dazu gehören Carboxylesterasen (EC 3.1.1.1), Poly(ethylenterephthalat)-Hydrolasen (EC 3.1.1.101), Lipasen (EC 3.1.1.3) und Cutinasen (EC 3.1.1.74). Aus der Gruppe der Dienelacton-Hydrolasen (DLHs, EC 3.1.1.45) war bislang noch kein Enzym mit PETase -Aktivität bekannt.

Dienelacton-Hydrolasen sind Enzyme, die eine zentrale Rolle beim Abbau zyklischer Ester spielen. In der vorliegenden Studie zeigen wir, dass Bakterien aus der Gruppe der Bacteroidota (Klasse Flavobacteria) DLHs besitzen, die auf PET-Folie und -Pulver wirken. In dieser Arbeit wurden zwei marine Stämme isoliert, *Arenibacter palladensis* UHH-Hm9b und *Maribacter dokdonensis* UHH-5R5, die Biofilme auf PET-Folie bilden und nach 5–7 Tagen mikromolare Mengen an Terephthalsäure freisetzen. Mittels Genomsequenzierung und funktioneller Analysen konnten zwei sekretierte DLHs, PET93 und PET94, identifizierten werden, die am PET-Abbau beteiligt sind, . Obwohl die vorhergesagten aktiven Zentren und Substratbinde-Taschen mit denen der bereits publizierter PETasen identisch waren, unterschieden sich beide Enzyme in ihren strukturellen Merkmalen deutlich von den bekannten PETasen und stellten neuartige

Gerüste dar. Ebenfalls fehlte ihnen die typische PorC-Domäne, die für die bekannten PETasen aus Flavobakterien charakteristisch ist.

Für die beiden rekombinanten Enzyme PET93 und PET94 konnte Aktivität gegenüber PET sowie den primären Abbauprodukten Bis(2-Hydroxyethyl)terephthalat (BHET) und Mono-(2-Hydroxyethyl)terephthalat (MHET) nachgewiesen werden. Beide Enzyme konnten PET-Folie und -Pulver mit niedrigen, aber signifikanten Raten hydrolysieren. Damit handelt es sich um die ersten beschriebenen DLHs mit Aktivität gegenüber Kunststoffen. Dies zeigt, dass Flavobakterien eine größere Vielfalt an PET-aktiven, wenn auch unspezifischen Enzymen besitzen, als bislang angenommen.

Außerdem liegt das PET94-Gen stromab eines Fur-ähnlichen Transkriptionsregulators, was die Begründung für die Untersuchung einer Eisenzugabe in diesem Experiment liefert. Tatsächlich zeigte diese Studie, dass der BHET-Abbau unter Eisenzugabe zunahm, wobei eine bis zu neunfache Erhöhung der MHET-Konzentration mittels UHPLC nachgewiesen wurde. Die Transkriptomanalyse zeigte jedoch unter den getesteten Bedingungen keine Expression von PET94, was darauf hindeutet, dass Eisen den PET-Abbau auf posttranskriptionaler Ebene modulieren könnte oder dass die eingesetzten Konzentrationen nicht ausreichten, um eine transkriptionelle Aktivierung auszulösen.

Zusammenfassend unterstreicht diese Arbeit die Bedeutung der Erforschung enzymatischer Diversität und erweitert die bislang bekannte Biodiversität von PET-hydrolysierenden Enzymen innerhalb der marinen Bacteroidota. PET93, PET94 und deren Homologen aus der Gruppe der Bacteriodota sind weltweit in unterschiedlichen Klimazonen zu finden, was auf eine wichtige Rolle beim Abbau von Plastikpartikeln in marinen Ökosystemen hindeutet.

Declaration on oath

I hereby declare and affirm that this doctoral dissertation is my own work and that I have not used any aids and sources other than those indicated. If electronic resources based on generative artificial intelligence (gAI) were used in the course of writing this dissertation, I confirm that my own work was the main and value-adding contribution and that complete documentation of all resources used is available in accordance with good scientific practice. I am responsible for any erroneous or distorted content, incorrect references, violations of data protection and copyright law or plagiarism that may have been generated by the gAI.

Eidesstattliche Versicherung

Hiermit versichere ich an Eides statt, die vorliegende Dissertationsschrift selbst verfasst und keine anderen als die angegebenen Hilfsmittel und Quellen benutzt zu haben. Sofern im Zuge der Erstellung der vorliegenden Dissertationsschrift generative Künstliche Intelligenz (gKI) basierte elektronische Hilfsmittel verwendet wurden, versichere ich, dass meine eigene Leistung im Vordergrund stand und dass eine vollständige Dokumentation aller verwendeten Hilfsmittel gemäß der Guten wissenschaftlichen Praxis vorliegt. Ich trage die Verantwortung für eventuell durch die gKI generierte fehlerhafte oder verzerrte Inhalte, fehlerhafte Referenzen, Verstöße gegen das Datenschutz- und Urheberrecht oder Plagiate.

Hamburg, 17/09/2025

Trinh, Thi Truc Ly

List of Abbreviations

BSA	Bovine serum albumin
DAP	Diaminopimelic acid
BMB	Bacto Marine Broth
IMAC	Immobilized metal affinity chromatography
TAE	Tris-acetate-EDTA buffer
LDPE	Low-density polyethylene
TCA	Tricarboxylic acid cycle
PULs	Polysaccharide utilization loci
CAzymes	Carbohydrate-Active Enzymes
HGT	Horizontal gene transfer
CLSM	Confocal laser scanning microscope
T9SS	Type IX secretion system
BSA	Bovine serum albumin
BHET	Bis(2-hydroxyethyl) terephthalate
C2	4-Nitrophenyl acetate
C4	4-Nitrophenyl butyrate
C6	4-Nitrophenyl hexanoate
C8	4-Nitrophenyl octanoate
C10	4-Nitrophenyl decanoate
C12	4-Nitrophenyl dodecanoate
C14	4-Nitrophenyl myristate
C16	4-Nitrophenyl palmitate
C18	4-Nitrophenyl stearate
Carb	Carbonate-bicarbonate buffer
Cit	Citrate buffer
DMSO	Dimethyl sulfoxide
ε	Extinction coefficient

EC	Enzyme Commission (number)
EG	Ethylene glycol
EPS	Extracellular Polymeric Substances
gDNA	genomic DNA
HMM	Hidden Markov Model
IMG	Integrated Microbial Genomes and Microbiomes
IPTG	Isopropylthio-β-galactoside
*Is*PETase	PET enzyme from Ideonella sakaiensis
PPB	Potassium phosphate buffer
LB	Lysogeny broth
LCC	Leaf-branch compost cutinase
MHET	Mono(2-hydroxyethyl) terephthalate
Ni-NTA	Nickel-chelating nitrilotriacetic acid
OD600	Optical density at a wavelength of 600 nm
PA	Polyamide
PBS	Phosphate-buffered saline
PCL	Polycaprolactone
PCR	Polymerase Chain Reaction
PDB	Protein Data Bank
PE	Polyethylene
PET	Polyethylene terephthalate
PETase	PET enzyme
*p*NP	para-Nitrophenol PP Polypropylene
PS	Polystyrene PUR Polyurethane
PP	Polypropylene
PVC	Polyvinylchloride rpm revolutions per minute
rRNA	ribosomal RNA
SDS-PAGE	Sodium Dodecyl Sulphate PolyacrylAmide Gel Electrophoresis
TBS	Tris-buffered saline
TBST	Tris-buffered saline with tween-20

TBT	Tributyrin
Tg	Glass transition temperature
T_{ann}	Annealing temperature
TPA	Terephthalic acid
TRIS	Tris(hydroxymethyl) aminomethane
UHPLC	Ultra-High-Performance Liquid Chromatography

List of Figures

List of Tables

List of publications (or manuscripts under revision at the time of submission)

1. Polyethylene terephthalate (PET) primary degradation products affect c-di-GMP-, cAMP-signaling, and quorum sensing (QS) in *Vibrio gazogenes* DSM 21264.

Preuss, L., Alawi, M., Dumnitch, A., **Ly T.T. Trinh**., Maison, W., Burmeister, N., Poehlein, A., Daniel, R., Vollstedt, C., & Streit, W. R. (2025). Polyethylene terephthalate (PET) primary degradation products affect c-di-GMP-, cAMP-signaling, and quorum sensing (QS) in *Vibrio gazogenes* DSM 21264. *Microbiology spectrum*, *13*(7), e0018125.

2. Role of Dienelactone Hydrolases in PET Biodegradation by Flavobacteria *Maribacter dokdonensis* and *Arenibacter palladensis*

Ly T.T. Trinh, Ifey Alio, Pablo Perez-Garcia, Sabine Keuter, Robert Dierkes, Lena Preuss, Christel Vollstedt and Wolfgang R. Streit (Submitted to Applied and Environmental Microbiology journal)

Table of Contents

1.INTRODUCTION

1 INTRODUCTION

1.1 Bacteroidota in marine ecosystems

The phylum Bacteroidota represents a major evolutionary lineage within the domain Bacteria. It is highly diverse and ecologically significant group that have successfully colonized a wide range of environments (Alonso et al., 2007). These rod-shaped, Gram negative and non-spore forming bacteria are dominant species of microbial communities in wide range of habitats such as animal guts, soils, freshwater (Thomas et al., 2011), especially in coastal marine waters (Alonso et al., 2007)

Recent genome sequencing projects have provided deeper insights into the diversity and functionality of this Bacteroidota phylum. They are highly abundance and specialize in the decomposition of high molecular weight polymer and algal polysaccharides in marine systems. It has been reported that they are also major contributors to global carbon and nutrient recycling (Larsbrink & McKee, 2020; Pan et al., 2023, Lian et al., 2025). With more than 32.000 genome sequenced and assembled, Bacteroidota is now classified into six distinct classes, including *Saprospiria, Sphingobacteriia*, *Bacteroidia, Cytophagia, Flavobacteriia and Chitinophagia* (NCBI, August 2022, https://www.ncbi.nlm.nih.gov/data- hub/taxonomy/976/). Within this phylum, the class Flavobacteria stands out as the largest and most widely distributed group, particularly in the aquatic environment, and are known for their surface-active properties and are frequently associated with marine algae and sponges (Mann Alexander et al., 2013; Yoon & Oh, 2012).

Genome analysis of Bacteroidota has confirmed the presence of polysaccharide ultilization loci (PULs) gene clusters which encode carbohydrate-active enzymes

(CAZymes) (Lapébie et al., 2019). These loci are essential for Bacteroidota to efficiently metabolize a wide range of polysaccharides, such as complex glycans derived from plants, fungi and plankton (Pan et al., 2023). PULs are often linked to the gliding motility of this phylum to facilitate the secretion and release of CAZymes into the surrounding environment and support efficient substrate degradation (Larsbrink & McKee, 2020; McKee et al., 2021; Pan et al., 2023). The CAZymes encoded by PULs include glycoside hydrolases, polysaccharide lyases and carbohydrate lyases which enable the efficient degradation of polysaccharide, pectins and other biopolymers using these enzyme combinations (McKee et al., 2021).

In addition, Bacteroidota genomes are very flexible so they can undergo changes through gene duplications, rearrangements, deletions and horizontal gene transfer (HGT). Thanks to this flexibility, they could evolve new abilities, adapt to new ecological niches and survive in competitive environmental conditions (Thomas et al., 2011). Recent studies have highlighted that they also can colonize synthetic polymers which suggest a potential role in marine plastic degradation (Vaksmaa et al., 2022). All together, these characteristics make Bacteroitoda a key phylum for maintaning ecological process and environmental sustainability.

1.2 Plastic pollution: a growing burden

1.2.1 Plastic “overload”

Synthetic plastics were first developed in 1860 and then gradually they have significantly supported global industries with numerous sectors relying heavily on a variety of plastic materials from 1907. Today, plastics are deeply integrated in our modern life. Global plastic production has expanded dramatically with rapid industrial development. Annual

production increased from approximately 2 million metric tons in 1950 (Geyer et al., 2017) to 368 million metric tons in 2019 (an estimate of 180-fold increase). Worldwide plastic output had reached approximately 400.3 million metric tons by 2022 (Figure 1) (Plastic Europe, 2023). If these current trends continue, production is thus predicted to approach almost 600 million metric tons by 2050 (Rafey & and Siddiqui, 2023; Statista, 2023).

Plastics offer many notable environmental, social and economic benefits such as saving fuel use and energy, improving food packaging and distribution or offering less production cost. However, their widespread has led to a significant increasing of plastic waste entering the environment. An estimated 8-10 million tons of plastic waste enter the ocean each year (Eriksen et al., 2014; Jambeck et al., 2015; OECD, 2022; Nayanathara Thathsarani Pilapitiya, 2024 & Ratnayake, 2024). Because most plastics are highly resistant to natural degradation (Sokolova et al., 2023), this pollution has become a serious global concern nowadays.

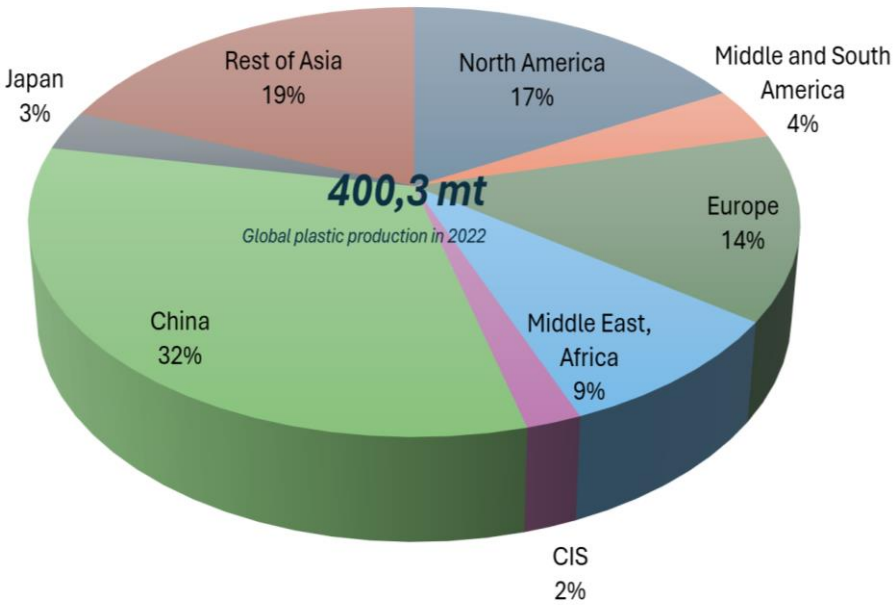

Figure 1. Global plastic production by regions of the world. The data adapted from PlasticEurope (2023)

1.2.2 Polyethylene terephthalate (PET) and its growing concern

Polyethylene terephthalate (PET) is commonly produced by the polymerization of terephthalate acid (TPA) and ethylene glycol (EG) (Figure 2). It is classified among the seven primary types of plastics according to the Plastics Identification System (Pudack et al., 2020). PET accounts for approximately 6% of total plastics production and is among the most widely used synthetic plastics worldwide due to their strong, lightweight, and resistant to moisture, temperature and chemicals (Figure 3). These properties make it a ideal material for producing products such as water bottles, food packaging, cosmestics and pharmaceuticals (Muringayil Joseph et al., 2024; Nisticò, 2020, Sin & Tueen, 2023).

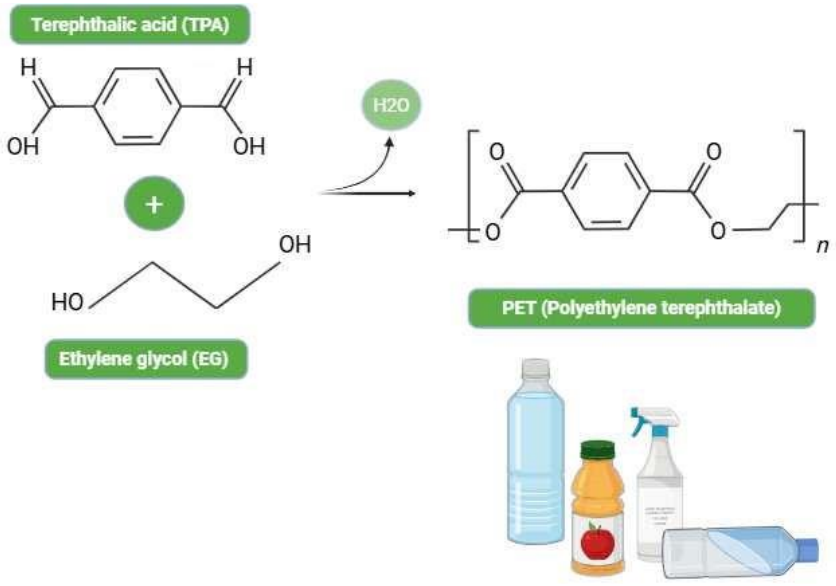

Figure 2. Schematic representation of the condensation reaction leading to the formation of polyethylene terephthalate (PET), in which terephthalic acid (TPA) reacts with ethylene glycol (EG), releasing water as a byproduct. The chemical structures were drawn with Biorender. Adapted from (Garcia Simão et al., 2024).

The global market of PET has grown continuously from 19 million metric tons in 2015 to approximately 25 million metric tons in 2022. Alarmingly, this number is predicted to continue to increase up to 36 million metric tons before 2030. Large amounts of PET end

up in our ecosystem around the world, raising and leading to serious global issues such as risks to microbial biodiversity and environmental health. It is estimated that out of every million PET bottles sold globally every minute, over 90% of them eventually end up in landfills and oceans. There, PET can take hundreds of years to allow fully degrading (Enache et al., 2024; Maitlo et al., 2022; Plastic Europe, 2023; Wawer et al., 2025).

1.2.3 Impacts of plastics

Most plastic products are designed for single use, typically with short life cycle of less than a month and limited recyclability (Panda et al., 2010; Walker et al., 2023). Therefore, it is substantially accumulated in the environment Currently, approximately 70% of global plastics ends up as waste, among them 41% goes through recycling and incineration, 40% goes into the landfills and about 19% leaks directly into natural environment (Figure 3) (Soong et al., 2022; Zhao et al., 2019). Plastics are initially present as larger floating fragments with different particle sizes, from macro (>25 mm) to meso (5-25 mm) (Chen et al., 2021; Gabbott et al., 2020; Hurley et al., 2020). Over time, weathering factors such as sunlight, wind and water currents gradually break them down into micro- to nano-plastics (<5 mm) (Chow et al., 2023.

Kaandorp et al., 2023). These small particles can spread through air, water and soil, and then threaten ecological systems as well as human health (Muringayil Joseph et al., 2024; Soong et al., 2022). Along with the chemical addictives, these particles negatively affect biodiversity across all environments (Osman et al., 2023; R. J. Wright et al., 2020).

Although plastics require centuries to fully degrade in nature, micro- and nano-plastics are available and can be ingested by marine organisms. They then enter the food chain, appearing in the form of seafood, salt and even drinking water. Current estimates

indicated that nearly 51 trillion microplastics are floating in the oceans (ASEZ, 2024) and can harm organisms by blocking or damaging their digestive systems, releasing heavy metals and other pollutants into the environment, or transporting invasive microorganisms (Chiappone et al., 2005; Pawar et al., 2016; Wang & Qian, 2021). Plastic pollution is reported to cause the deaths of around 100,000 marine species each year (Cózar et al., 2014; Van Sebille et al., 2015) and threaten approximately 43% mammals, 44% seabirds, 86% sea turtles worldwide and numerous fish & crustacean worldwide (Thushari & Senevirathna, 2020).

In addition to environmental concerns, micro- and nano-plastics are also being recognized as potential human health risk (Enyol et al., 2019; Huang et al., 2020). These particles can enter human body and build up in tissues and then cause serious long-term problems for human health (Campanale et al., 2020; Cui et al., 2021). Therefore, managing the plastics environmental impacts while still maintaining societal benefits is attracting increasing attention nowadays for sustainable development.

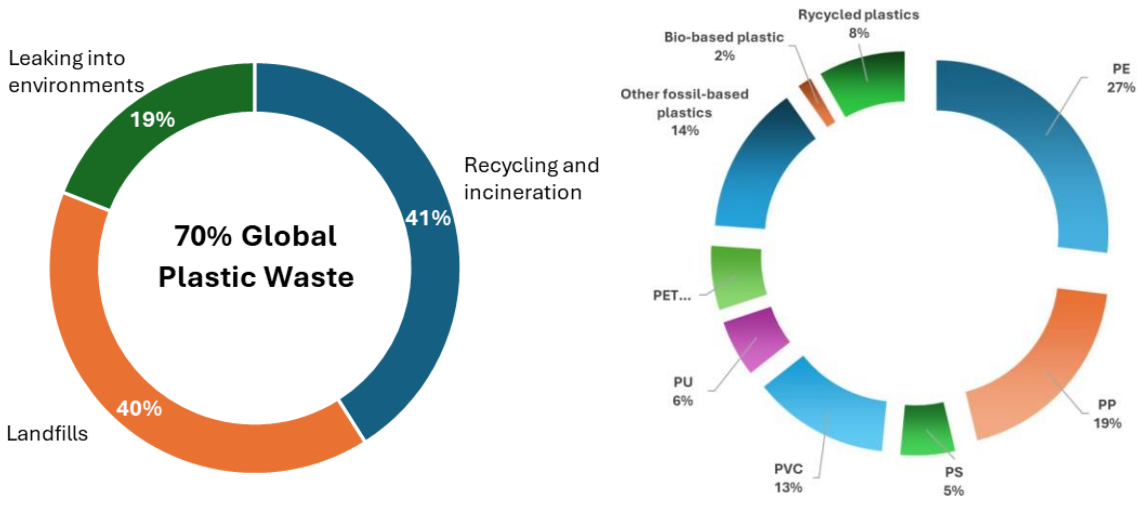

Figure 3. Global plastic waste and Global plastic polymers production by type in 2021, according to Plastics Europe.

1.3 From persistence to biodegradation

Petroleum based plastics are generally highly stable and durable, which is why they are considered largely non-degradable in nature (Webb et al., 2013). Nonetheless, once released into the environment, plastic waste undergoes slow degradation process. In case of PET, complete degradation may take hundred years (Müller et al., 2001). Mechanical forces such as waves, wind, or the movement of solids across the plastic surface can fragment plastics into microplastics, which possess much greater surface than larger fragments and are therefore more susceptible to further abiotic or biotic factors degradation.

For PET, abiotic degradation commonly referred to as “weathering” or “photodegradation” is a critical initial process, although it remains not fully understood. The aromatic ring of the terephthalic acid contains a strong chromophore, making PET sensitive to UV light. UV radiation is therefore a major factor causing changes in properties of PET, such as decrease in molecular weight or color change from clear to yellow. Other contributing factors include ambient and surface temperature, as well as moisture, which promotes hydrolysis when combined with UV exposure (Fagerburg & Clauberg, 2004).

Currently, conventional methods for PET treatment include incineration, mechanical and chemical recycling. Over 60% of plastic waste ends up in landfills, where its degradation is slowed by UV resistance and anaerobic conditions. Incineration can convert plastic into heat and gases for energy recovery but also releases to greenhouse gas. Mechanical recycling, the most widely used method, produces lower-quality fibers, films, or sheets, with polymer quality declining. After several repeated cycles, the recycled PET is no longer be usable and is often eventually incinerated (Hopewell et al., 2009; Koshti et al., 2018;

Soong et al., 2022). Meanwhile, chemical recycling can efficiently depolymerize PET into its original monomers, but the process is not economic friendly, as virgin plastic is cheaper to produce (Sardon & Dove, 2018).

In response, biological recycling has emerged as a promising sustainable alternative (Wei & Zimmermann, 2017). This strategy relies on microorganisms or enzymes to depolymerize PET into monomers. Microorganisms often colonize PET surface via biofilm formation, facilitated by the hydrophilic properties of bacterial cell surface. This helps them to attach better and allows them to use the carbon from the plastic as an energy source and accelerate the degradation process (Gross & Kalra, 2002; Koshti et al., 2018). Several studies have demonstrated enzymatic modification of plastic topology and physio-chemical properties, and microorganisms capable of polymer breakdown have also been identified (Webb et al., 2013; Wei et al., 2019). However, the efficiency of biological recycling is constrained by the type of organism, the structural properties of the polymer, and the necessity of pretreatment (Koshti et al., 2018). Factors such as molecular weight, crystallinity, melting temperature, functional groups, and the presence of additives strongly influence PET biodegradability (Mergaert & Swings, 1996). Optimizing and modifying these factors are key challenges that must be addressed to improve the feasibility of large-scale biorecycling (Koshti et al., 2018).

1.4 Marine Bacteroidota as potential plastic-degrading microorganism

Microbial communities in marine environments are essential players ocean ecological process, especially in nutrient and carbon cycling (Agostini et al., 2021). Besides their ecological functions, these microbes can break down pollutants in the environment, as well as minimize harmful effects caused by human and industrial activities (Carr et al.,

2020; Oliveira et al., 2020). Many enzymes derived from marine microbes often exhibit novel catalytic properties, reflecting chemical complexity of marine habitats and unique substrate they encounter (Trincone, 2010). While Actinobacteria dominates as sources of terrestrial hydrolases, a growing number of putative PET-active enzymes from marine environments have been linked to the Bacteroidota phylum (Danso et al., 2018). Members of this phylum are known to be equipped with multiple hydrolases and binding molecules for degrading polymers such as xylan, cellulose, and pectin (Dodd et al., 2011; Thomas et al., 2011). Two functional PET-active enzymes, PET27 and PET30, were recently identified from marine Bacteroidota genera Kaistella and Aequorivita, respectively. Their characterization revealed PET hydrolytic activity and underlined the potential of marine Bacteroidota as a source of novel biocatalysts for PET recycling (Zhang et al., 2022).

Flavobacteria in this Bacteroidota phylum are among the dominant colonizers of floating plastic particles such as LDPE, PP and PET (Dudek et al., 2020; Pinto et al., 2020; Vaksmaa et al., 2021). This class is particularly notable for its potential ability to degrade marine polysaccharide through enzyme complexes (Lapébie et al., 2019). Their frequent association with plastic debris suggests an important role in potential degradation of synthetic polymers in marine environments. Recently, a growing interest has shifted from terrestrial ecosystems to marine ecosystems as a promising source of microbes which could harbour novel biodegradable activities (Carr et al., 2023; Dharmaraj, 2010; Olaniyan & Adetunji, 2021; Yang et al., 2020).

1.5 Enzyme classes involved in PET degradation.

To date, 125 PET microbial hydrolases (wildtype enzymes) have been described (for a complete list see PAZy database, www.pazy.eu, accessed on 22.07.2025) (Buchholz et al., 2022).

PET degradation is primarily carried out by non-specific and secreted enzymes of esterase class (EC 3.1.1-.). They are either designated as carboxylesterases (EC 3.1.1.1), poly(ethylene terephthalate) hydrolases (EC 3.1.1.101), lipases (EC 3.1.1.3) or cutinases (EC 3.1.1.74) and produced by different types of microorganisms, including bacteria, fungi and archaea (Figure 4). Notably, among the currently known and functional PETases no dienelactone hydolases DLHs (3.1.1.45) are listed. Most of these enzymes can act on a broad range of substrate and often cleave PET in a non-specific manner (D. Danso et al., 2019; Tournier et al., 2023; Wei & Zimmermann, 2017).

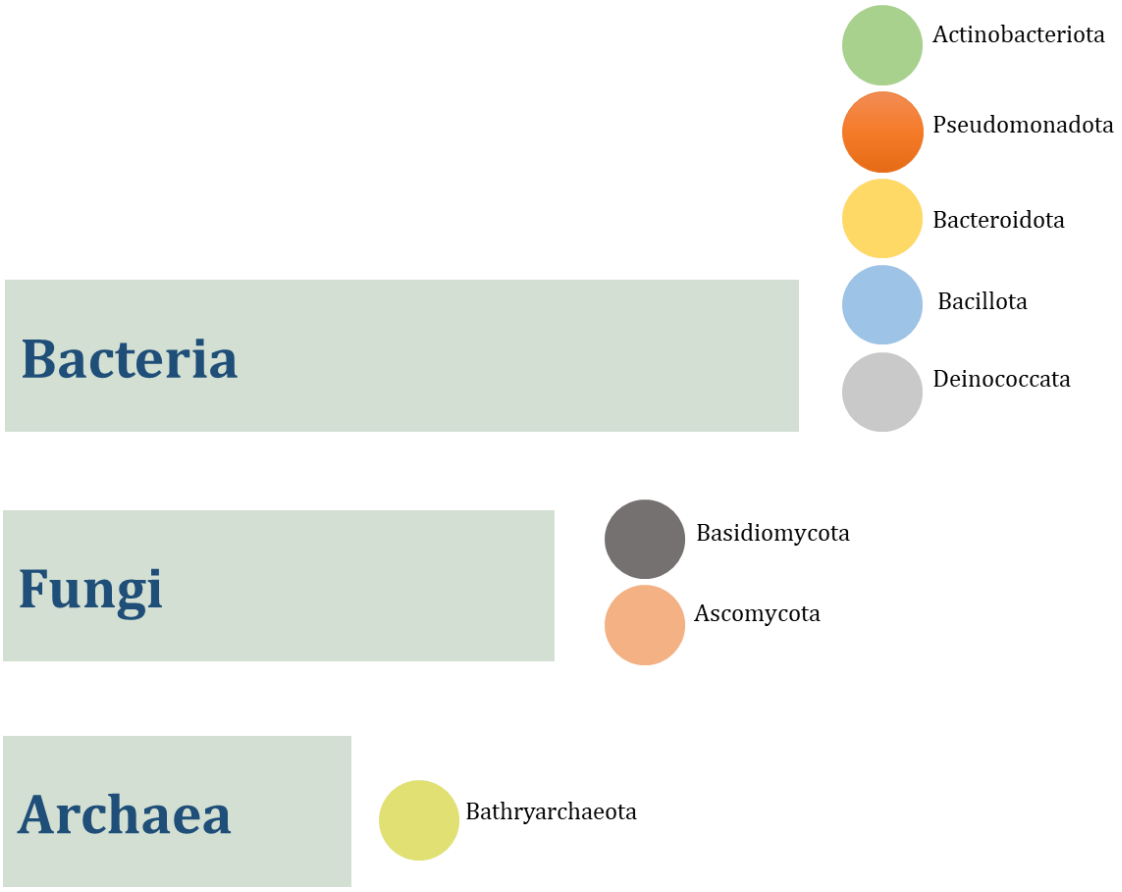

Figure 4. The origins of PET-degrading enzymes from different domains of life. (Data were derived from PAZy - The Plastics-Active Enzymes Database, June 2025: 125 functional PETases)

However, the efficiency of enzymatic PET degradation is not determined by the enzyme itself. Factors, such as polymer chemical composition, its physical characteristics, and how effectively the enzymes interact with PET surface, all play important roles (Mueller, 2006; Urbanek et al., 2020). Cutinases possess a shallow, wide-open active site exposed on the enzyme surface, which facilitates the hydrolysis of water-insoluble, hydrophobic polyesters (Biundo et al., 2018; Fecker et al., 2018). In contrast, lipases and esterases contain the active site in a tunnel-forming structure, leading to vertical-type hydrolysis mechanism (Biundo et al., 2018). While only cutinases have been shown to cleave the inner block of PET films, though lipases, esterases, and cutinases are all capable of modifying PET surfaces (Kawai et al., 2019). Notably, dienelactone DLHs (3.1.1.45) are not commonly known as functional PETases to degrade PET.

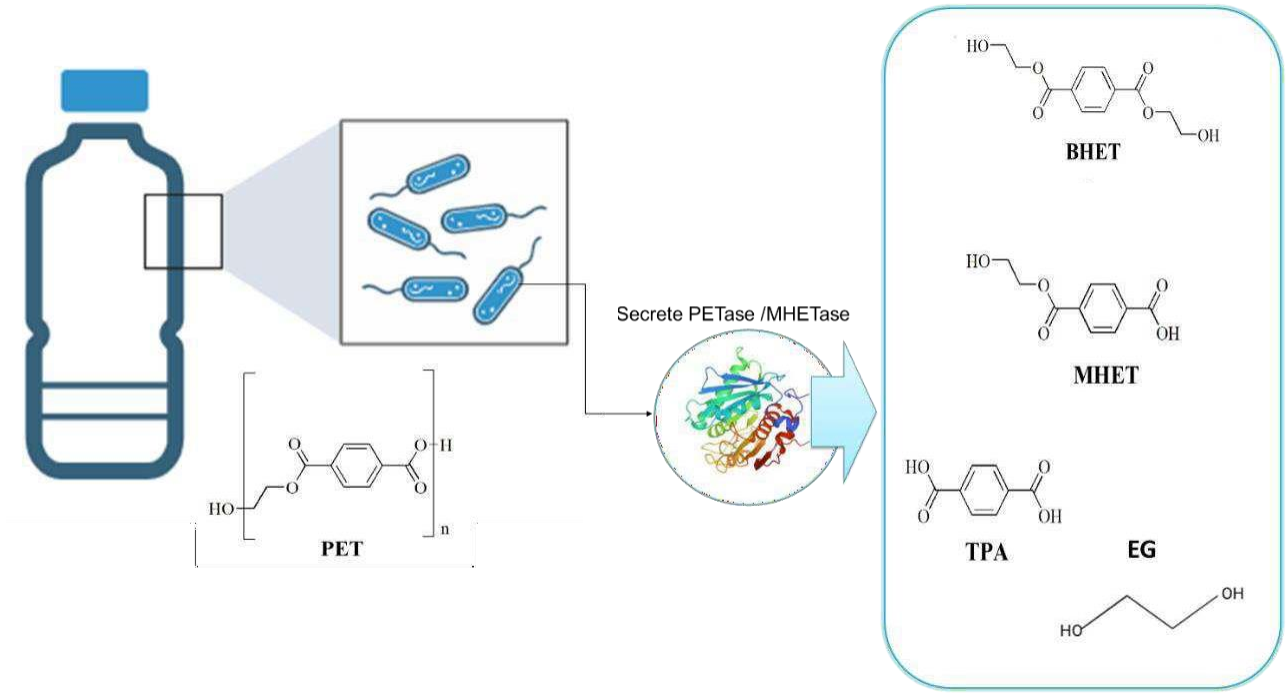

Figure 5. Attachment of Ideonella sakaiensis to PET film. The strain utilizes PET as its sole carbon source. Upon attachment, the bacterium secretes PETase to hydrolyze PET into MHET (mono(2- hydroxyethyl) terephthalate). MHET is then transported into the cell and further degraded into terephthalic acid (TPA) and ethylene glycol (EG) (Yoshida et al., 2016). Adapted from (Bornscheuer, 2016).

1.5.1 Cutinases (EC 3.1.1.74)

Cutinases represent one of the largest and most versatile classes of PET-degrading enzymes. The earliest PET-active enzymes were derived from the Gram positive *Thermobifida fusca* (Müller et al., 2005), with the strains DSM43793 producing hydrolases BTA-1 (TfH) and BTA-2, and KW3 expressing cutinases TfCut1 and TfCut2 (EC 3.1.1.74) (Wei & Zimmermann, 2017). As reported, TfH resulted in an about 50% weight loss of PET bottles after 3 weeks at 55^{o}C (Müller et al., 2005), while TfCut2 variants reduced amorphous PET film weight by 45 % in 50-hours at 65°C (Carr et al., 2020). Ronkvist et al. reported a highly active and thermostable enzyme designated HiC (EC 3.1.1.74) isolated from fungal species *Humicola insolens*. HiC achieved nearly complete degradation of low crystalline PET within 96 hours (97%± 3%weight loss) (Ronkvist et al., 2009). Accordingly, these cutinases can break down PET plastic effectively at the temperature neat glass transition temperature of PET (Tg) (Wei et al., 2019).

1.5.2 Poly(ethylene terephthalate) hydrolases (EC 3.1.1.101)

The first identified PET-degrading hydrolases was *Is*PETase from *Ideonella sakaiensis 201-F6*, which hydrolyzes PET into MHET and along with minor amounts of TPA at mesophilic temperature (~30°C). The subsequent step to complete PET degradation process is carried out by second enzyme, MHETase, which converts MHET into TPA and ethylene glycol (Figure 5) (Bornscheuer, 2016; Taniguchi et al., 2019; Yoshida et al., 2016).These products are then metabolized via the TCA cycle (Palm et al., 2019; Satta et al., 2024; Yoshida et al., 2016). Since its discovery in 2016, *Is*PETase has been extensively engineered to improve its hydrolysis efficiency, thermostability and activity. Typical variants include DuraPETase (Cui et al., 2021), thermoPETase

(S121E/D186H/R280A) (Son et al., 2019) and HotPETase (Bell et al., 2022). In addition to the best-characterized *Is*PETase, cutinase-like enzyme LCC (Leaf-Branch Compost Cutinase) is recognized as a PET hydrolase because of its remarkable PET degrading efficiency (S. Sulaiman et al., 2012). LCC-G, a variant of LCC, has been introduced as one of the most promising enzymes for industrial PET recycling which capable of depolymerizing up to 90% of PET within 10 hours at 72°C (Shirke et al., 2018).

1.5.3 Carboxylesterases (EC 3.1.1.1)

The Carboxylesterases (EC 3.1.1.1) are a diverse group of enzymes catalyzing ester bond cleavage in PET and its intermediates. Several PET-degrading bacteria produce carboxylesterases: PE-H from *Halopseudomonas aestusnigri* hydrolyzed amorphous PET film at 30°C, however it is inactive on commercial PET. Its variant Y250S shows limited activity on this form of PET plastic (Bollinger et al., 2020). Recently we showed that *Vibrio gazogenes* DSM 21264 secretes an active polyethylene terephthalate (PET) hydrolase PET6 and degrades PET in biofilms on foils and microplastic particles (Preuß et al., 2025). Notably, two carboxylesterases Ces19_14 and Ces39_5 isolated from *Caldibacillus thermoamylovorans* were found to work synergistically with a cutinase (ICCG) from compost, achieving higher TPA yields (Yan et al., 2024). Recently, the first two promiscuous and cold-active esterases from Bacteroidetes have been identified and characterized: PET27 (*Aequorivita* sp.) and PET30 (*Kaistella jeonii*.) Both enzymes were active on polycaprolactone (PCL), amorphous PET foil and on the polyester polyurethane Impranil® DLN (Zhang et al., 2022).

1.5.4 Lipases (EC 3.1.1.3)

Lipases are enzymes typically associated with hydrolysis of triglycerides but also exhibit

activity against synthetic polyesters. Examples include LipA from *Caldibacillus thermoamylovorans* (Yan et al., 2024), CALB from *Candida antarctica* (Carniel et al., 2017) and LipMRD9 from *Bacillus safensis* (Vidal et al., 2024). CALB has limited activity in breaking down intact PET polymers, it efficiently hydrolyzes intermediates such as BHET. Its combination with HiC (a fungal cutinase) significantly improves TPA yield, achieving a 7-fold increase over HiC alone (Carniel et al., 2017). LipMRD9 is a true lipase that is capable of degrading PET at both nanosized particle and film forms and retaining more than 80 % of its activity at 35–40 °C (Vidal et al., 2024).

The functionally identified bacterial enzymes listed above are mostly phylogenetically affiliated with Actinobacteria and Proteobacteria. Danso et al. highlighted Bacteroidota as a key phylum rich in PET-degrading enzyme candidates, predominantly detected in marine metagenomes (Danso et al., 2018). However, only two enzymes from Bacteroidota have been found to be active on PET to date. Further, although diverse bacterial enzyme classes have been identified for PET degradation, notably among the currently known and functional PETases no DLHs (3.1.1.45) are reported.

1.6 Microbial PET colonization on plastic surface

The microbial communities colonizing plastic particles (i.e. the plastic microbiota), termed **‘**plastisphere’, have attracted increasing research interest (Amaral-Zettler et al., 2020; Kirstein et al., 2019; Yang et al., 2020; Zettler et al., 2013). These plastisphere communities are highly diverse and typically dominated by Proteobacteria, Firmicutes, Cyanobacteria and Bacteroidota (Lee et al., 2008; Zhai et al., 2023). In marine ecosystems, larger plastic debris gradually breaks down into micro- and nanoparticles through both biotic and abiotic processes. The greater surface areas of micro- and

nanoplastic particles facilitate better microbial attachment and biofilm formation (Flemming et al., 2016). It has been reported that colonization does not necessarily imply any biodegradation, as many of the microorganisms observed on plastic surfaces are opportunistic colonizers that utilize the substrate for attachment as ecological niche without metabolizing the polymer (Chow et al., 2023). However, microbial biofilm formation is critical in plastic biodegradation because this helps microbes attach better to hydrophobic plastic surfaces and then improve enzyme access to the plastic surface (Nauendorf et al., 2016; Orr et al., 2004; Tribedi & Sil, 2014; Wilkes & Aristilde, 2017). Once attachment occurs, further degradation steps can proceed more effectively (Jaiswal et al., 2020).

1.7 Intention of this study

Global plastics pollution is a major environmental challenge, and we still have limited knowledge of marine microbiota involved in possible remediation. While PET is one of the commodity polymers that can be degraded under laboratory and industrial scale conditions, there is little knowledge on the microbiota potentially involved in marine PET degradation. This study is necessary to expand the ecological diversity of PET-degrading enzymes and suggests a broader role for aquatic microorganisms in plastic degradation. Here, we asked:

1. Do marine Bacteroidota contribute to PET degradation and if so, which strains and enzymes are involved?
2. Are also additional hydrolases family involved in the degradation of man-made polymers such as PET?
3. Does iron availability affect the activity of PET-degrading enzymes?

2. MATERIALS AND METHODS

2 MATERIALS AND METHODS

2.1 Bacterial strains and culture conditions

Name, characteristics and the source of strains used within this study are shown in Table 1. All media and buffers used in this study were autoclaved for 20 min at 121 °C. Antibiotics and heat-sensitive supplements (Table 2) were sterilized separately using sterile filtration and were added to the media only after the media had cooled to approximately 60°C. The prepared media containing supplements were subsequently stored at 4°C to maintain stability and prevent contamination. Bacterial glycerol stocks were prepared by mixing 1 ml of the overnight inoculum to 500 µL of 86% glycerol and stored at -70^{o}C for long-term use. All media could be prepared as solid plates by adding 12 or 15 g/L of agar prior to sterilization.

Table 1. Bacterial strains used in this study.

Strain	Characteristics	Reference/source
E. coli DH5α	supE44 ΔlacU169 (Φ80 lacZ ΔM15) hsdR17 recA1 endA1 gyrA96 thi-1 relA1	Invitrogen, Karlsruhe, Germany
E. coli BL21 (DE3)	F-, ompT, hsdS B (rB- m B-) gal, dcm, λDE3	Novagen/Merck Darmstadt, Germany
E. coli WM3064	thrB1004 pro thi rpsL hsdS lacZΔM15 RP4-1360 Δ(araBAD)567 ΔdapA1341::[erm pir(wt)]	W. Metcalf, University of Illinois, Urbana-Champaign
Maribacter dokdonensis UHH-5R5	Isolated strain from environmental sample	This work
Arenibacter palladensis UHH-Hm9b	Isolated strain from environmental sample	This work
ReporTPA_UHH04	C. thiooxidans S23_UHH01, carrying pReporTPA, Cm^R	(Dierkes Robert et al., 2022)

2.1.1 Cultivation of *E. coli* strains

Unless otherwise indicated, the *E. coli* strains was grown overnight in LB medium (1% tryptone/peptone, 0.5% yeast extract, 1% NaCl) (see section 2.3.1) (Bertani, 1951),

supplemented with appropriate antibiotics (Table 2) under appropriate aerobic conditions at 37°C. Cultures harbouring a plasmid were supplemented with antibiotics to keep selection pressure.

Table 2. Antibiotics and supplements used in this study.

Antibiotic/supplement	Solvent	Stock solution	Working concentration
Ampicillin	70% EtOH	100 mg/ml	100 µg/ml
Chloramphenicol	EtOH	50 mg/ml	50 µg/ml
IPTG	H2O	100 mg/ml	100 µg/ml

To cultivate *E. coli* WM3064, the same media and culture conditions as above was applied. After the media cooled down to approximately, sterile DAP was added to final concentration of 0.3 mM.

2.1.2 Cultivation of *Maribacter dokdonensis* UHH-5R5 and *Arenibacter palladensis* UHH-Hm9b

Maribacter dokdonensis UHH-5R5 and *Arenibacter palladensis* UHH-Hm9b were grown in BMB medium (composition as described in section 2.3.2) at 28 °C for overnight and two days, respectively, with shaking at 150 rpm.

2.1.3 Enrichment, isolation and identification of Bacteroidota strains

Microbial communities from marine and aquatic environments were enriched in 100ml R2A or BMB media with 1g of PET powder. Enrichment cultures were then incubated at 22ºC and 28ºC under continuous shaking conditions. After enrichment, 100µl of the cultures were spread on the R2A/BMB agar plate. The 16S rDNA gene of the colonies was amplified using standard 16S primers. The amplified fragments were Sanger sequenced afterwards at Eurofins (Elsberg, Germany). The colonies were then screened for their hydrolysis activity on tributyrin (TBT), polycaprolactone (PCL) and bis-(2-

hydroxyethyl) terephthalate (BHET). The strains with hydrolytic activities observed towards TBT, PCL or BHET were later selected for whole-genome sequencing. Genomic DNA (gDNA) were extracted with the NucleoSpin® Microbial DNA Kit from MN (Düren, Germany) from 5 mL cultures and then sequenced using IIlumina NextSeq 500 sequencing method at Eurofins (Germany).

2.2 Vectors, primers and constructs used in this study.

Primers, vectors and constructs used in this study are shown in Table 3 and Table 4. The pET21a (+) vector contains T7 promotor for expressing putative PET-degrading genes, antibiotic resistance gene (Amp^r) to apply for selection pressure, and His-6-tag for Immobilized Metal Affinity Chromatography (IMAC) purification.

The pBBR1MCS-1 vector carries chloramphenicol resistance gene (CAM^r), enabling the selection of transformants on media containing chloramphenicol.

Table 3. Primers used in this study.

Primer	Sequence (5' to 3')	Length	T_m (°C)	Source
616v (16S)	AGAGTTTGATYMTGGCTC	18	60	(Juretschko et al., 1998)
1492r (16S)	GGYTACCTTGTTACGACTT	19	60	(Frank Jeremy et al., 2008)
PET93_F	GCTCCATATGAAATTTAGAGCACTATTA TTTTCGGCATCG	40	51	This work
PET93_R	CCGACTCGAGGTTTGCAGGTTGTGCAT GTAACAATTCC	38	51	This work
PET94_F	CATATGACCGGGTCTTTTGTTTSTGGC	21	58	This work
PET94_R	GCGCTCGAGTGGAGCAGGTTT GTCATGAAGAAG	33	55	This work
T7 Promotor	TAATACGACTCACTATAGGG	20	53	Eurofins (Elsberg, Germany)
pET reverse	TCCGGATATAGTTCC	15	54	Eurofins (Elsberg, Germany)

Table 4. Vectors and constructs used in this study.

Vector	Properties	Reference/source
pET21a(+)	Expression vector: *lacI,* Amp^R, T7-promotor, C-terminal His_6-tag coding sequence	Novagen/Merck (Darmstadt, Germany)
pBBR1MCS-1	Broad host-range cloning vector, *Cm^R, mob*	(Kovach et al., 1995)
pET21a(+)::PET93	pET21a(+) carrying His-6-tag containing-PET93 gene in the MCS between NdeI and XhoI restriction site	This work
pET21a(+)::PET94	pET21a(+) carrying His-6-tag containing-PET94 gene in the MCS between NdeI and XhoI restriction site	This work
pBBR1-MCS-1::*amcyan*	*pBBR1MCS-5 carraing the amcyan gene in the* MCS *between Xba*I *and Bam*HI *restriction site*	This work
pBBR1MCS-1::pRo5::Cyan	*pBBR1MCS-1*, carrying PET93 promotor and Cyan fluorescence sequence *pRo93::Cyan*	This work
pBBR1MCS-1::pRo9::Cyan	*pBBR1MCS-1*, carrying PET94 promotor and Cyan fluorescence sequence *pRo93::Cyan*	This work

2.3 Culture media and supplements

2.3.1 LB media

Tryptone	10 g
Yeast extract	5 g
(Agar	12-15 g
H2O	*up to* 1000 ml

2.3.2 Bacto Marine Broth (BMB) media (Difco 2216)

Bacto peptone	5 g	SrCl2	34.00 mg
Bacto yeast extract	1 g	H3BO3	22.00 mg
Fe (III) citrate	0.1 g	Na-silicate	4.00 mg
NaCl	19.45 g	NaF	2.40 mg
MgCl2 (anhydrous)	5.9 g	(NH4) NO3	1.60 mg
Na2SO4	3.24 g	Na2HPO4	8.00 mg
CaCl2	1.8 g		
KCl	0.55 g		
NaHCO3	0.16 g		
KBr	0.08 g		

Distilled water: *up to* 1000 ml
Final pH should be adjusted to 7.6 ± 0.2 at 25°C.

2.3.3 R2A media

Proteose Pepton (Difco no. 3)	0.50 g
Casamino Acids	0.50 g
Glucose	0.50 g
Starch	0.50 g
Na-Pyruvat (Brenztraubensäure)	0.30 g
Dikaliumhydrogenphosphat [K_2HPO_4]	0.30 g
Magnesiumsulfat-Heptahydrat [$MgSO_4$ x 7 H_2O]	0.05 g
$H_2O_{dest.}$	ad 1000 ml

2.3.4 Artificial seawater media (AS)

Solution A		**Solution B**	
NaCl	28.13 g	Yeast extract	34.00 mg
KCl	0.77 g	Peptone	22.00 mg
$CaCl_2.2H_2O$	1.6 g	Agar	4.00 mg
$MgCl_2.6H_2O$	4.8 g	H_2O	Up to 250 mL
NaHCO3	0.11 g	pH=7.3,	
MgSO4. $7H_2O$	3.8 g		
H_2O	Up to 1L		

Autoclave
And then mix Solution A: Solution B according to ratio 3:1

2.4 Preparation of indicator plates

2.4.1 TBT indicator plates

The final concentration of TBT was 1 % (v/v). 5 mL TBT were added to 500 mL sterile media containing agar and homogenized at 14,000/min until the media became homogenous.

2.4.2 PCL containing plate

A 500 mg/mL solution of polycaprolactone (PCL) was prepared by dissolving in acetone and incubating at 60 °C until the polymer was fully dissolved. The complete solution was poured into 500 ml of sterile medium containing agar under constant stirring. Acetone was

allowed to evaporate completely under a fume hood, after that other supplements were added as needed.

2.4.3 BHET containing plate

A stocking concentration of 1M bis-(2-hydroxyethyl) terephthalate BHET was prepared by mixing 0,245 g BHET in 1 ml of dimethyl sulfoxide (DMSO), then heat the solution to 60^{o}C and mix by agitation to dissolve BHET. 5 ml of BHET was then mixed with 500 ml of sterile media containing agar to have a final working concentration of 10 mM, after that other supplements were added as needed.

2.5 Initial screening for polyesterase activities in marine Bacteroidota isolates

Single colonies were then screened for their hydrolysis activity on TBT, PCL and BHET. The strains with hydrolytic activities observed towards PCL or BHET were later selected for whole-genome sequencing. Genomic DNA (gDNA) were extracted with the NucleoSpin® Microbial DNA Kit from MN (Düren, Germany) from 5 mL cultures and then sequenced using IIlumina NextSeq 500 sequencing method at Eurofins (Germany).

For the activity test, the strains or the enzymes were conducted on agar plates containing appropriate media (BMB/R2A) and the substrates. The bacterial strains or purified enzymes were streaked/drop on the plates and incubated at an optimal temperature until halo was observed on the plates.

2.6 Whole genome sequencing for putative PET-degrading genes

Genomic DNA from Bacteroidota isolates were then isolated with the NucleoSpin® Microbial DNA Kit from MN (Düren, Germany) and sequenced using IIlumina NextSeq 500 sequencing method at Eurofins (Germany). To identify putative PET esterases within

the genome datasets of the Bacteroidota isolates, a profile Hidden Markov Model (HMM) was constructed based on the already known and functionally tested enzymes.

2.7 Biofilms on PET surface: growth and degradation product analysis

The starter culture of Bacteroidota strains were grown in BMB media at 28ºC with continuous shaking at 130 rpm. After 48 hours, the cultures were diluted to an OD_{600} of 0.05 and then 7 ml of each diluted cultures were transferred to 6-well plate. PET foil platelets were sterilized by Ethanol 70% for 10 mins and then added the cultures, which were subsequently incubated at 28ºC under static condition to facilitate biofilm formation. Samples were collected after 3, 5 and 7 days of incubation. Each 6 ml of collected samples was vacuum dried to a final volume of 600 µl. The concentrated samples were further analysed by both method UHPLC (see section 2.9.1). PET foils incubated in media without bacterial cells served as negative control. The Bacteroidota strain NS50, grown on PET foil under the same conditions, was used as a negative control because preliminary analyses revealed no hydrolytic activity on model substrates, suggesting that this strain lacks potential PET-degrading enzymes (Table 8). All experiments were performed in triplicates.

2.8 Imaging analysis of biofilms on PET foil platelets

The starter cultures of Bacteroidota isolates UHH-5R5 and UHH-Hm9b were grown in BMB medium at 28ºC with shaking 130 rpm until reaching an optical cell density OD600 of 1. These starter cultures were then diluted to the OD600 of 0.05 in fresh BMB medium, followed by addition of PET foil. The cultures were incubated at 28ºC without shaking. After incubation, the PET foils were removed, wash three times with 1x PBS and transferred to µ-Slide 8 well plates (ibidi GmbH, Martinsried, Germany). The cells were

stained using 100 µL of the LIVE/DEAD® BacLight™ Bacterial Viability Kit (Thermo Scientific), which contains propidium iodide (PI) for labeling dead cells (red fluorescence) and SYTO-9™ for staining live cells (green fluorescence). PI and SYTO-9™ were mixed at a 1:1 ratio, and then 15 µl of this mixture was pipetted into 5 ml PBS. The PET foils were incubated in this staining solution for 1 hour at room temperature in the dark. The biofilms forming on foils after 1, 2, 3 , 6 and 7 days of incubation were then analysed using under the Axio Observer Z1/7, LSM 800 confocal microscope equipped with an objective C-Apochromat 63x/1.2 W Korr UV VisIR (Carl Zeiss Microscopy GmbH, Jena, Germany), utilizing the SYTO-9 channel (emission wavelength: 528/20 nm) and the PI channel (emission wavelength: 645/20 nm) and Plan-Apochromat 100×/1.40 Oil DIC M27 objective. Image analysis and processing was carried out using ZEN software (Version 2.3, Carl Zeiss Microscopy GmbH).

2.9 Expression of recombinant putative enzymes

2.9.1 Cloning of PET genes in *E. coli*

PET93 and PET94 were amplified from genomic DNA of UHH-5R5 and UHH-Hm9b using specific primers listed in Table 3. PCR conditions for DNA amplification process are as described in Table 5. The amplified fragments were cut with restriction enzymes NdeI and XhoI and the overlapping ends were used to ligate the inserts into pET21(a)+ vector. Constructs were checked after ligation with the same restriction enzymes. Size estimation was done on an agarose gel (0.8% TAE agarose gel, 120 V, 25 min). Positive clones were further confirmed by Sanger sequencing at Microsynth Seqlab GmbH (Goettingen, Germany) to verify the integrity of the inserts.

Verified plasmids were subsequently used for downstream expression and functional analyses.

Table 5: 3-step PCR conditions for amplification of PET hydrolase genes.

Step	Temperature (°C)	Time (min:sec)	
Initial denaturation	95	3:00	
Denaturation	95	1:00	Repeat 35 cycles
Annealing	T_m + 3°C	0:20	
Elongation	72	0:40	
Final elongation	72	5:00	
Hold	4	end	

2.9.2 Overexpression

Sequences coding mature PET94 (sequence devoid of the signal peptide) and PET93 protein were heterologous expressed in *E. coli* BL21 (DE3) using *β*-D-1-thiogalactopyranoside (IPTG) induction. Cultures grew aerobically in LB medium with ampicillin 100 µg/ml at 37°C. When OD_{600} reached 0.7-0.8, the expressions were induced with IPTG 1mM, followed by incubation at 22°C and 17°C for 20 hours. Cells were harvested and lysed with pressure using a French press. Afterwards the proteins with C-terminal 6x histidine tag were purified via Nickle-ion affinity chromatography using Ni-NTA agarose (Qiagen, Hilden, Germany) and analysed by SDS-PAGE. The elution buffer was exchanged against

0.1 mM potassium phosphate buffer pH 7.0 in a 30 kDa Amicon Tube (GE Health Care, Solingen, Germany).

2.9.3 Protein purification

The expression culture was centrifuged at 5000 g for 15 min to obtain a cell pellet. The pellet was washed and resuspended in an appropriate amount of NPI-10 buffer for further processing, or frozen at -20 °C for long term storage. Cells were disrupted using a French

Press (1,200 Pa) and additional sonication rounds (Amplitude height was 70% and duty cycle set at 0.5 sec.) in order to degrade high molecular weight DNA. The lysate was centrifuged (30 min, 4 °C, 20,000 rpm) and the supernatant was then collected. Ni-NTA agarose was added to the crude extract in a ratio 1:4 v/v and incubated on a rotatory shaker at 4 °C for 1 hour to allow binding of His-tagged proteins.

The purified proteins were obtained using Protino® Ni-NTA Agarose as described in the manufacturer's instruction. Elution fractions of target proteins were checked by SDS-PAGE (section 2.9.4) and western blot (section 2.9.5)**.** Protein fractions were pooled, and the elution buffer was exchanged against 0.1 M potassium phosphate pH7 using dialysis method with a centrifugal concentrator and 30kDa ultrafiltration column. Protein concentration was determined via the Bradford Assay at 595 nm according to the manufacturer (Roti®-Quant, Carl Roth, Karlsruhe, Germany) or NanoPhotometer® (PET93: ε = 58790 M^{-1} cm^{-1}, PET94: ε = 57300 M^{-1} cm^{-1}). The centrifugation steps were carried out at 8 °C and at manufacturer recommended speed in case of buffer exchange. For activity tests, purified recombinant proteins were utilized. Agar plates were prepared containing 10mM bis-(2-hydroxyethyl) terephthalate (BHET) and 500 mg L^{-1} polycaprolactone (PCL). 10 µl of eluate from protein purification were spotted onto the plates to observe the halo formation.

2.9.4 SDS-PAGE

Samples were added to denaturing loading dye (5x) in a 4:1 ratio and heated at 95 °C for 5 min. Electrophoresis was performed at 80 V until the dye front reached the stacking gel, then shifted to 120 V. The SDS gel was stained for an hour and de-stained for 3 hours or until bands were visible. The expected size of purified proteins is shown in Table 6.

Table 6. Size of purified proteins (kDa)

Enzyme	Protein (kDa)	Characteristics
PET93	48.1 kDa	His-6-tag containing PET hydrolase
PET94	45.6 kDa	His-6-tag containing PET hydrolase

2.9.5 Western blotting analysis

Fractions of purified protein were prepared for analysis by denaturing with 5x loading dye at a ratio of 4:1. The mixture was heated at 95 °C for 5 mins to ensure complete degradation. The denatured proteins were then loaded on SDS polyacrylamide gels (12% separating gel, 7% stacking gel). Protein separation was then carried out by gel electrophoresis. The gel was equilibrated in transfer buffer and subsequently transferred onto a nitrocellulose membrane using a wet transfer system. The transfer was performed at 0.7 A and 25 V for 25 mins to ensure efficient protein immobilization on the membrane. After the transfer, the membrane was washed twice with TBS buffer for 10 mins each to remove residual transfer buffer.

To block non-specific binding sites, the membrane was incubated in TBST buffer containing 5% milk at 4 °C overnight. In the next day, the membrane was washed three times with TBST buffer for 10 minutes per wash to remove unbound blocking reagent. Membrane was then incubated with the primary antibody (1:5000 dilution for Anti-His). The incubation was carried out for 1 hour at 4 °C in TBST buffer with 5 % milk to allow specific binding of antibody to His-tag proteins. Afterwards, the membrane was washed three times with TBST for 10 mins each to remove unbound primary antibody. For detection, the membrane was incubated with secondary antibody for an appropriate time at room temperature until the proteins bands were visible.

2.10 Biochemical characterization of PET93 and PET94

The biochemical properties of PET hydrolases PET93 and PET94 were analysed using purified proteins (from Section 2.9.3). Enzymatic activities were normalized to relative percentages, with the untreated sample serving as the reference standard (100% relative activity).

For activity tests, purified recombinant proteins were utilized. Agar plates were prepared containing 10mM bis-(2-hydroxyethyl) terephthalate (BHET) and 500 mg L^{-1} polycaprolactone (PCL). 10 µl of eluate from protein purification were spotted onto the plates to observe the halo formation.

The detection of hydrolytically active enzymes was performed using para-nitrophenyl (*p*NP) esters as substrates (Table 7). These colorless substrates release chromogenic para-nitrophenol (*p*NP) upon the hydrolysis of ester bond, which can then be detected and quantified photometrically at a wavelength of 405 nm in a plate reader (Biotek, Winooski, USA). The assays were performed in 96-well microplates with a total reaction volume of 200 µl.

Measurement was taken using the Synergy HT plate reader from BioTek (Winooski, USA). Unless otherwise specified, each reaction contained of 10 µL purified enzyme (0.1 mg mL^{1}), 20 µL of 10 mM pNP-substrates dissolved in isopropanol and about 170 µL of 0.2M buffer. The reaction mixture was incubated at a specific temperature and pH and was terminated after 10 minutes by adding 20 µL of 2M Na_2CO_3. After the incubation period, the reactions were immediately measured for absorbance at 405 nm to determine enzymatic activity. The sample with enzyme-free was used as a control. All measurements were performed in triplicate.

Table 7. para-nitrophenyl substrates used in pNP ester assay.

Chain length	Substrate name
C2	4-nitrophenyl acetate
C4	4-nitrophenyl butyrate
C6	4-nitrophenyl hexanoate
C8	4-nitrophenyl octanoate
C10	4-nitrophenyl decanoate
C12	4-nitrophenyl dodecanoate
C14	4-nitrophenyl myristate
C16	4-nitrophenyl palmitate
C18	4-nitrophenyl stearate

2.10.1 Dilution series

A serial dilution of enzyme concentration with different dilution factors of 2, 4, 8, 16, 32, 64, 128, 256 were used to identify the optimal concentration of the enzymes which yields optimal enzyme activity while minimizing dilution effects. Each diluted enzyme solution was incubated with a substrate solution containing 1 mM 4-nitrophenyl hexanoate (*p*NP-C6) in 0.1 M potassium phosphate buffer at pH 7. The temperature for the reactions was maintained at 37^{o}C.

2.10.2 Substrate specificity

Fatty acids containing even numbers of carbon atoms from C2 to C18 were tested at a concentration of 1 mM (Table 7). The reactions were conducted in sodium phosphate buffer pH 7 and 1 µg enzyme, incubated for 10 min at 37 °C.

2.10.3 pH optimum

To determine the suitable buffer and optimal pH, various buffers were tested across different pH ranges: 0.1 M citrate buffer (pH 3–6), 0.1 M potassium phosphate buffer (pH 6–8), 0.1 M tris buffer (pH 7–9) and 0.1 M carbonate-bicarbonate buffer (pH 9–10). Reactions were performed using 1 mM *p*NP-C6 as the substrate and incubated at 40 °C.

After identifying the optimal temperature, the pH assay was repeated to confirm whether the enzymatic activity remains optimal under combined conditions of the optimal pH and temperature.

2.10.4 Temperature optimum and stability

The optimal temperature for enzyme activity was evaluated between a range of 10 to 90°C. The amount of enzyme and incubation time was kept as previously mentioned. The buffer and pH used was determined by the previous pH optimum tested, and 1 mM *p*NP-C6 substrate was applied.

2.11 PET degradation assays

Purified proteins at the concentration of 0.1mg mL^{-1} were incubated with MHET (1 mM), BHET (5 mM). After 24 hours of incubation at 37^{o}C with MHET/BHET and 120 h with PET, the supernatant was filtered through 0.22 µm filter paper. The release of TPA was then analyzed using UHPLC and TPA reporter strain *C. thiooxidans* UHH04 (Dierkes Robert et al., 2022). BSA incubated with PET substrates under the same conditions served as a negative control.

2.11.1 UHPLC-based activity assay for PET, MHET and BHET degradation

The concentration of breakdown products in supernatants after incubations with PET and its intermediates was analyzed using UltiMate™ 3000 UHPLC system (Thermo Fisher Scientific, Waltham, MA, USA). The Triart C18 column (YMC Europe GmbH, Dinslaken, Germany), 100 × 2.0 mm with 1.9 µm diameter was employed for separation. Isocratic elution was performed with a mobile phase consisting of 20:80 (v/v) acetonitrile (AcN) and water (acidified with 0.1% v/v trifluoroacetic acid) at flowrate of 0.4 mL min^{-1}.

For UHPLC sample preparation, 50 µl of incubation supernatant was mixed with 200 µl of AcN (acidified with 1% vol trifluoroacetic acid), followed by centrifugation at 10,000 × g for 3 min. A 200 µl aliquot of the mixture was then diluted with 600 µl water. Each 15 µl of sample was then injected for each measurement. Breakdown products were detected at 254 nm using a VWD-3400 detector (Thermo Scientific, Waltham, MA, USA). Peak quantification was conducted using a data analysis software supplied with the Compass HyStar software package (Bruker, Billerica, MA, USA).

2.11.2 *C. thiooxidans* S23 reporter strain preparation for TPA Assays

The protocol for this experiment was adapted from Dierkes's original method (Dierkes Robert et al., 2022). The *C. thiooxidans* S23 biosensor strains ReporTPA_UHH04 were incubated overnight at 130 rpm in 50ml LB medium containing 25 µg/mL chloramphenicol and additionally supplemented with 10 mM gluconate in an Erlenmeyer flask. Before performing the TPA assays, the OD600 of the cultures was measured, and an appropriate volume was centrifuged at 4,500 rcf and 4°C for 5 minutes. The resulting pellet was resuspended in 50 ml Wx medium containing 25 µg/mL chloramphenicol to achieve a final OD600 of 0.6. The resuspended cultures were incubated at 37°C and 130 rpm for 30 minutes before being added to the samples.

For standard assay, 100 µL of the sample was added to each well of a black-walled 96-well microtiter plate (ThermoFisher, Waltham, MA, USA) designed for fluorescence-based assays. An additional 100 µL of reporter cells UHH04, prepared as described above, was added to each sample well. The plate was incubated at 28°C on a Vibration Shaker 3023 (Gesellschaft für Labortechnik mbH, Burgwedel, Germany) at 150 rpm. Fluorescence and

OD600 measurements were taken at intervals of 0.5 to 2 hours using a Synergy HT plate reader with Gen5 software (BioTek, Winooski, VT, USA).

2.12 Fluorescence microscopy of *C. thiooxidans* S23 reporter strain

Microscopic imaging of reporter cells was performed with a confocal laser scanning microscope Axio Observer.Z1/7 LSM 800 (Carl Zeiss Microscopy GmbH, Jena, Germany) using Plan-Apochromat 100×/1.40 Oil DIC M27 objective. Image analysis and processing was conducted using ZEN software (Version 2.3, Carl Zeiss Microscopy GmbH).

2.13 Accessing the effect of iron on PET intermediate degradation

2.13.1 BHET degradation assay

Pre-cultures of *Maribacter dokdonensis* UHH-5R5 and *Arenibacter palladensis* UHH-Hm9b were prepared in artificial seawater media (AS media, section 2.3.4) and incubated at 28°C for 1-2 days. For liquid culture experiments, the cultures were diluted to an optical density OD_{600} of 0.05. The medium was supplemented with BHET at a final concentration of 5 mM, and iron (Fe^{+3}) was added to the media at two different concentrations (0.5 mM and 1 mM), while control cultures contained BHET without additional iron. Samples were collected at day 3, 5, and 7 after incubation. The concentrations of degradation products were quantified by UHPLC.

For plate-based assays, artificial seawater agar plates were prepared and supplemented with BHET (5 mM) and iron (1 mM). Both strains were streaked onto the plates and incubated at 28 °C. The plates were observed after 5 days of incubation. All experiments were performed in triplicate.

2.13.2 Transcriptomic analysis via RNA sequencing

UHH-Hm9b precultures were diluted to an OD_{600} of 0.05 in 4ml AS medium per well in 6-well cell culture plates (Nunc cell culture plate. catalog no. 130184; Thermo Fisher Scientific, Waltham, MA). BHET was added as a substrate to each well, and cultures were incubated for 3 days at 28°C under gently shaking conditions. Following incubation, cells were then harvested by centrifugation, and then stabilized with 2 ml of 20% stop mix (solution composed of 95% ethanol and 5% phenol), and centrifuged for 20 minutes at 4°C. The resulting pellets were washed three times with PBS buffer and afterwards immediately frozen in liquid nitrogen and stored at -70 °C until processing. Cell pellets were sent to Goettingen Genomics Laboratory (University of Goettingen, Germany) for RNA sequencing. Sequencing was performed using 75-bp single-end read on an Illumina NextSeq 500 system.

2.14 Global distribution of PET93 and PET94 homologs

The IMG/M scans for PET93 and PET94 homologs were completed on April 20, 2025. When available, Geo locations were used as provided on IMG. In case the data was missing, we attempted to retrieve Geo coordinates using details about isolation source/location/city/country on IMG database. The map illustrates both the frequency and geographical distribution of the homologs of dienelactone hydrolases in the strains UHH-5R5 and UHH-Hm9b was created using the Cartopy Python package (version 0.24.0) that is freely available on https://scitools.org.uk/cartopy. A similarity threshold of 50% was applied in homology searches. Only bacterial hits classified within the Bacteroidota phylum were included in the final dataset.

2.15 Data availability and bioinformatic analysis

The genome of isolates UHH-5R5 and UHH-Hm9b were submitted to IMG.gov under the submission IDs 294449 and 294450, respectively. The sequence reads were assembled using SPAdes (v.3.15.0) (Bankevich et al., 2012) and initial annotated with Prokka (v 1.14.6) (Seemann, 2014). To identify putative PET esterases within the Bacteroidetes genome datasets, a profile Hidden Markov Model (HMM) was constructed based on the known, functionally tested enzymes. The HMM analysis identified PET93 and PET94 as homologues of known-PET degrading enzymes, which were subsequently investigated further.

Nucleotide and amino acid sequences of putative PET esterases were obtained from genomic data of isolates UHH-5R5 and UHH-Hm9b from IMG. Sequence data were processed and analyzed using Snapgene (GSL Biotech LLC, San Diego, CA, USA). Conserved domains in the protein sequences were identified using CD-search (Marchler-Bauer & Bryant, 2004). A phylogenetic tree was constructed with MEGA-X, employing maximum bootstrap of 1000 for enhanced accuracy (Kumar et al., 2018). Structural information was retrieved from the RCSB-PDB database (Berman et al., 2000), and protein structures were predicted using AlphaFold2 with default parameters (Jumper et al., 2021). The 3D protein models were visualized in UCSF Chimera, further the structural alignment with homologous protein were generated with Chimera MatchMaker tool (Pettersen et al., 2021). SignalP 5.0 server was used to predict the native signal peptide sequences (Almagro Armenteros et al., 2019)

3. RESULTS

3 RESULTS

3.1 Enriching for PET-active enzymes affiliated with the Bacteroidota

In this study, we expanded the biodiversity of known PET-degrading microorganisms within the phylum Bacteroidota by selectively enriching Bacteroidota species capable of utilizing PET as their carbon source. Enrichment cultures were established using either BMB or R2A medium, both supplemented with PET powder to promote the growth of bacteria with PET-degrading potential. This approach led to the successful isolation of 19 novel and phylogenetically distinct strains, as summarized in Table 8. To determine their taxonomic identity, we performed 16S rRNA gene sequencing, which confirmed that all isolates were affiliated with the phylum of the Bacteroidota and belong to the genus Flavobacterium.

As a first measure to assess if any of these newly isolated Bacteroidota were cable of secreting PET-active hydrolases (i.e. esterases E.C. 3.1.1.1) we screen all isolates for their ability to hydrolyse typical model substrates commonly used to screen for PET-active bacteria (e.g. TBT, PCL and BHET). The assays were performed on agar plates supplemented with each substrate, and halo formation around the colonies was used as indicator of enzymatic activity, reflecting the production and secretion of active hydrolases into the surrounding medium.

Table 8 presents the substrate degradation abilities of the isolated microbial strains when exposed to three model substrates. Out of the 19 isolates tested, several showed activities against one or more substrates. Among all isolates, only two, UHH-5R5 and UHH-Hm9b, showed hydrolytic activity on BHET and only UHH-5R5 acted on both substrates PCL and BHET (Figure 6). Other isolates like UHH-ER2 and UHH-SO2 showed activity on TBT and PCL while most of the remaining strain only showed no detectable activity on any substrates or on only one substrate TBT or PCL (Table 8).

To dedermine their taxonomic identity and evolutionary relationships, 16S rRNA gene sequencing followed by phylogenetic analysis. The isolate UHH-Hm9b was identified as a novel species of *Arenibacter palladensis* while the isolate UHH-5R5 was affiliated with *Maribacter dokdonensis.* The 16S rDNA phylogenetic tree revealed that the novel species UHH-5R5 and UHH-Hm9b are placed very close together within the phylum and form a distinct branch from other known strains on the tree. Their placement on a separate branch from other known strains suggests a shared evolutionary history and possibly the development of specialized adaptations (Figure 7). Thus, the two isolates UHH-5R5 and UHH-Hm9b were expected to be an interesting candidate for further investigation in the context of polyester degradation.

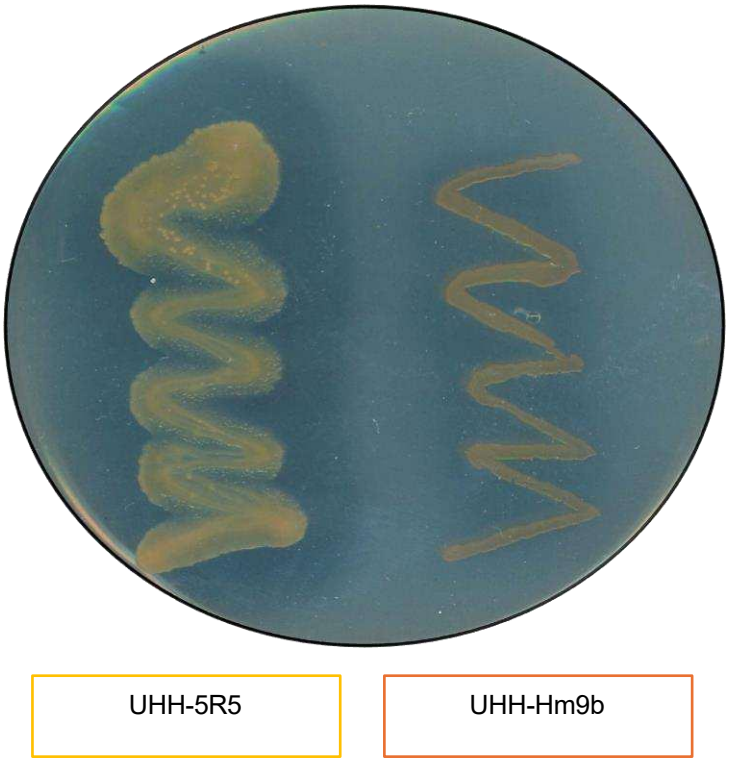

Figure 6. Visualization of BHET-hydrolyzing activity by the isolates Maribacter dokdonensis UHH-5R5 and Arenibacter palladensis UHH-Hm9b. Clear zones (halos) formed around bacterial colonies grown on BHET agar plates indicate enzymatic hydrolysis of the substrate. Plates were incubated at 28°C for 5 days.

Table 8. Flavobacterium isolates enriched in this work using PET powder as substrate and plate assay for activity screening on TBT, PCL and BHET substrates. The presence of a "+" indicates positive degradation activity, while a "–" indicates no observable activity.

Isolate	***Affiliated Species*** *(Based on 16S rDNA sequencing and at > 99% identity)*	***IMG Accession number***	***Origin***	***Substrates***		
				TBT (1.5% vol/vol)	**PCL (500mg/l)**	**BHET (5mM)**
UHH-Hm2a	*Aequorivita vladivostokensis **	298716	Marine aquaculture, Büsum, Germany	+	-	-
UHH-Hm9b	*Arenibacter palladensis**	294450	Marine aquaculture, Büsum, Germany	**+**	**-**	**+**
UHH-3NH2	*Muricauda taeanensis**	298717	Marine aquaculture, Büsum, Germany	+	-	-
UHH-5R5	*Maribacter dokdonensis**	294449	Marine aquaculture, Büsum Germany	**+**	**+**	**+**
UHH-ER1	*Flavobacterium cheniae**	341742	North Sea, Hamburg, Germany	**+**	**-**	**-**
UHH-ER2	*Flavobacterium bizetiae**	298720	Elbe River sediment, Hamburg, Germany	+	+	-
UHH-ER3	*Flavobacterium gyeonganense**	341743	Elbe River sediment, Hamburg, Germany	+	-	-
UHH-SO1	*Flavobacterium chungangense**	341744	Terrestrial isolate, Hamburg, Germany	+	-	-
UHH-SO2	*Flavobacterium proteolyticum**	298719	Terrestrial isolate, Hamburg, Germany	+	+	-
UHH-ER5	*Flavobacterium cheonhonense*	N/A	Elbe River sediment, Hamburg, Germany	-	-	-
UHH-EL5	*Flavobacterium reichenbachii*	N/A	Lake 'Außenalster', Hamburg, Germany	-	-	-
UHH-SP2	*Flavobacterium cheonhonense*	N/A	Lake Stadtpark, Hamburg, Germany	-	-	-
UHH-NS2	*Flavobacterium johnsoniae*	N/A	North Sea, Hamburg, Germany	-	-	-
UHH-NS50	*Flavobacterium laiguense*	N/A	North Sea, Hamburg, Germany	-	-	-
UHH-NS15	*Unclassified flavobacterium*	N/A	North Sea, Hamburg, Germany	-	-	-
UHH-NS30	*Flavobacterium psychroterrae*	N/A	North Sea, Hamburg, Germany	-	-	-
UHH-NS31	*Flavobacterium frigidimaris*	N/A	North Sea, Hamburg, Germany	-	+	-
UHH-NS47	*Unclassified flavobacterium*	N/A	North Sea, Hamburg, Germany	-	-	-
UHH-FTS11	*Mariniflexile jejuense*	N/A	Marine aquaculture, Büsum	-	-	-

Sequenced genomes are marked with an asterisk (*)

3.2 *Maribacter dokdonensis* UHH-5R5 and *Arenibacter palladensis* UHH-Hm9b form dense biofilms on PET foil and release TPA

Intrigued by the above-made observations, we further asked if both isolates would grow on PET, form biofilms and release TPA as the primary PET degradation product. To

assess if UHH-5R5 and UHH-Hm9b degrade PET foil under biofilm conditions, we inoculated both strains in BMB medium with added PET foil. The attachment and biofilm formation of UHH-5R5 and UHH-Hm9b on PET foil was observed over a seven-day incubation period using laser scanning microscopy and potential PET degradation was analysed using UHPLC and measuring the released TPA.

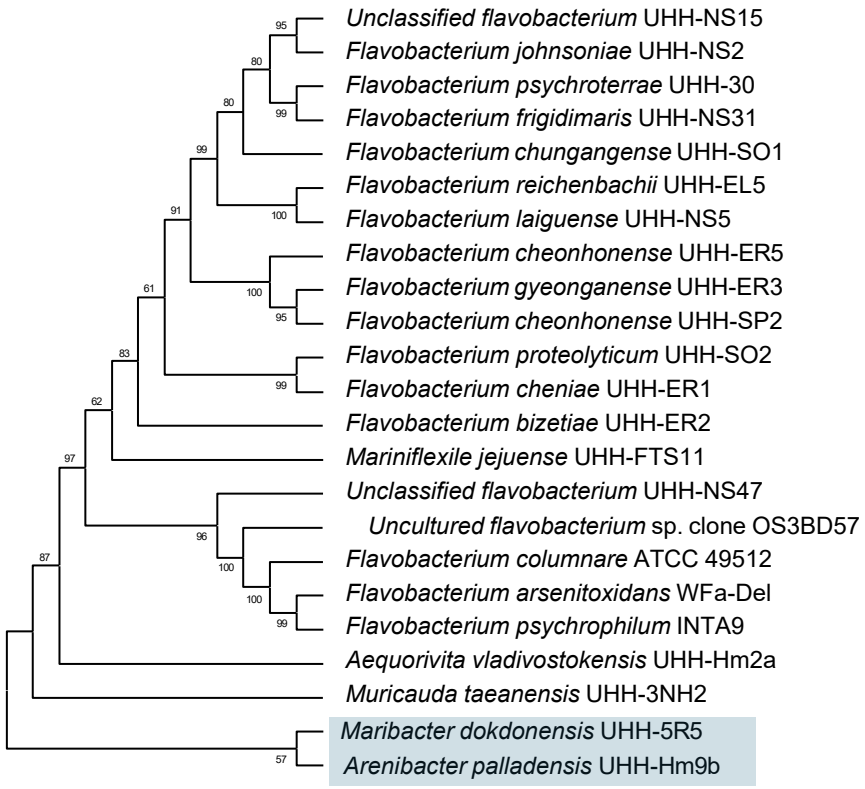

Figure 7. Phylogenetic tree based on 16S rDNA gene sequences of the two newly isolated strains (highlighted in blue) and other Bacteroidota strains. The tree was constructed using MEGAX and the number displayed at nodes are the bootstrap values based on 1,000 replications.

Initially, only a few individual cells of both strains were sparsely adhered to the PET surface, with no visible biofilm structures. However, on day 2, thin biofilm layers formed, accompanied by an increased number of attached cells (Figure 8). The 2-day old biofilms of UHH-5R5 and UHH-Hm9b exhibited an average thickness of 5.9±1.04 µm and 8.4±1.14 µm, respectively, corresponding to approximately 3–5 cell layers on foils. An increase in biofilm development was observed at day 3, with biofilm thickness

reaching 6.7±2.1 µm (UHH-5R5) and 12±3.2 µm (UHH-Hm9b). At day 6, both strains had developed well-structured, multilayered biofilms, reaching thicknesses of 14.5±1.8 µm (UHH-5R5) and 13.4±1.2 µm (UHH-Hm9b). Interestingly, while the biofilm thickness of UHH-5R5 decreased slightly to 11.3±2.5 µm by day 7, that of UHH-Hm9b remained stable at 15.1±3.1 µm.

To detect possible PET degradation products, supernatants were collected and concentrated from 3-, 5- and 7-day old biofilms grown on PET foil. UHPLC analysis revealed that strain UHH-5R5 released approximately 100-320 µM of TPA in the concentrated supernatants, equivalent to approximately 6-19 µM in the original samples (corresponds to 60-190 nmol in 10 ml culture volume), with smaller amounts of MHET and BHET detected throughout the observation period (Figure 9). The concentration of TPA steadily increased from day 3 to day 7, reaching a maximum of approximately 318±47.2 µM on day 7, indicating a slow but continuous degradation process over time. In contrast, strain UHH-Hm9b exhibited lower overall PET degradation activity. Nevertheless, UHPLC analysis confirmed its ability to release TPA from biofilms on PET foil at µM level. Interestingly, TPA concentration was highest on day 3 (41.6±13.2 µM in concentrated samples or 2.5±0.8 µM in original samples, corresponds to 25±8 nmol in 10 ml culture volume) but subsequently decreased to approximately 12±3.8 µM (7.2±2.2 nmol in 10 ml culture volume) on days 7 (Figure 9). No TPA were detected by HPLC in any of the negative controls, including Bacteroidota strain NS50 incubated with PET foil under the same experimental conditions. Altogether these findings imply that UHH-5R5 and UHH-Hm9b from dense biofilms on non-treated PET foil and can release minute amounts of TPA under the tested conditions in the laboratory.

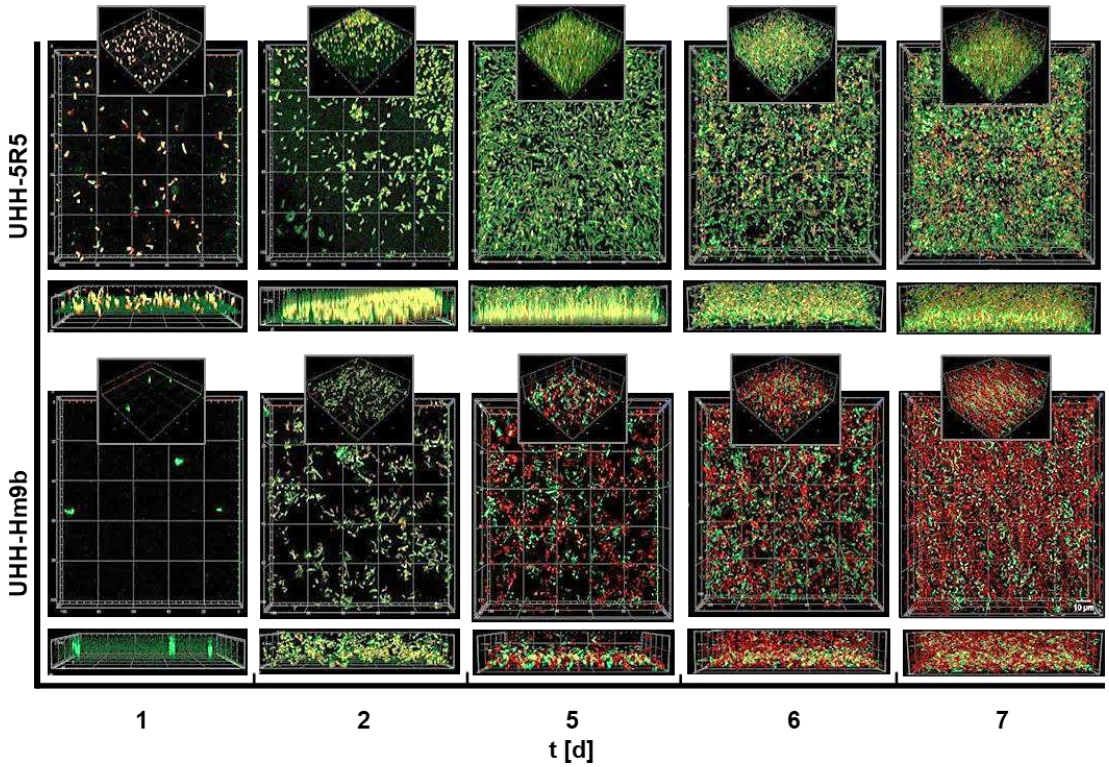

Figure 8. LSM microscopy images show the development of biofilms formed by the Bacteroidota isolates UHH-5R5 and UHH-Hm9b on PET foil over a 7-day incubation period. Biofilms were visualized using Live/Dead staining, where live cells are green (SYTO 9) and dead cells are red (Propidium iodide). Images were taken on days 1, 2, 5, 6, and 7 using a confocal laser scanning microscope (CLSM) with a 63× oil immersion objective. For each sample at least three different positions were observed and all images here are representative of three independent biological replicates.

Cell Viability during biofilm development

Live/dead staining imaging by LSM revealed the cell survival of the two strains during biofilm formation on PET foil. A large fraction of UHH-5R5 cells remained viable throughout the incubation period, with numerous live cells still present on the PET surface at later stage. In contrast, UHH-Hm9b exhibited a marked decline in viability, with majority of cells appearing non-viable from day 6 onward. These observations suggest strain-specific differences in survival and adaptation within PET-associated biofilms (Figure 8).

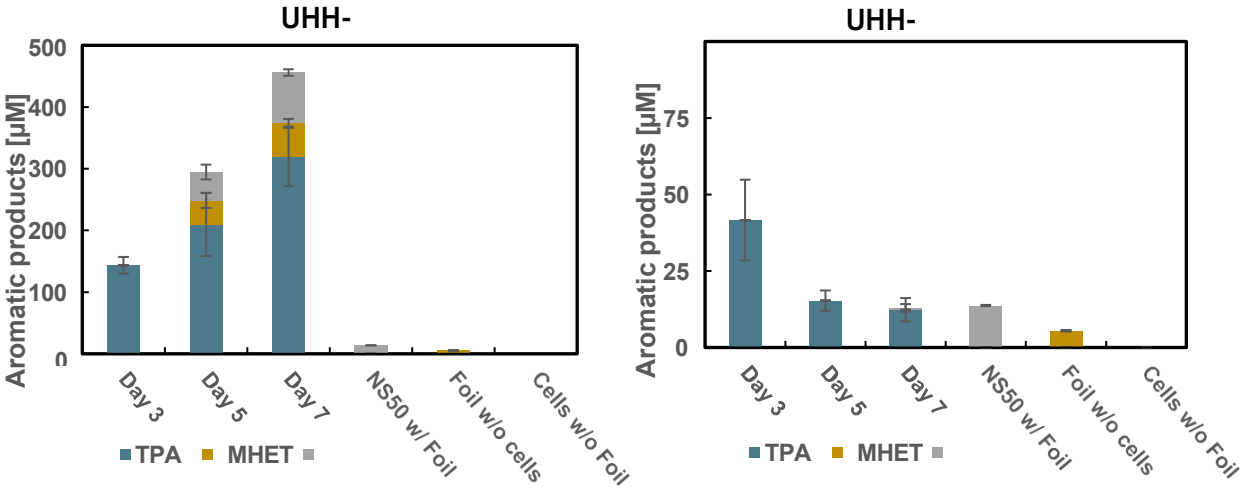

Figure 9. PET degradation products observed in supernatants from UHH-5R5 and UHH-Hm9b biofilms grown on PET film. Supernatants were collected after 3, 5, and 7 days and the degradation products were quantified using UHPLC as detailed in the Material and Methods section. Negative control samples were taken after 7 days of incubation. Data are normalized and corrected relative to E. coli DH5α growing on PET foil. PET degradation products in supernatants from UHH-5R5 and UHH-Hm9b biofilms grown on PET film. Values are mean of three biologically independent replicates, with error bars representing standard deviations.

3.3 Genome sequencing identifies two novel dienelactone hydrolases involved in PET degradation

To identify the possible genes linked to the observed hydrolytic activities, DNA of nine potential strains from Bacteroidetes collection were sent out for whole genome sequencing. Genomic DNA of these strains were sequenced using the Illumina NextSeq 500 system. The raw data was evaluated in terms of overall quality prior to genome assembly and annotation. Table 9 presents the results of genome assembly and gene annotations of sequenced strains. The genome assembly statistics indicate variation in genome size and contig number among the strains. The number of contig ranges from 105 in UHH-ER3 to 2.253 in UHH-5R5, reflecting differences in genome fragmentation and assembly completeness. Genome sizes vary significantly, with

UHH-5R5 having the largest genome (10.27 Mb) and UHH-SO2 having the smallest genome (2.85 Mb). Furthermore, the total number of predicted genes follows a similar trend, with UHH-5R5 encoding the highest number of genes (9,358) and UHH-SO2 the lowest (2,635). The number of coding sequences (Cds) closely correspond to the total gene count which indicates a high proportion of protein-coding potential across the genomes. GC content varies notably among the strains, ranging from 33.24% in UHH-SO2 to 49.93% in UHH-5R5. This suggests potential differences in their genomic stability and environmental adaptation.

Table 9. Summary of genome assemblies and annotations

ISOLATES	UHH-5R5	UHH-Hm9b	UHH-3NH2	UHH-SO2	UHH-Hm2a	UHH-ER2	UHH-SO1	UHH-ER3	UHH-ER1
IMG Accession number	294449	294450	298717	298719	298716	298720	341744	341743	341742
ASSEMBLY									
No. of contigs	2253	408	281	333	364	321	167	105	1850
Genome length	10 269 119	6 093 203	4 245 280	2 849 098	3 660 802	5 695 312	8 316 007	5 649 412	7 964 951
GENE									
No. of genes	9358	5056	3882	2635	3363	4735	7550	4951	8549
Cds	9261	5014	3842	2573	3324	4675	7340	4737	8290
GC (%)	49.93	39.7	45.51	33.24	38.54	34.3	48.99	34.12	33.64

Table 10. PETase-like genes in selected isolates based on sequence homology

No.	Isolate	Family/Species	Hits
1	UHH-5R5	Maribacter dokdonensis	NKFFJOOI_00264 (PET93)
2	UHH-Hm9b	Arenibacter palladensis	ICNPBAOJ_00709 (PET94)

The draft genomes of these isolates have been deposited at IMG under accession numbers listed in Table 8. The genome of those strains was mined for genes encoding potential PET-degrading enzymes using the previously published HMM search motifs for PETases. The genome assemblies implied a size of 10.2 Mbp for *Maribacter dokdonensis* UHH-5R5 and 6.1 Mbps for A*renibacter palladensis* UHH-Hm9b.

A detailed analysis of both draft genomes and using the previously published HMM search motifs (Danso et al., 2018) for PETases revealed a single hit for possible PETases in each strain. The potential PET-acting esterase in Arenibacter corresponded to the predicted ORFs Ga0596863_004_127947_129248 and in Maribacter the ORF Ga0596861_0008_300124_301428 was identified as potential PETase. The potential PET-esterase predicted in the two isolates were designated PET93 and PET94, respectively (Table 10 & Figure 10).

Interestingly we could not identify homologues of the previously identified Bacteroidetal PET degrading esterases (PET27 and PET 30) in the two draft genomes. Both hydrolase coding genes were not part of conserved regions on the bacterial chromosomes and only a few other strains were observed with similar gene neighbourhoods in the genomes available in IMG. None of the predicted genes were part of an operon and the flanking genes appeared to be transcribed in the opposite directions. For both predicted genes putative promoter sequences were identified using CNN Prom program (Umarov & Solovyev, 2017) with a SD sequence 5-6 bp upstream of the translational start point.

3.4 Computational protein analyses of predicted PET-degrading enzymes

The predicted esterase PET93 from *Maribacter dokodonensis* consisted of 434 amino acids with a possible secretion signal cleaving site identified between position 27 and 28 (VNA-QT) using the Sec/SPI secretion system. Similarly, the predicted protein PET94 derived from *Arenibacter palladensis* consisted of 433 amino acids and an N-terminal cleavage site between positions 25 and 26 (LNA-QT). Both amino acid sequences of the enzymes were highly similar (>99%) to precited DLHs in closely related species either affiliated with the genus Maribacter (PET93) or Arenibacter

(PET94) in the NCBI database. However, their overall amino acid similarity to known PETases from the phylum of the Bacteriodota was relatively low with less than 50% identity (Table 11).

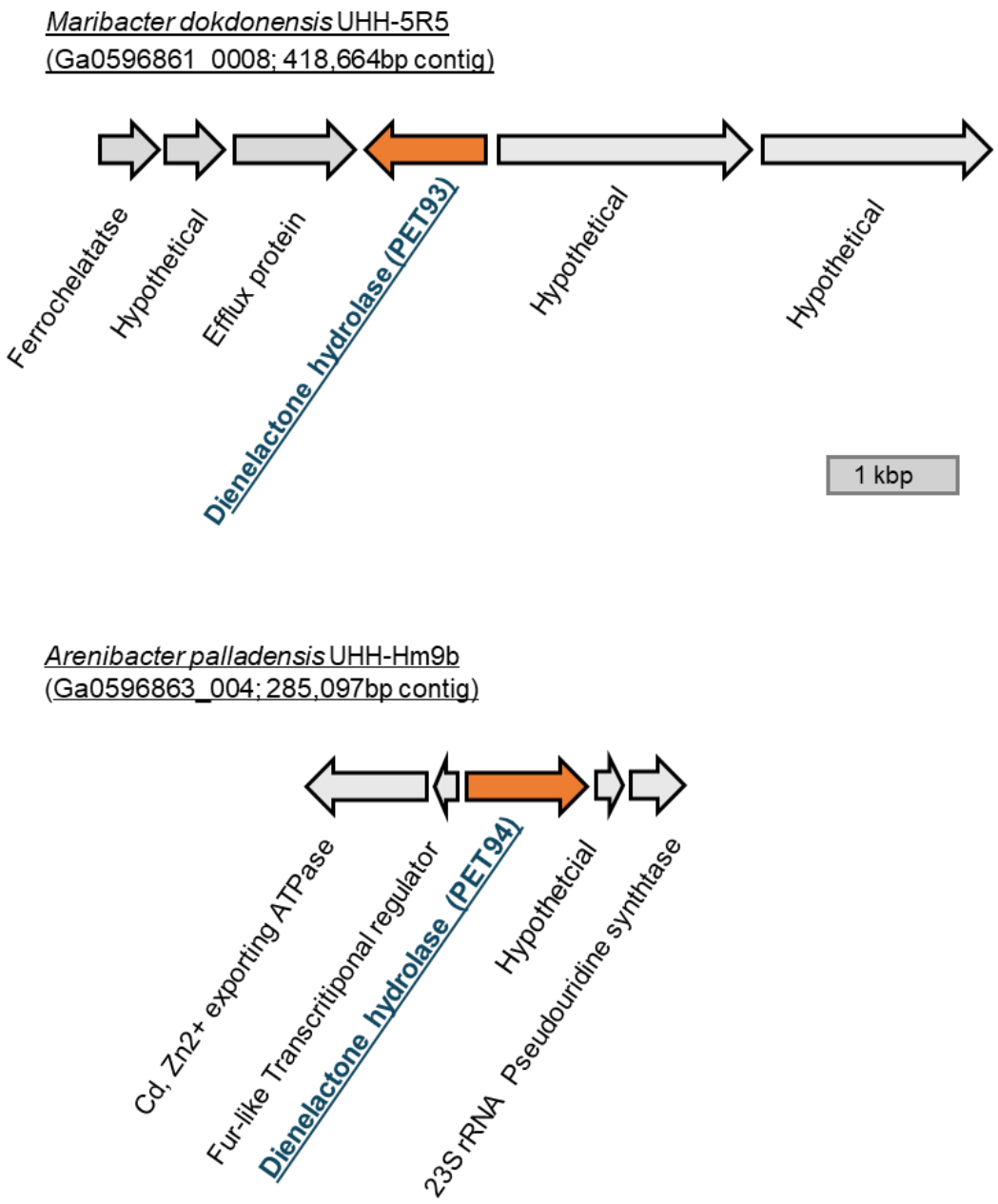

Figure 10. Genetic context of the dienelactone hydrolase PET93 and PET94 located in the Bacteroidota strains Maribacter dokdonensis UHH-5R5 and Arenibacter palladensis UHH- Hm9b, respectively

To gain further insight into the potential functional and evolutionary relationships among bacteroidetal-hydrolyzing enzymes, including PET93, PET94 and other known PETases, a phylogenetic tree was constructed using published and functionally verified PETases using MEGA-X with the maximum likelihood method and 1000 bootstrap replicates (Figure 11). The resulting consensus tree revealed that putative Bacteroidota PET-degrading hydrolases formed a distinct subcluster. Interestingly, PET93 and PET94 were not grouped within the subcluster that included the previously known Bacteroidotal enzymes PET27 and PET30 (Zhang et al., 2022). They differed also with respect to the secretion signal. While PET93 and PET94 are secreted enzymes and code for a predicted N-terminally secretion signal, PorC-like and C-terminal secretion signal was not observed as previously described for PET27 and PET30. This provides evidence for the broad diversity of bacteroidota enzymes capable of acting on PET.

Table 11. Sequence similarities generated for PET93 and PET94 against functionally verified PET hydrolases. Active site and PET binding motifs of PET93 and PET94 with selected and known PETases

Enzyme	**Origin**	**Sequence identity (%)**		**Active site**	**Binding site**
		PET93	**PET94**	Ser Asp His	Tyr Met Trp
*Is*PETase	*Ideonella sakaiensis*	49.5	48.6	Ser Asp His	Tyr Met Trp
PET27	*Aequorivita sp.*	50	48.6	Ser Asp His	Phe Met Trp
PET30	*Kaistella jeonii*	47.9	46.2	Ser Asp His	Phe Met Trp
LCC	*Leaf compost metagenome*	48.5	49.4	Ser Asp His	Tyr Met Trp

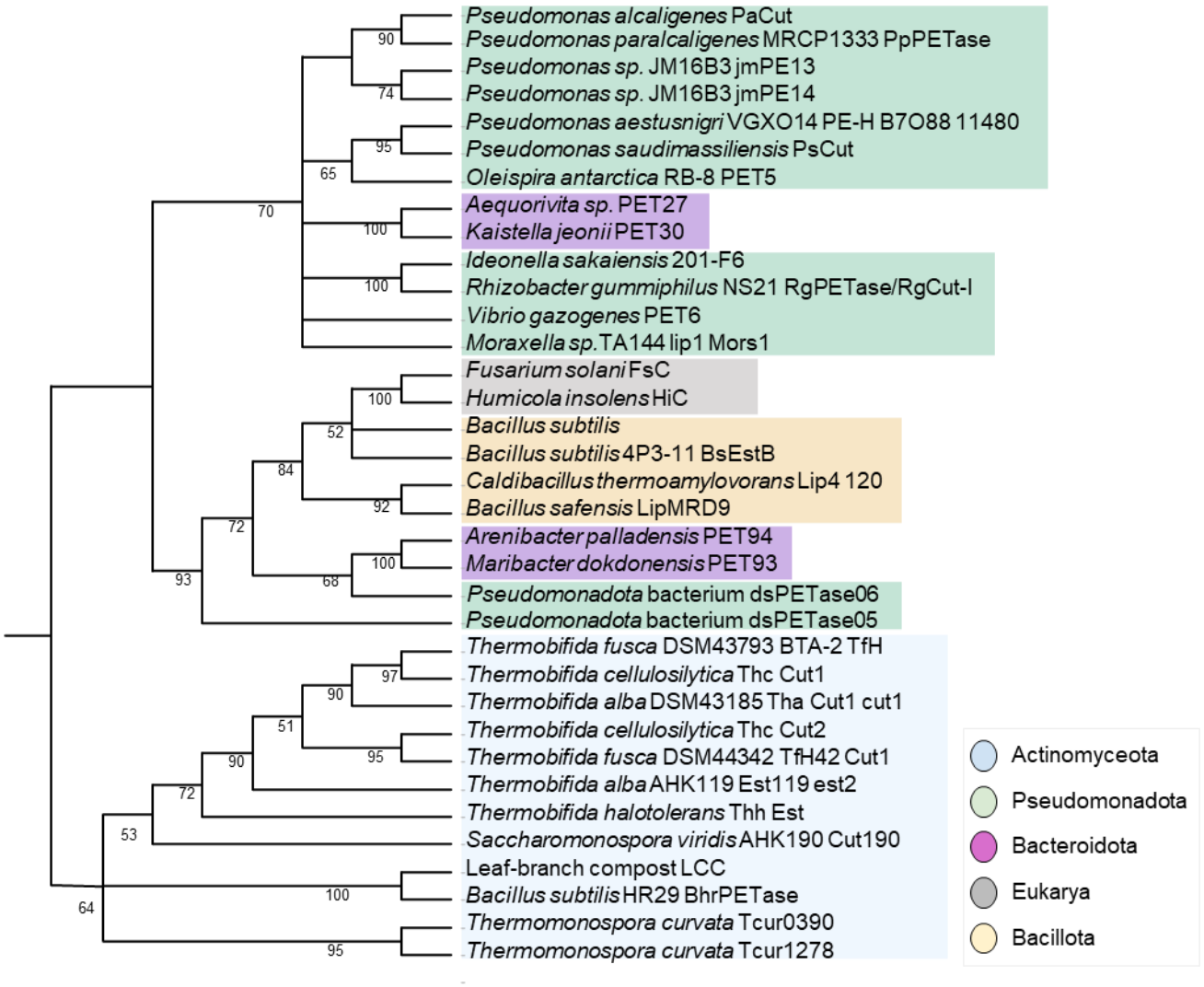

Figure 11. Neighbor-joining trees show the phylogenetic relationship of PET93 and PET94 with other well-characterized enzymes. The tree was constructed using MEGAX and the number displayed at nodes are the bootstrap values based on 1,000 replications

3.5 Binding mode prediction via molecular docking

Molecular docking simulations were conducted for the two target proteins, PET93 and PET94. We performed molecular docking using docking engine Autodock Vina via UCSF Chimera system to evaluate potential ligand-protein interactions. The ligands selected for docking were ester substrates that were also investigated experimentally in this study, namely mono(2-hydroxyethyl) terephthalate (MHET), bis(2-hydroxyethyl)

terephthalate (BHET), polycaprolactone trimer (PCL_3), tributyrin (TBT), 4-Nitrophenyl hexanoate (*p*NP-C6) and 4-Nitrophenyl caprylate (*p*NP-C8) (Figure 12 & Figure 13). Independent docking simulations were performed for each protein-ligand pair. For each simulation, the top-ranking binding pose was selected based on the lowest binding energy predicted by AutoDock Vina. The binding affinities (docking scores) for each substrate with PET93 and PET94 were summarized in Table 12. Overall, docking experiments generated binding modes with estimated binding affinity ≤ -5 kcal/mol for both enzymes with all substrates as ligand. Among the tested substrates, pNP-C8 exhibited the most stable/favorable binding energies (binding mode 1, RMSD value = 0.0) for both proteins (-6.199 kcal/mol for PET93 and -6.016 kcal/mol for PET94), suggesting a potentially better hydrophobic interaction with the active site residues

Table 12. Docking scores of the representative of best-scored cluster for all docking substrates.

Substrate	**Lowest docking energy**	
	PET93	**PET94**
MHET	-5.34	-5.835
BHET	-5.222	-5.331
*p*NP-C6	-6.013	-5.568
TBT	-5.539	-5.53
*p*NP-C8	-6.199	-6.016
PCL_3	-5.982	-5.322

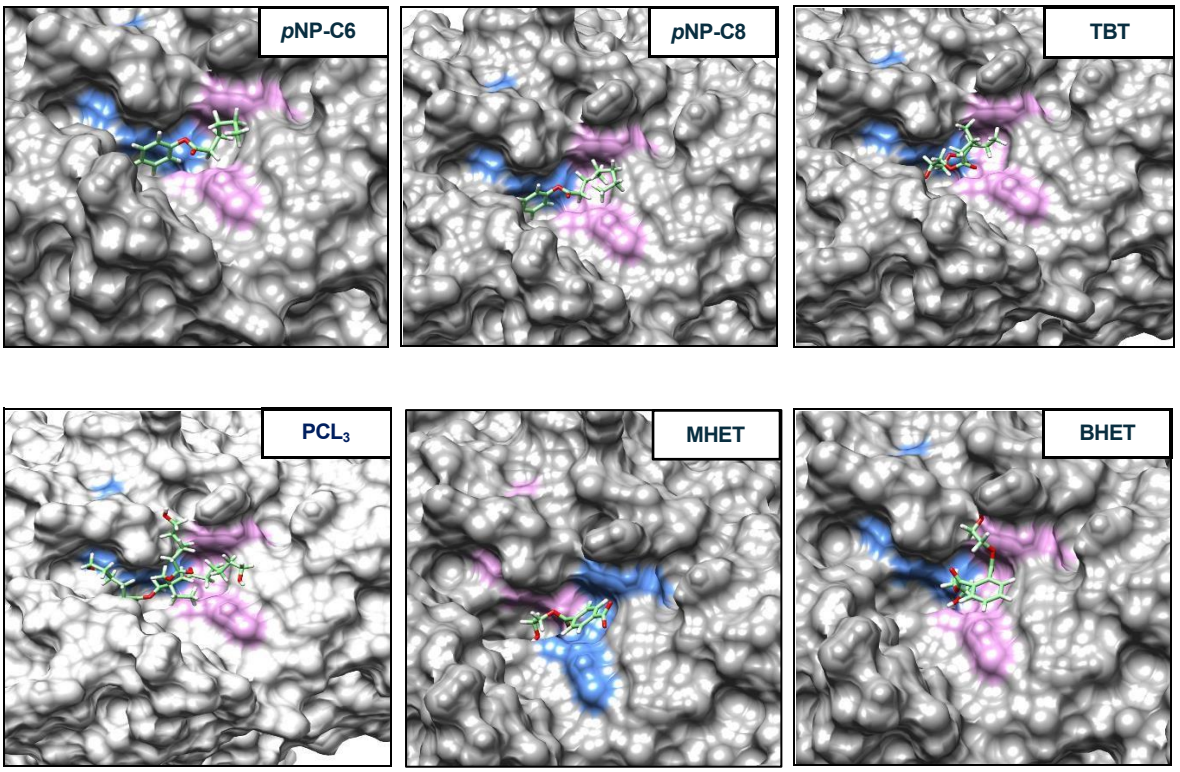

Figure 12. Molecular docking analysis facilitated by AutoDock Vina and the binding poses were visualized in ChimeraX. The PET93 structural model is displayed in surface representation with docked ligands BHET, MHET, and pNP-C6, pNP-C8, TBT and PCL_3 localized at the predicted active site pocket. The catalytic region is hightlighted in blue and the substrate binding region is indicated in pink.

Similarly, pNP-C6 and PCL_3 also showed relatively moderate docking energies, suggesting that both enzymes are well-suited to fitting the interacting with medium-chain ester substrates. BHET and MHET, which are the key intermediates in PET degradation, showed moderate binding affinities. PET93 and PET94 exhibited similar binding energies to TBT, BHET and MHET, ranging from -5.222 to -5.835 kcal/mol (Table 12). In general, the docking results suggest the idea that both PET93 and PET94 may interact with a broad range of ester-containing compounds

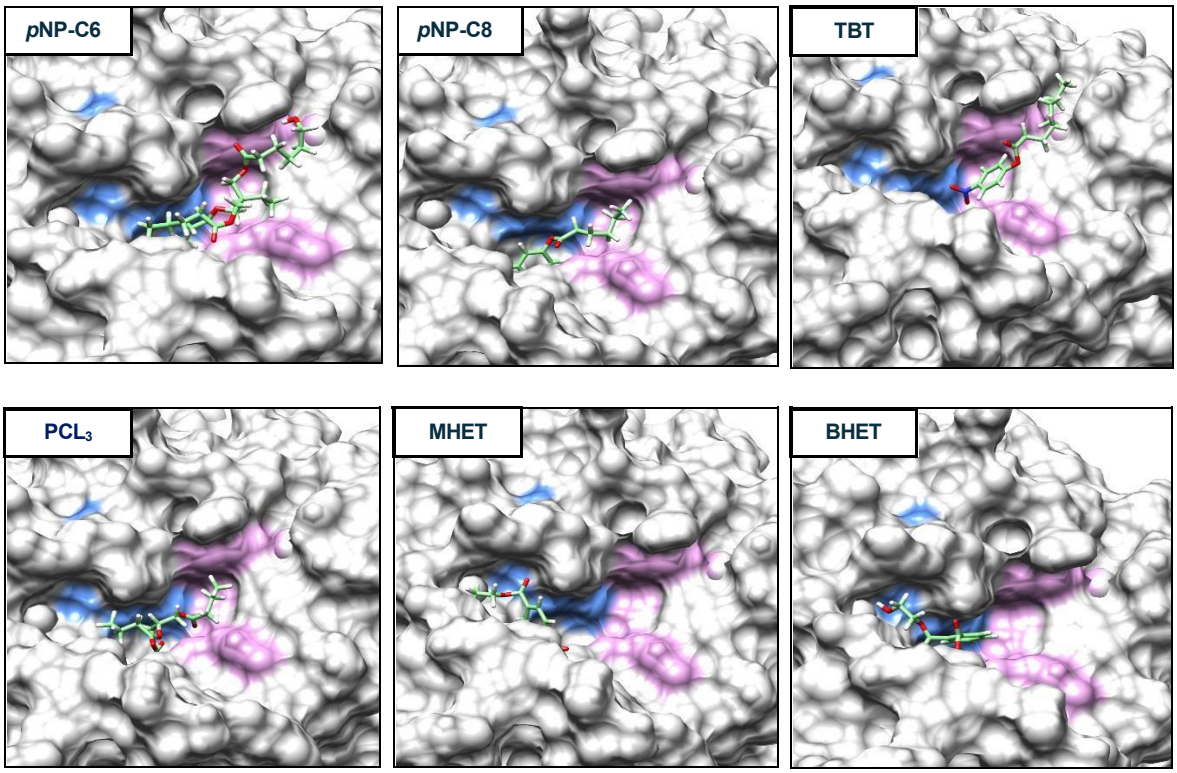

Figure 13. Molecular docking analysis facilitated by AutoDock Vina and the binding poses were visualized in ChimeraX. The PET94 structural model is displayed in surface representation with docked ligands BHET, MHET, and pNP-C6, pNP-C8, TBT and PCL_3 localized at the predicted active site pocket. The catalytic region is hightlighted in blue and the substrate binding region is indicated in pink.

3.6 Cloning, heterologous expression and purification of putative enzymes

To determine whether both genes do encode for proteins which are responsible for PET-degrading activities, the gene sequences obtained by HMM were amplified from corresponding organisms, cloned into expression vector pET21a(+) to generate the pET21a(+)::*PET93* and pET21a(+)::*PET94* constructs (Figure S3 and Figure S4). Following transformation into *E. coli* DH5α, the constructs were then heat shocked to get into the *E. coli* BL21(DE3) expression host. PET93 was successfully expressed when its native signal peptide was maintained in the expression construct. However, we encountered some difficulties with the expression and secretion of PET94. Expression of PET94 was initially unsuccessful. This failure was attributed to the

presence of the native signal peptide in the gene. To overcome this, the signal peptide was removed from the PET94 sequence, allowing proper expression of the protein.

The expression and purification of PET93 and PET94 were evaluated by SDS-PAGE and Western Blot analysis. The transformed cells produced 48.1 and 45.6 kDa proteins (Table 6) when induced with 1mM IPTG. For both these C-terminal 6x histidine tagged proteins we obtained recombinant proteins using Ni-NTA purification protocols with relatively high purity. Polyesterase activity was confirmed using BHET plate assay with hallo appearing on the plates after overnight incubation (Figure 14). The negative control i.e., *E. coli* BL21(DE3) containing plasmid without insert did not display such activity towards the BHET substrate.

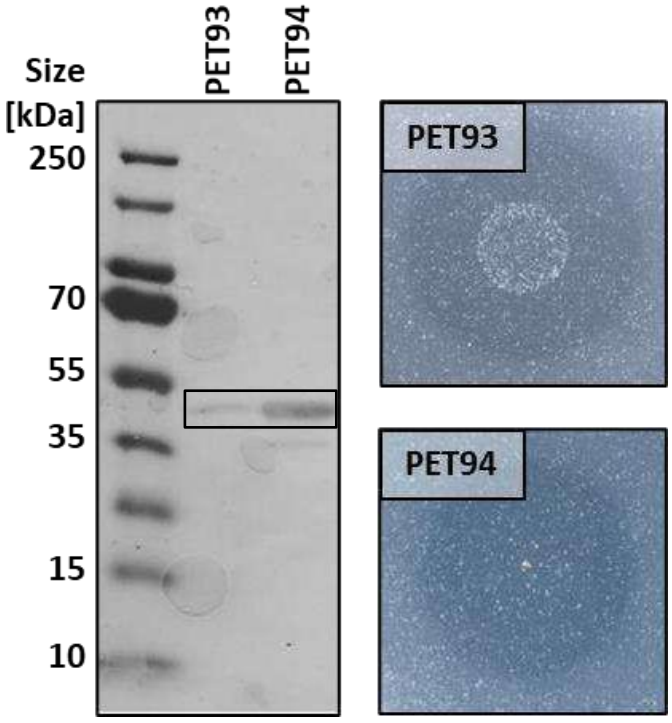

Figure 14. Purification and biochemical characterization of the dienelactone hydrolases PET93 and PET94. Purification of the His6-tagged dienelactone hydrolase PET93 (48.1 kDa) and PET94 (45.6 kDa) from Maribacter dokdonensis UHH-5R5 and Arenibacter palladensis UHH-Hm9b, respectively, and protein activity on BHET-containing plates

3.7 Initial characterization of enzyme activities with *p*NP assay

We first characterized the activity of two recombinant enzymes using *p*NP-assay (Kanta et al., 2021) with respect to substrate specificity, optimal temperature and optimal pH/buffer. With this assay, the released yellow para-nitrophenol products was measured with a spectrometer at 405 nm to determine relative enzyme activity.

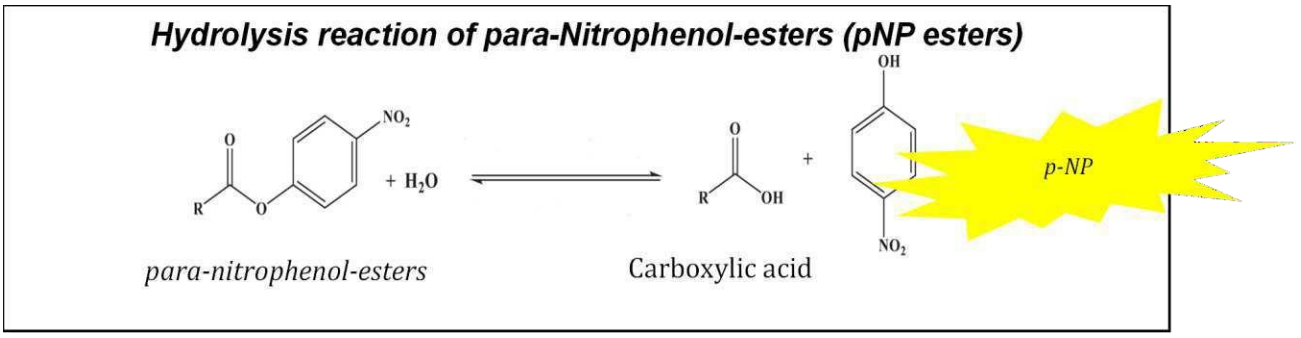

3.7.1 Substrate specificity

A substrate spectrum was recorded with *p*NP-esters which have acyl chain lengths of 4-18 carbon atoms to evaluate the active site preferences of the enzymes (Table 7). PET93 and PET94 revealed a narrow spectrum of substrates they hydrolyzed. The substrate specificity test clearly shows that PET93 and PET94 both are capable of hydrolyzing ester bonds of a chain length of 6-10 carbon atoms but exhibit highest activity to hydrolyze a chain length of C8 *p*NP-octanoate (Figure 15A). The degradation of *p*NP-acetate, -butyrate, and -hexanoate (C2–C6) occurred at less than 60% of the highest catalytic activity. The enzymatic activities of both enzymes were gradually reduced after *p*NP-octanoate (C8) and were no longer detected after *p*NP-myristate (C14). Thus, the results clearly showed that these enzymes preferred short chain substrates.

3.7.2 Temperature optimum

The hydrolyzing activity of both enzymes was also accessed within the temperature range from 4 to 90°C. In general, both enzymes were mesophilic, displaying the highest

activity at 20-50ºC and were much less active over 50ºC, where the relative activities decreased significantly. Both enzymes were shown to perform best at 40ºC and interestingly they were able to act at 4ºC where they could retain over 80% enzyme activity (Figure 15B), implying a possible cold adaptation.

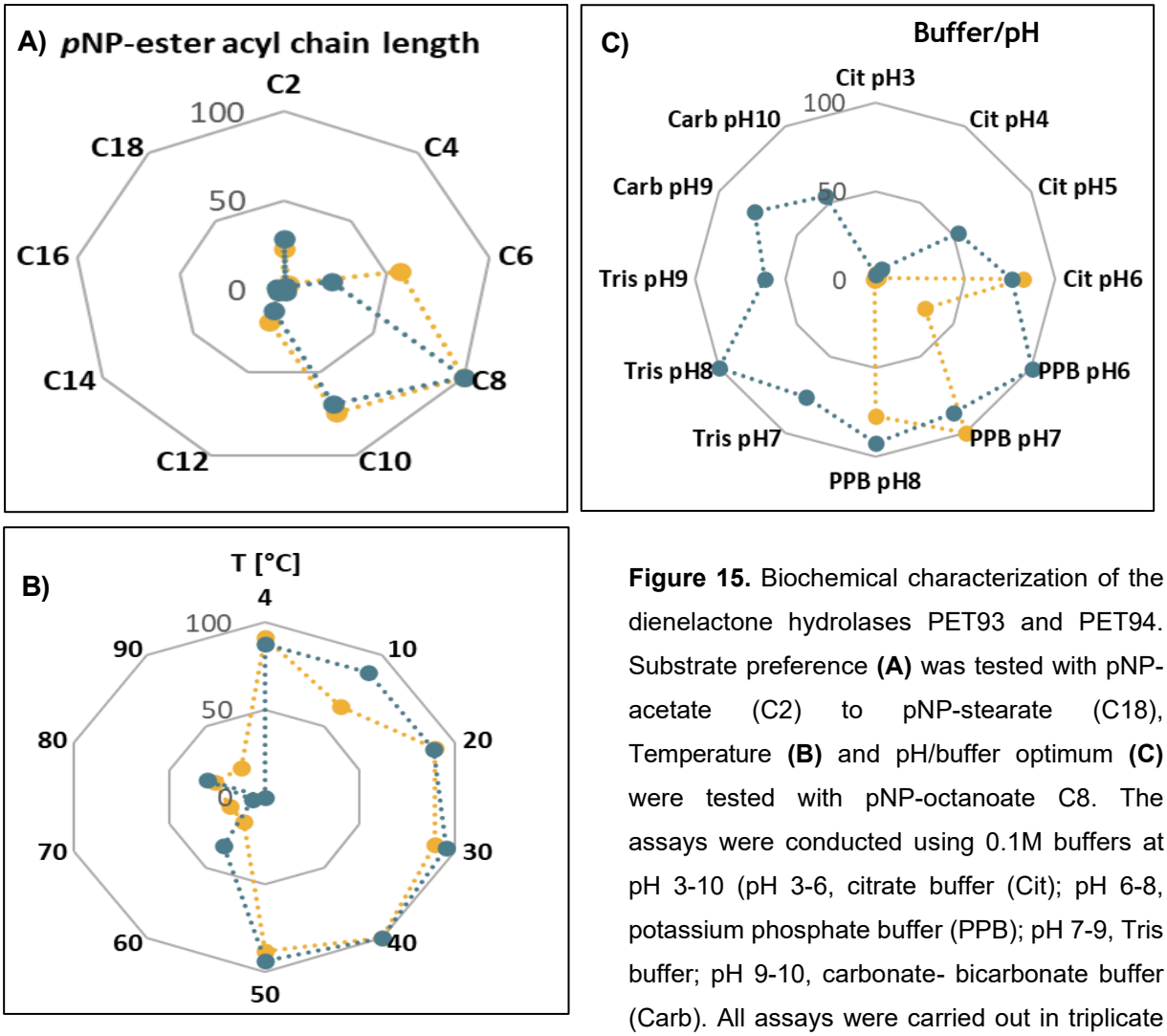

Figure 15. Biochemical characterization of the dienelactone hydrolases PET93 and PET94. Substrate preference **(A)** was tested with pNP-acetate (C2) to pNP-stearate (C18), Temperature **(B)** and pH/buffer optimum **(C)** were tested with pNP-octanoate C8. The assays were conducted using 0.1M buffers at pH 3-10 (pH 3-6, citrate buffer (Cit); pH 6-8, potassium phosphate buffer (PPB); pH 7-9, Tris buffer; pH 9-10, carbonate- bicarbonate buffer (Carb). All assays were carried out in triplicate at 37 °C using purified enzymes (0.1 mg mL^{-1}). Data represents the mean values of three independent replicates, with standard deviation (SD) ≤ 10% for all measurements.

3.7.3 pH optimum

Different buffers including citrate (Cit), potassium phosphate (PPB), TRIS and carbonate-bicarbonate (Carb) with overlapped pH range of 3-10 were used to verify the optimal pH conditions for PET93 and PET94. With C8 *p*NP substrate, it was shown

PET93 was most active in 0.1M citrate buffer pH 6 and in 0.1M potassium phosphate buffer pH 7 while PET 94 was highly active in potassium phosphate buffer pH 6-8. PET93 lost its activity nearly completely in the citrate buffer at pH below 5, Tris buffer at pH values 7-9, and Carb buffer at pH values 9-10 (Figure 15C). Further it is shown that PET94 was almost inactivated under acidic conditions pH<4.

3.8 PET93 and PET94 activity towards MHET, BHET and PET

Given that PET93 and PET94 are most active at 30-40°C in pH 7 potassium phosphate buffer, the recombinant enzymes were further assayed with substrates MHET (1 mM) and BHET (5 mM) under these conditions. Therefore, UHPLC analysis was performed to identify the PET degradation product TPA (Table 13). Both enzymes can hydrolyse BHET and MHET to TPA and 0.2 mg mL^{-1} of PET93 released an average of 2642.8 ± 46.9 µM TPA from BHET and 776.3 ± 29.5 TPA µM TPA from MHET after 24 hours in 200 µl reaction volume. Under the same conditions, PET94 (0.2 mg mL^{-1}) also released a similar amount of 2659.8 ± 99.6 and 684.5 ± 49.1 µM TPA when incubated with BHET and MHET, respectively.

Notably, when non-treated PET foil or powder was used as substrate for these two enzymes at pH 7 and 37°C, no TPA was detected by UHPLC after 5 days incubation. However, both enzymes were able to degrade UV-treated PET (Figure 16). After 5 days incubation with UV-treated PET powder, reasonable levels of PET degradation product were observed in a 200 µl reaction volume by UHPLC analyses, reaching 40.4 ± 18.67 µM and 54.7 ± 21.9 µM TPA released by PET 93 and PET94 (corresponds to 8.08 ± 3.73 nmol and 10.94 ± 4.38 nmol), respectively. However, only about 29.8± 1.76 and 37.3±11.5 µM TPA by PET93 and PET94 (corresponds to 5.96 ± 0.35 nmol and 7.46 ± 2.30 nmol) was detected under the same conditions with UV-treated foil (Figure 16). This suggests that UV probably helps promote the initial breakdown of PET.

Table 13. Recombinant and purified PET 93 and PET94 (0.2 mg mL^{-1}) enzymatic hydrolysis of MHET (mono(2-hydroxyethyl) terephthalate), BHET (bis(2-hydroxyethyl) terephthalate) and PET (polyethylene terephthalate) with their final degradation product TPA (terephthalic acid). The controls of an equal amount of BHET and MHET were incubated at the same conditions without added enzymes to rule out non-enzymatic TPA release. The concentration of the substrates and products was determined by UHPCL. The samples were incubated at 37^0C for 24 hours with continuous shaking at 200 rpm and were analyzed in triplicates. BHET and MHET were added at 5 mM and 1 mM concentrations, respectively. (*): PET substrates were pretreated with UV light for 1 week as indicated in the Material and Methods section.

Substrate added	Treatments	BHET detected (µM)	MHET detected (µM)	TPA detected (µM)
		Mean ± SD	Mean ± SD	Mean ± SD
BHET	Control	2244 ± 38.4	286.6 ± 11.5	n.d
	PET93	n.d	n.d	2642.8 ± 46.9
	PET94	n.d	n.d	2659.8 ± 99.6
MHET	Control	n.d	736 ± 31.5	20.1 ± 0.73
	PET93	n.d	n.d	776.3 ± 29.5
	PET94	n.d	n.d	684.5 ± 49.1

n.d: not detected

Since we observed that the recombinant proteins had relatively low turnover rates in the µM range, we used the recently published *Comamonas thiooxidans (C. thiooxidans)* S23 reporter strains (Dierkes RF (2013) that is able to detect nM concentrations of TPA in further tests. Using this reporter strain (ReporTPA_UHH04, Table 1) we were able to detect TPA release on PET foil incubated with recombinant PET93 and PET94 (Figure 17). Controls incubated with BSA showed no fluorescence (Figure 18). Unfortunately, the biosensor cannot be used for a quantitative analysis of TPA release, therefore only the presence or absence of TPA was recorded in this experiement. Altogether the data implied that the recombinant enzymes PET93 and PET94 are both active on PET albeit at relatively low levels.

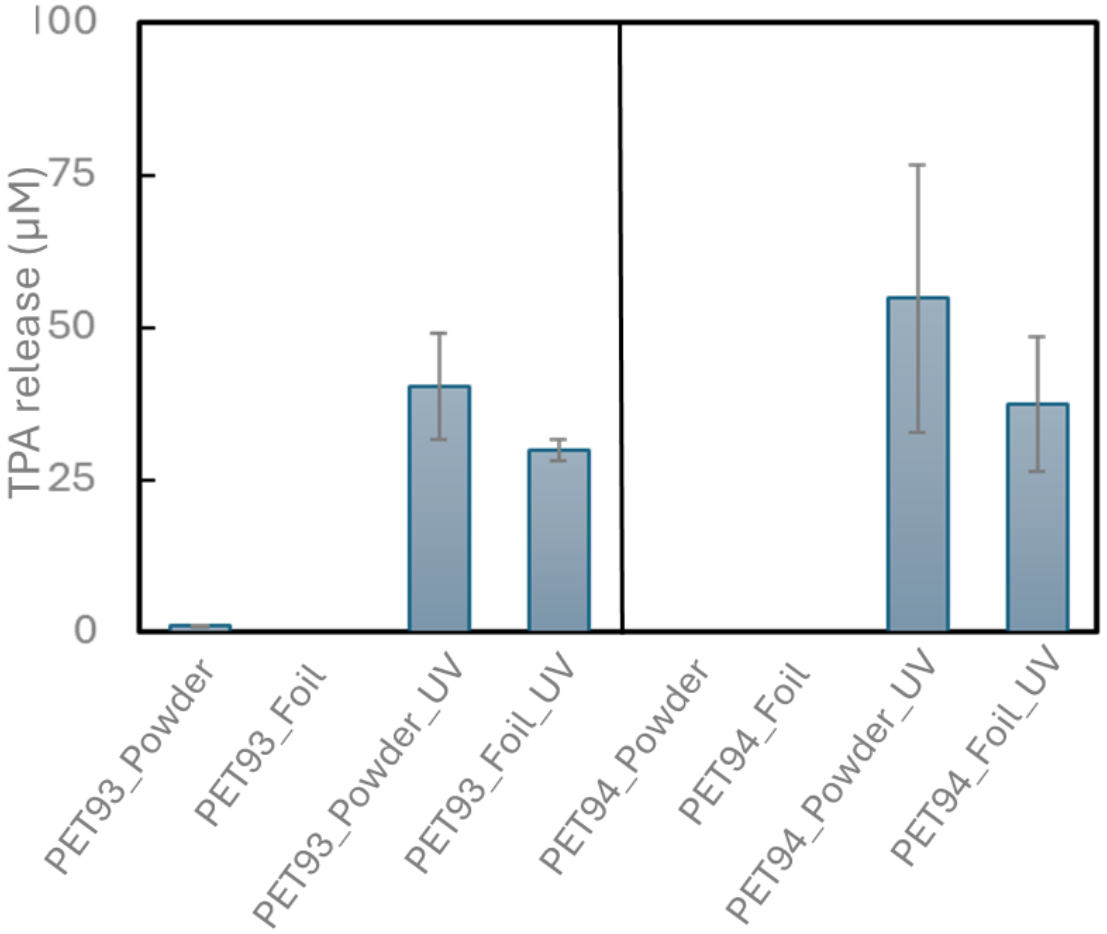

Figure 16: PET degradation assay of PET93 and PET94; TPA concentration after 5 days incubation of the purified enzymes (0.2 mg mL^{-1}) with PET powder and PET foil at 28°C. P: powder; F: foil; UVP: UV-treated PET powder and UVF: UV-treated PET foil. Values are means of triplicates; error bars indicate standard deviations. PET substrates were pretreated with UV light for 1 week as indicated in the Material and Methods section.

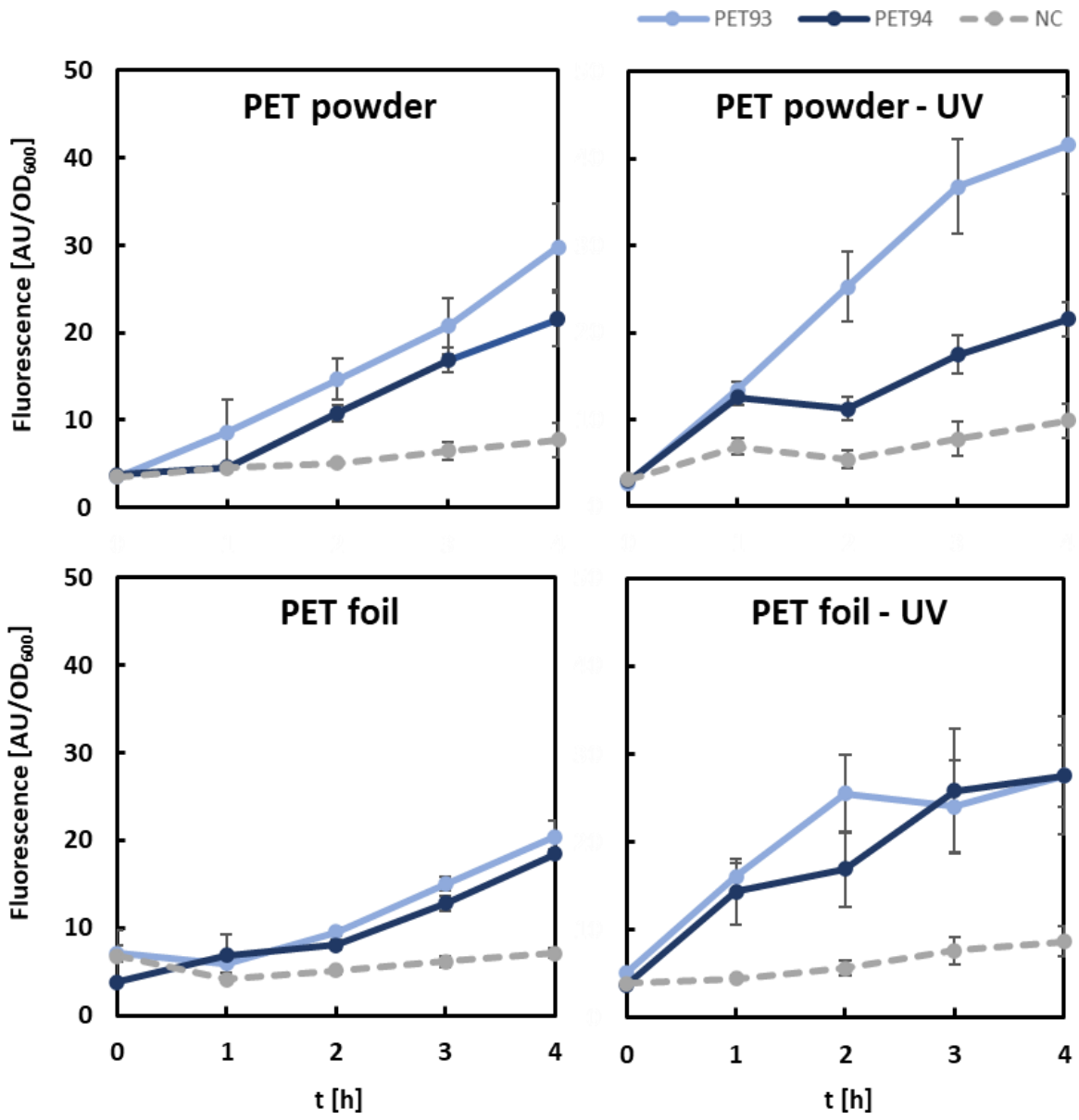

Figure 17. Detection of enzymatic TPA release from untreated and UV-treated PET Powders and Foils by *Comamonas thiooxidans* UHH04. Fluoresence response of *C. thiooxidans* UHH04 reporter cells (Dierkes, 2022) to supernatants from incubations of PET93 and PET94 with PET powder and foil, both untreated and UV-treated. Respectively 0.1 mg mL^{-1} of each enzyme and BSA as a negative control (NC) were incubacted with PET for 5 d in 0.1 M potassium phosphate buffer pH 7 before the addition of the UHH04 reporter to the supernatant. Fluorescence signals of sfGFP were normalized to the absorbance of the reporter cells at 600 nm. Data points represent mean values of 6 measurements, with standard deviation indicated by error bars.

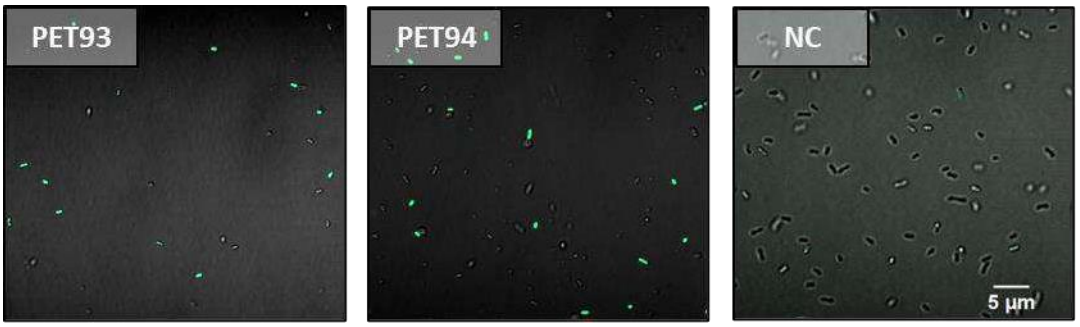

Figure 18. CLSM images of UHH04 reporter cells incubated with supernatants from the enzymatic reactions of PET93, PET94, and BSA (NC) on PET. The sfGFP channels were applied and were set at the same intensities for all pictures to allow for comparison.

3.9 Protein structural modelling for PET93/PET94 and comparative Analysis with other Well-known PETases

Homology models that represent three-dimensional structures often offer insights into their conformation and functionality and enable the visualization of important features. The structure of PET93 and PET94 were predicted using Alphafold2 for 3D protein modelling and Chimera for structural alignment. The well- characterized enzymes *Is*PETase from *Ideonella sakaiensis* and LCC from the leaf- branch compost cutinase are currently still considered as the reference models for PET degradation.

To explore how structural differences might influence PET degradation, the predicted 3D structures of PET93 and PET94 were compared with the high-resolution crystal structure of *Is*PETase (PDB: 6EQE), LCC (PDB: 4EBO) and two PET-degrading enzymes PET27 and PET30 originating from Bacteroidota. The structural analysis revealed that PET93 and PET94 generally share less than 50% sequence identity with the other well-known/characterized PETases (Table 11), yet both contain a predicted N-terminal signal peptide for secretion (Figure 19). Sequence alignment with *Is*PETase, LCC, PET27 and PET30 showed that the catalytic triad (Ser Asp His) is

highly conserved in PET93 and PET94 (Table 14). However, while substrate binding residues are similar to those of *Is*PETase and LCC (Figure 20), they differ significantly from PET27 and PET30, which appear to use distinct residues for substrate binding (Table 14). Amino acid sequence analysis revealed that PET 93 and PET 94 contained N-terminal signal domains for protein transport as predicted with SignalP 5.0. The predicted cleavage site was located between amino acid (aa) positions 26 and 27 for PET93 and positions 25-26 for PET94 with the signal peptide using the standard secretory signal peptides (likelihood of 0.93) (Table 14)

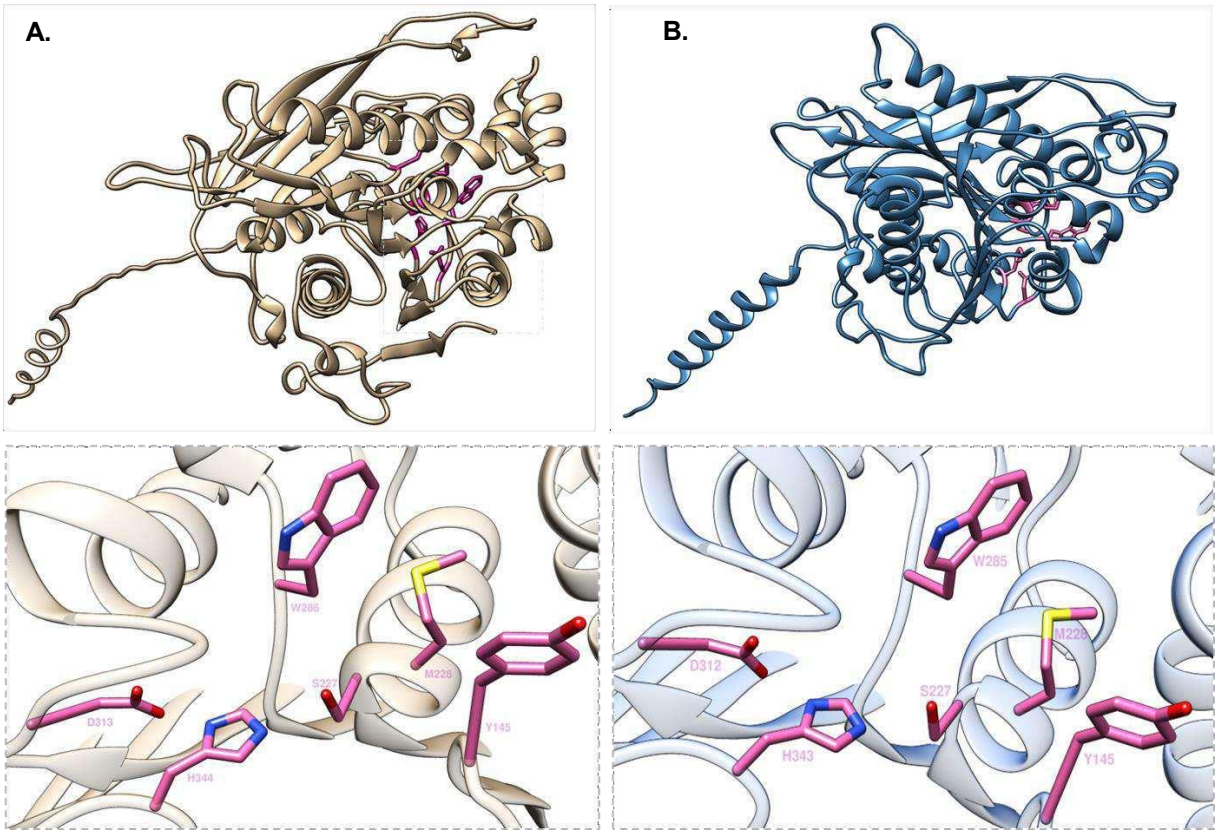

Figure 19. Structural model of PET-hydrolyzing enzymes from Bacteroidota. **A.** Overall structure of PET93 including active site and potential substrate binding site (showed in light brown); **B.** Overall structure model of PET94 including active site and potential substrate binding site (showed in light blue).

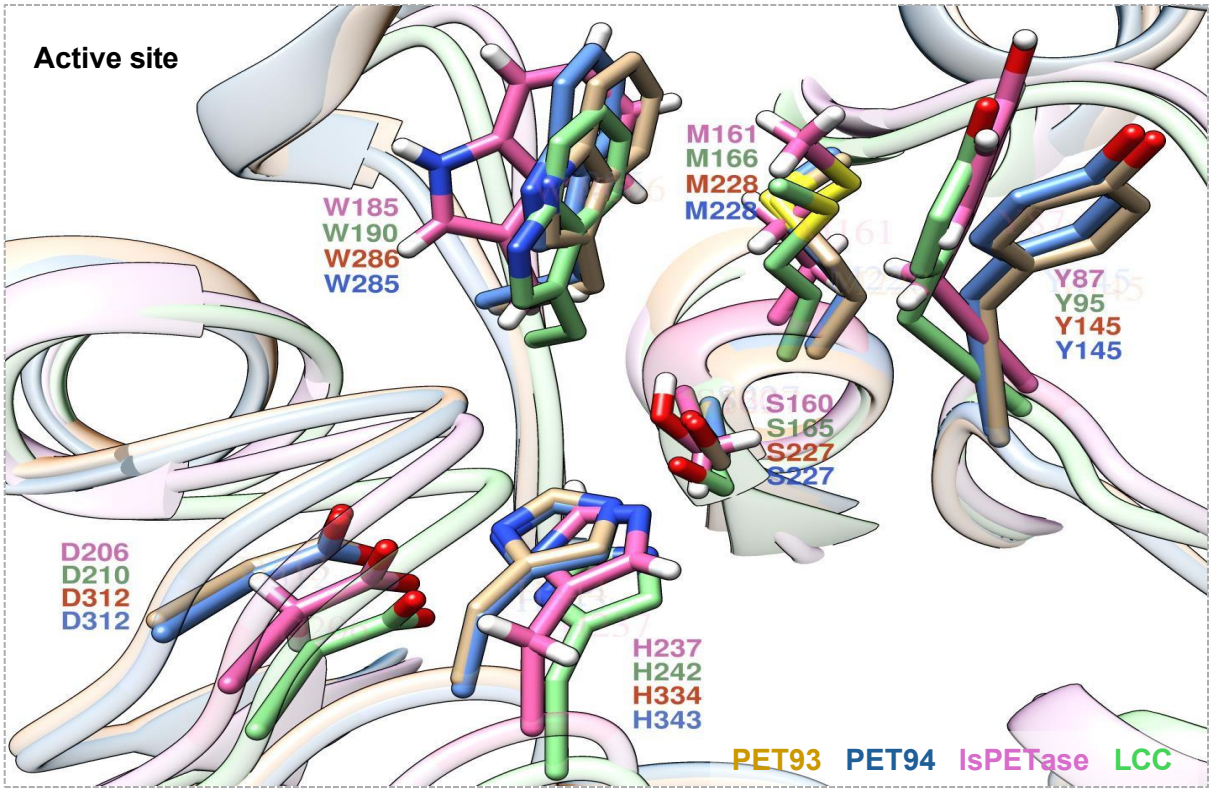

Figure 20. Comparison of active site residues. All four enzymes PET93 (light brown), PET94 (blue), IsPETase (pink, PDB 6EQE) and LCC (green, PDB 4EBO) have the typical residues of Ser-hydrolases at the catalytically active positions (Ser, His and Asp) and have the same amino acids associated with PET-binding. The residues of IsPETase and LCC are indicated in pink and green, respectively.

Even though PET93 and PET94 share conserved amino acids in the predicted substrate binding pocket with previously published PETases, such as *Is*PETase or LCC, both enzymes differed largely in their structural features from known PETases and represent novel scaffolds. Their actual PET-degrading activity was very low under the tested conditions. This was confirmed by product detection via HPLC measurements and ReporTPA_UHH04 assays, indicating that the presence of conserved residues alone is not sufficient for effective degradation process. Meanwhile, PET27 and PET30 have a single amino acid substitution in the predicted substrate binding pocket of PET93 and PET94. Notably, PET27 and PET30 carry a

Phe-Met-Trp motif in their binding sites. PET93 and PET94, however, carries a Tyr-Met-Trp motif. Further they lacked the typical porC-domain of these known PETases PET27 and PET30 from the Flavobacteria (Table 14).

Table 14. Conserved motifs and structural features identified in PET93 and PET94 and other well-known PETases. The Ideonella sakaiensis PETase (*Is*PETase, PDB: 6EQE), LCC (4EB0), the Bacteroidetal enzyme PET27 and PET30 were included as reference enzyme for benchmarking purposes.

Enzyme	Signal peptide cleavage site	Catalytic triad	Substrate binding residues	Secretion pathway	C-terminal domain
*Is*PETase (*Ideonella sakaiensis)*	27–28	Ser Asp His	Tyr Met Trp	Sec/SPI	None
PET27 (*Aequorivita sp.*)	23-24	Ser Asp His	Phe Met Trp	Sec/SPI	PorC secretion system
PET30 (*Kaistella jeonii)*	23-24	Ser Asp His	Phe Met Trp	Sec/SPI	PorC secretion system
LCC (*Leaf compost metagenome*)	21-22	Ser Asp His	Tyr Met Trp	Sec/SPI	None
PET93 (*Maribacter dokdonensis)*	26-27	Ser Asp His	Tyr Met Trp	Sec/SPI	None
PET94 (*Arenibacter palladensis*)	25-26	Ser Asp His	Tyr Met Trp	Sec/SPI	None

3.10 Global occurrence and spread of Maribacter and Arenibacter PET enzymes

We further analysed the global distribution of PET93 and PET94 and their homologs. It is notable that we were able to identify homologs in more than 250 currently available genome sequences of other closely related strains from publicly available databases IMG/MER (threshold of 50% sequence identity and over 80% coverage) (Chen et al., 2022; Mukherjee et al., 2022). Analysis of their occurrence and frequency of PET93 and PET94 raised the question of to what extent these enzymes could impact plastic

degradation in the natural environment. For a focused view, we selected 99 homologs assigned to the Bacteroidota phylum in our global search to construct a global distribution map (Table S2 & Table S3). Interestingly these homologs originated from a broad range of countries and regions, suggesting that the Bacteroidetal-derived enzymes PET93 and PET94 are widespread and may play a significant role in the global degradation of PET in nature (Figure 21).

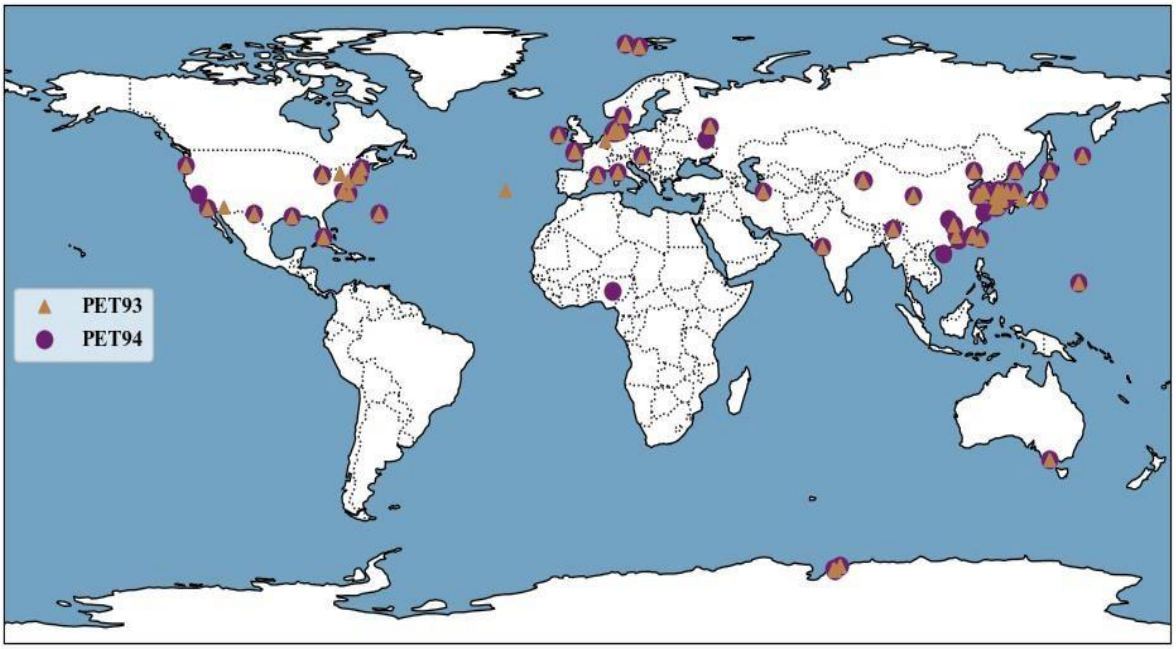

Figure 21. Global distribution of PET93 and PET94 homologs.

3.11 Response of PET93 and PET94 to iron supplementaion

The plate-clearing assay demonstrated halo formation around the polyester-degrading strain UHH-5R5 and UHH-Hm9b. The plates were incubated for 5 days at the optimal temperature 28^{o}C to support for bacterial growth and allow halo formation to proceed.

Figure 6 illustrates the polyesterase activities of Bacteroidota strains UHH-5R5 and UHH-Hm9b on the BHET plates with and without iron supplementation. Notably, a visual comparison of the plates revealed distinct differences in halo formation between

iron-supplemented and iron-free conditions (Figure 22). The halos surrounding UHH-Hm9b colonies were significantly larger on plates supplemented with 1 mM iron compared to those without iron. This suggests that iron availability possibly enhances the ability of the strain UHH-Hm9b to produce esterase enzymes involved in BHET degradation.

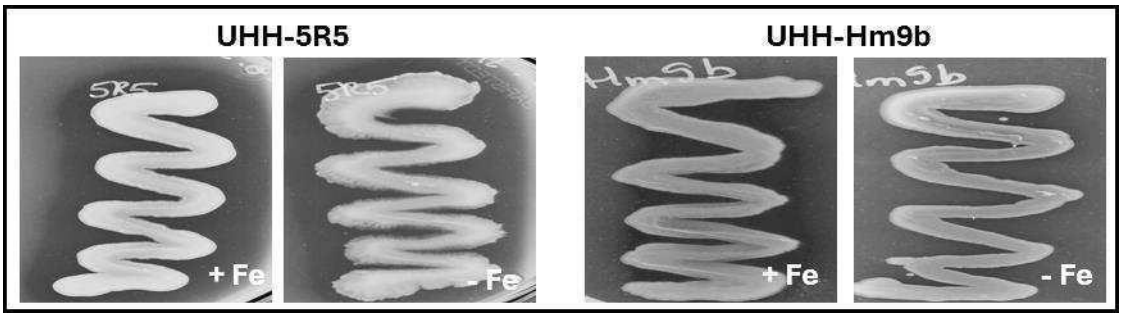

Figure 22. The effect of the supplementation of Fe^{3+} 1mM on BHET degradation of Bacteroidota strains UHH-5R5 and UHH-Hm9b on the BMB agar plate. Hydrolytic activity is indicated by a halo formation. The pictures were taken after 5 days of incubation at 28°C.

To further access the impact of iron, we incubated bacterial strains with 10mM BHET in the presence of different iron concentrations and quantified the degradation products MHET and TPA over a 7 day-period. MHET was the predominant degradation product across all conditions, with the highest accumulation observed at 0.5 mM Fe. After 3 days of incubation, the concentration of MHET, a primary degradation product, was approximately 9-fold increase in UHH-Hm9b cultures supplemented with 0.5 mM and 1mM iron compared to iron-free controls (Figure 23A). In contrast, TPA levels remained relatively low but increased consistently over time in iron-supplemented cultures. TPA was produced in much lower amounts compared to MHET but showed a clear iron-dependent increase, particularly under 0.5- and 1-mM Fe. This suggests that iron may promote the further breakdown of MHET into TPA. This shows that specific iron concentrations could optimize product turnover in microbial degradation systems. These findings highlight strain-specific responses to iron supplementation and indicate

that UHH-Hm9b may possess an iron-regulated enzymatic mechanism for BHET degradation.

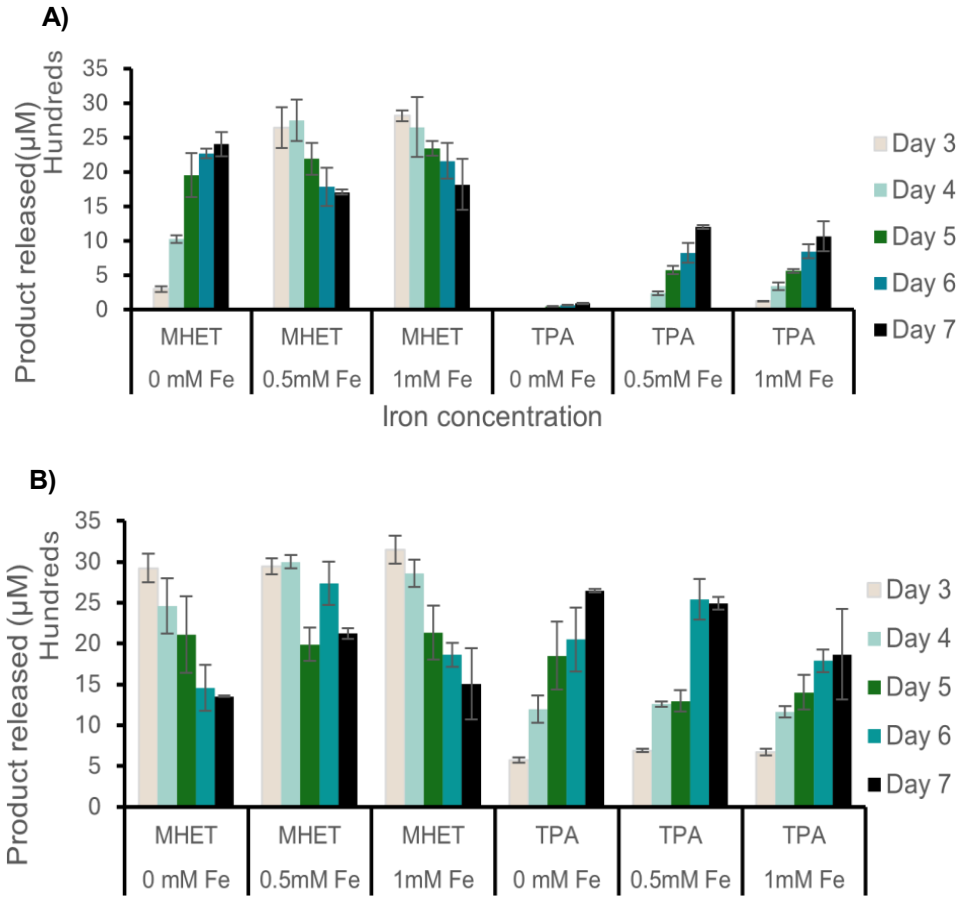

Figure 23. UHPLC data of culture supernatants from cultivation of UHH-5R5 and UHH-Hm9b strains with supplementation of iron 1mM. Degradation products released from BHET with UHH-Hm9b (**A**) and UHH-5R5 (**B**) growing on media supplemented with different concentrate of iron.

Similarly, to evaluate the effect of iron on BHET degradation for strain UHH-5R5, we compared MHET and TPA concentration over time in cultures with and without iron supplementation. Across all conditions (0 mM, 0.5 mM and 1 mM Fe), MHET accumulates strongly on Day 3, indicating rapid initial hydrolysis of BHET (Figure 23B). From Day 3 to Day 7, MHET concentrations decrease gradually, suggesting further enzymatic conversion (likely to TPA). However, the rate of MHET decline appears similar across all iron conditions, indicating that iron supplementation does not

significantly enhance MHET breakdown indicating that BHET degradation occurs effectively even in the absence of added iron. Further, TPA accumulates over time in all conditions, including in 0 mM Fe. Although there is a trend toward increased TPA production with iron, no significant differences in degradation product concentrations were observed for strain UHH-5R5 between iron-supplemented and iron-free conditions. This suggests that, unlike UHH-Hm9b, the effect of iron on BHET degradation in Strain UHH-5R5 appears limited or unclear, indicating that iron may not be a critical factor for BHET metabolism under these conditions.

Based on the above-made observations, we further asked if iron availability resulted in major transcriptional changes and if PET94 were affected by iron. To address these questions, we performed transcriptome analysis of the strain UHH-Hm9b growing on BHET 1mM supplemented with and without iron 1mM, with the goal to obtain an insight into the global gene expression pattern of this strain in response to iron. Analysis was conducted in 3 biological triplicates. Obtained reads were mapped against the established genome sequence of UHH-Hm9b which is available under accession numbers 294450 at IMG/IMGER. Figure 24 shows the bar chart of differently expressed genes under different conditions, highlighting the upregulation and downregulation of genes in UHH-Hm9b. Figure 25 provides a summary of top highly expressed genes under the stated conditions.

Iron has no effect on the expression of PET94 under tested condition

When we compared iron-supplemented BHET medium control, expression of PET94 was almost no detectable at 1 mM BHET and iron (only 6-7 transcribed genes). The expression level of this PET94 gene which is related to PET degradation was not upregulated (log_2=0.2, adjusted p value >0.05) in iron-supplemented BHET medium

compared to the control. For this transcriptome data set iron had no impact on the level of PET94 gene expression. This observation is not in line with the slow degradation of the BHET/polymer in biofilm cultures and as described in the observation above (Figure 22 and 23). In summary the data implies that PET94 gene expression is not activated by 1mM iron and 1mM BHET supplementation. This does not support the previous hypothesis that iron supplementation modulates gene expression related to both iron acquisition and potential PET degradation pathways.

Iron supplementation (1 mM) had the most pronounced effects on the overall gene expression levels in UHH-Hm9b with >63 upregulated and >33 downregulated genes compared to the controls (without iron). Top 5 upregulated genes (log2-fold ≥ 2) were detected for Tryptophan 2%2C3-dioxygenase, Iron-sulfur cluster repair protein YtfE, Quinolinate synthase A, HTH-type transcriptional regulator IscR and L-aspartate oxidase (Figure 24). These genes were significantly up-regulated in iron-supplemented samples compared to the control.

RNA-seq analysis also revealed differential expression of top 30 highly expressed genes as illustrated in Figure 25**.** This figure presents a comparative analysis of gene expression levels of the top-expressed genes under two experimental conditions: one with iron and the other without iron, in a bacterial culture incubated with BHET (bis(2-hydroxyethyl) terephthalate), an intermediate compound in PET plastic degradation. We noticed that in this experiment there were notable transcriptional changes in response to iron availability. Several genes were found to be among the most highly transcribed across both conditions, including *long-chain aldehyde dehydrogenase, chaperone protein DnaK, glutamate dehydrogenase, catalase peroxidase and negative regulator of genetic competence ClpC/MecB, RNA polymerase sigma factor SigA*. Notably, these gene exhibited higher expression levels under the iron-depleted

condition compared to the iron-supplemented treatments (p-value <0.05), indicating their potential role in stress adaptation and metabolic alterations when iron is limited.

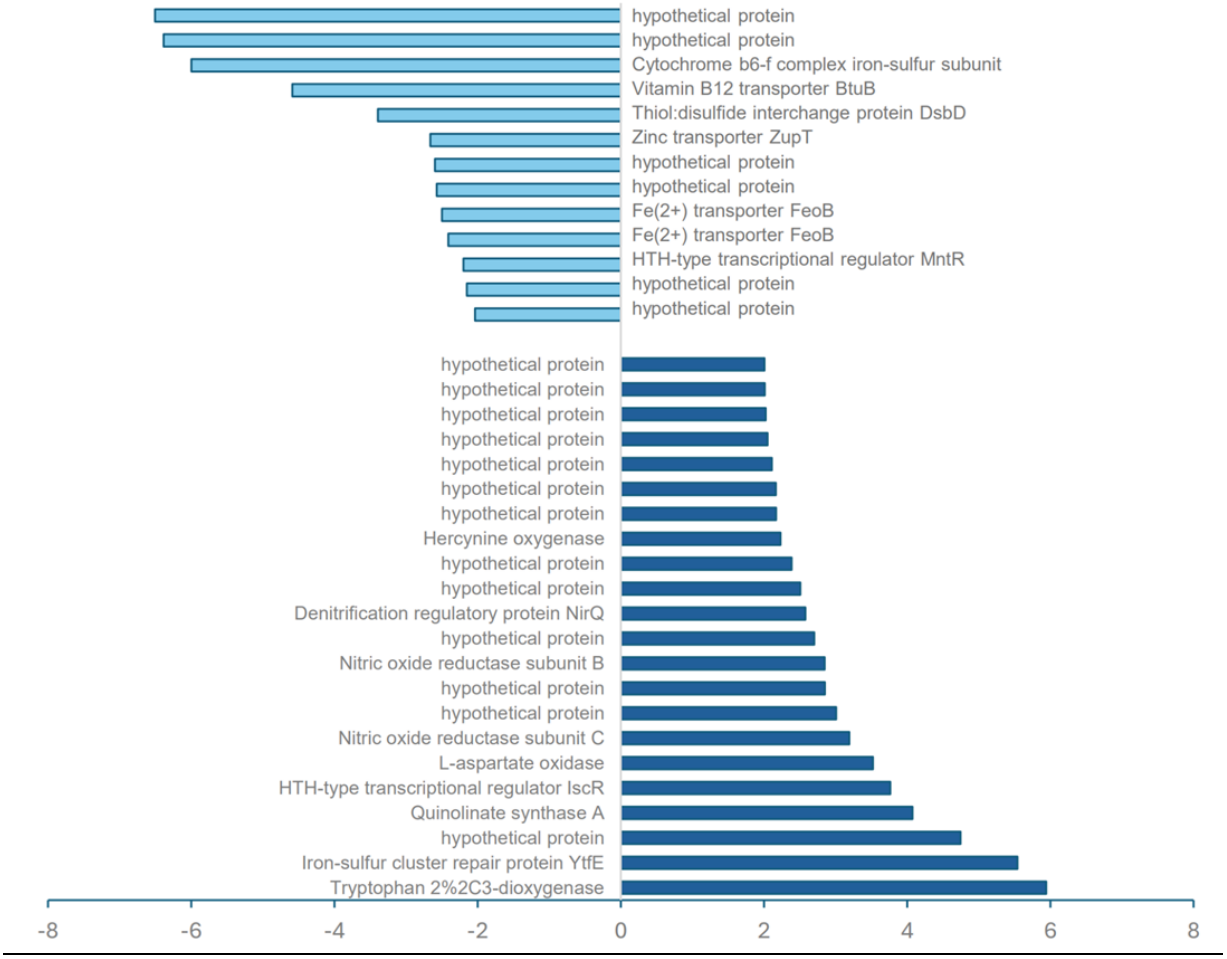

Figure 24. Up- and down-regulated genes with log2 > 2. Differentially up-regulated genes are represented by dark blue colors; pale blue colors are down-regulated genes.

Conversely, transcription of 8-amino-7-oxononanoate synthase was higher under iron-supplemented condition (Figure 25). This gene is involved in biotin biosynthesis, and its increased transcription in the presence of iron suggests an iron-responsive regulatory mechanism, suggesting that iron availability may influence general metabolism and cofactor biosynthesis through an iron responsive regulatory mechanism

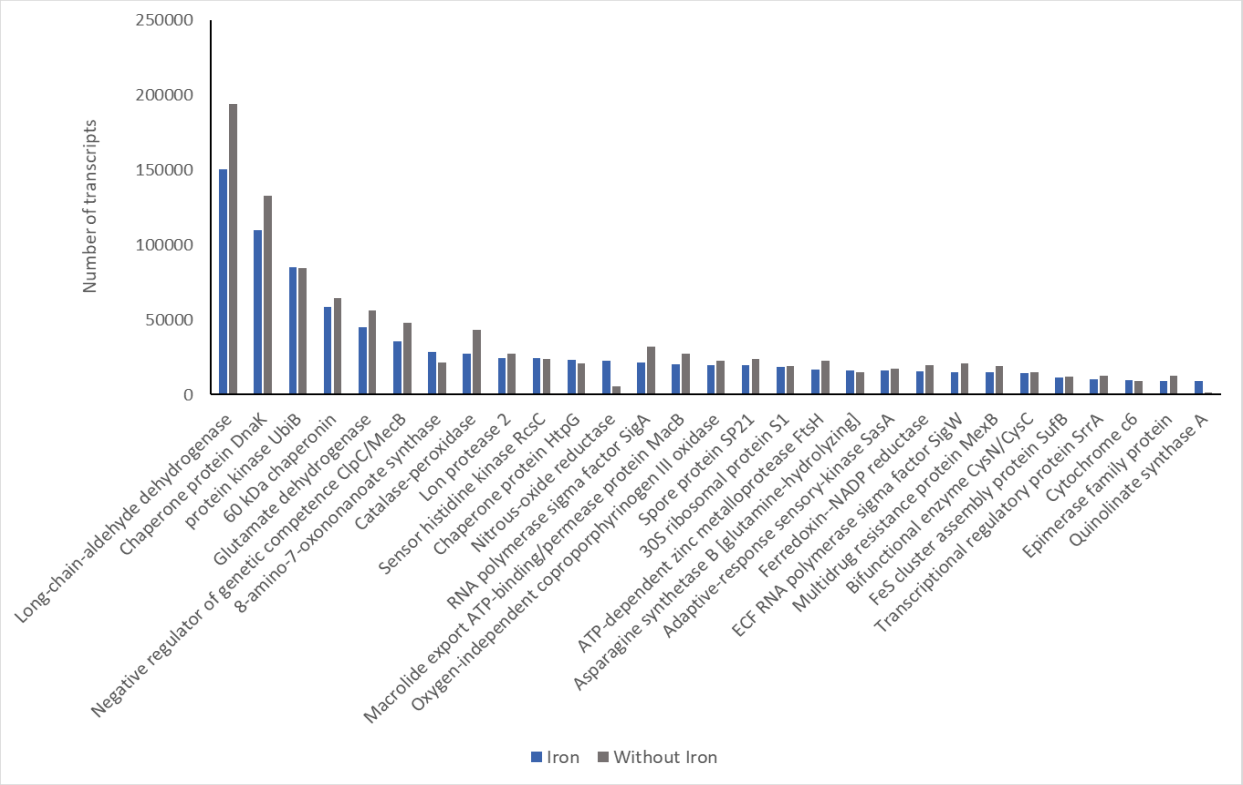

Figure 25. Top 30 expressed genes in iron-supplemented medium (Iron) compared to the control (without Iron)

.

4. DISCUSSION

4 DISCUSSION

Although PET has been accumulating in the oceans over the past decades, we still have a limited understanding of and to which extent this polymer can be degraded by microorganisms. We report here on the isolation of two marine bacteroidetal strains, *Arenibacter palladensis* UHH-Hm9b and *Maribacter dokdonensis* UHH-5R5, forming biofilms on PET foil and releasing µM amounts of terephthalic acid. Our research further shows that these strains harbor the potential for PET degradation using dienelactone hydrolases (DLHs, EC 3.1.1.45), providing the first bacterial DLHs involved in PET degradation. The widespread distribution of these microorganisms and the notion that these enzymes are secreted may imply a possible role in marine PET remediation.

4.1 Novel PET-degrading Bacteroidota from environmental samples

A recent study revealed that plastics from deep-sea in the Southwest Atlantic harbor core microbial communities with potential plastic-degrading capabilities (Agostini et al., 2021). Such abilities are likely to be as a result of their prolonged exposure of marine microorganisms to plastics and microplastics in the oceans (Eriksen et al., 2014). The phylum Bacteroidota has recently been predicted as an underexplored reservoir of PET-degrading enzymes, especially in marine environment (Danso et al., 2018). However, to date, most studies on Bacteroidota have focused on describing new species (Bakunina et al., 2013; Zhan et al., 2017) and sequencing their genome (Gutierrez et al., 2016; Wolter et al., 2021a; Zhan et al., 2017).

With this phylum, two genera Maribacter and Arenibacter are commonly found in marine sediments, coastal environments, and algae-associated habitats (Alejandre-Colomo et al., 2021; Avcı et al., 2020; Khan et al., 2020; López-Sánchez et al., 2024)

Lu et al., 2023; Sun et al., 2025), where they contribute in the marine carbon cycle by breaking down complex polysaccharides (Bakunina et al., 2013; Gao et al., 2023; Kalenborn et al., 2024; Wolter et al., 2021b). Further, to our knowledge, only small number of enzymes from the genus Maribacter and Arenibacter have been specifically characterized, primarily for their ability to degrade polysaccharides (Lee et al., 2016; Lu et al., 2022).

Notably, both genera have recently been detected in the plastisphere (Du et al., 2022; Marques et al., 2023). PET provides a surface for attachment, colonization and biofilm formation by marine bacteria, and can be served as a carbon source for PET-degrading bacteria (Guo et al., 2023). Studies using different plastic debris (PE, PET, PS and PP) consistently reported Bacteroidota as a dominant colonizers in these plastic biofilms (Debroas et al., 2017; Delacuvellerie et al., 2019; Jiang et al., 2018). Colonization process typically begins with Grammaproteobacteria and Alphaproteobacteria and then transition to more diverse microbial communities with Bacteroidota as the biofilm matures (Lee et al., 2008; Pinto et al., 2019). While it is well-known that bacteria in the plastisphere usually form biofilms on micro- or nanoparticles, it is commonly accepted that they mostly do not degrade the polymer (Linda A. Amaral-Zettler et al., 2020; Chow et al., 2023; Qian et al., 2024; Vaksmaa, Hernando-Morales, et al., 2021). However, it is assumed that they do primarily feed on the additives contained in the polymers and /or simply use the surface to attach and form biofilms (Chow et al., 2023; Robyn J Wright et al., 2020; Yang et al., 2020).

Although Bacteroidota remain abundant and ecologically important members, PET-active enzymes from this phylum remain underexplored compared to those from Actinobacteria and Proteobacteria (Dominik Danso et al., 2019; Danso et al., 2018). Recently, the first two promiscuous and cold-active enzymes PET27 (*Aequorivita* sp.)

and PET30 (*Kaistella jeonii)* were shown to act on polycaprolactone (PCL), PET, and Impranil ® DLN (Zhang et al., 2022).

To expand this diversity, we did initial screening of 19 marine Bacteroidota isolates. Two strains, *Arenibacter palladensis* UHH-Hm9b and *Maribacter dokdonensis* UHH-5R5, were demonstrated to degrade PET model substrates, formed biofilms on PET foil and released µM amounts of terephthalic acid. From these, we identified two new PET-active enzymes, PET93 and PET94, complementing the first two enzymes PET27 and PET30 previously reported (Zhang et al., 2022). Despite their low activities toward PET, we hypothesize that the intrinsic promiscuity of hydrolase enzymes enables these strains to recognize and facilitate the acceptance of an unnatural substrate such as PET plastic in marine environments, where rising levels of plastics and microplastics continuously shape microbial interactions with synthetic polymers. This supports the view that Bacteroidota has evolved the ability to degrade PET and verifies the prediction that this trait may be widespread within the phylum (Danso et al., 2018).

Within the phylum, Flavobacteria are the second most abundant group on plastic surfaces and colonizing various polymers (PE, PS, PP and PET) and showing higher abundance on PET and PS than on natural substrates (Oberbeckmann et al., 2018; Oberbeckmann et al., 2016). Our strains UHH-5R5 and UHH-Hm9b attached to and slowly metabolized PET, potentially overtime contributing to reducing the spread of nano- and micro-plastics in marine environment. In addition, biofilms are known to negatively affect surface of microplastics through additives degradation, enzymatic modification and metabolic byproducts (Ahmad et al., 2020; Sharma et al., 2025).

4.2 Bacteroidota harbor the first dienelactone hydrolases acting on PET

Genomic DNA from Bacteroidota isolates were sequenced using the Illumina HiSeq Next Generation Sequencing system. The raw sequence data were assessed for quality prior to genome assembly and annotation. The genome of two isolates UHH-

5R5 and UHH-Hm9b were subsequently mined for genes encoding potential PET polyesterase using hidden Markov models (HMMs) based on reference PETase-like domains. Two candidate genes, PET93 and PET94, were identified in strains UHH-5R5 and UHH-Hm9b, respectively. These genes were selected as the promising candidate for PET-degrading activity and for further investigation.

To assess the activity of the predicted PET-degrading enzymes, the candidate genes were cloned into an expression vector and transformed into *E. coli* BL21 (DE3) for heterogeneous expression. The purified proteins were used for initial functional tests. The expression of PET94 gene was initially hindered due to its native N-terminal signal peptide. Removing this sequence enabled detectable enzyme activity, suggesting that this signal peptide interferes with expression, folding, or stability in the heterologous host. (Jomrit et al., 2023). The peptide may cause mis localization, stress, or degradation and might not function effectively in the recombinant system, hindering proper transcription or translation (Gao et al., 2024; Kaushik et al., 2022).

The obtained biochemical characteristics revealed that both enzymes preferentially hydrolyze a spectrum of *p*NP substrates with a medium carbon chain length (C6-C10). Similar substrate preferences also reported for other PET-active enzymes such as PET2, PET27, PET30 and PET40 (Danso et al., 2018; Gao et al., 2024; Zhang et al., 2022). To further verify their hydrolytic activity against PET, the purified enzymes were incubated with PET powder or foil under defined conditions, and the resulting degradation products were analysed using UHPLC. However, detecting clear PET-degrading activity was challenging because UHPLC method can only detect above 1 µM degradation products (Dierkes et al., 2023; Sintawee Sulaiman et al., 2012; Yoshida et al., 2016). However, it is still notable that the UV-treated PET substrates yielded detectable degradation products.

To further confirm the enzymatic activity on PET, an alternative approach using ReporTPA_UHH04 was investigated (Dierkes et al., 2023). By combining these approaches, we confirmed that PET93 and PET94 can degrade PET and releasing TPA monomer as the degradation product, but only at nanomole concentrations. Quantification of TPA, however, was not feasible using this reporter strain system (Dierkes et al., 2023).

To date, the PET-degrading enzymes that have been identified are typically cutinases (EC 3.1.1.74), lipases (EC 3.1.1.3) and carboxylesterases (EC 3.1.1.1). Although various microbes and PET degrading enzymes have already been reported, the diversity of bacteria with PET degradation, especially in the ocean, still needs to be discovered. The newly discovered enzymes PET93 and PET94 in this study are both promiscuous DLHs (E.C. 3.1.1.45). PET only emerged as an environmental contaminant in recent decades, so it is likely not to be a native or preferred substrate for these hydrolase enzymes. While the native substrate of both enzymes remains currently unknown, our data showed a significant but slow turnover of PET (Figure 3 and 6). Here we reported the first two Dienelactone hydrolases from the phylum Bacteriodota PET93 and PET94 showing activity towards PET and are affiliated with *Maribacter dokdonensis* and *Arenibacter palladensis*, respectively.

Although the efficiency of these *Maribacter* sp. and *Arenibacter sp.* towards PET degradation do not yet meet the level of industrial application, their ecological significance should not be underestimated as they were discovered in the marine environment, a major accumulation zones for plastic waste. Importantly, PET-degrading genes derived from these Bacteroitota species are distributed across diverse regions worldwide, suggesting that these microbes may play an important but not yet fully understood role in natural bioremediation of marine plastic pollution.

4.3 Unexpectedly wide range of PET-active promiscuous enzymes from Flavobacteria

High molecular weight polymers like PET are too large for intracellular enzymes to access directly, bacteria typically secrete PET-degrading enzymes into their surroundings where they can act on these large substrates (Son et al., 2019; Taniguchi et al., 2019; Yoshida et al., 2016). Genome sequencing and functional analyses identified two DLHs designated PET93 and PET94 involved in PET degradation. The presented N-terminal signal peptide suggested that both enzymes are secreted proteins, as identified with all known active enzymes to date (Chow et al., 2023). While their predicted active sites and substrates binding pockets were identical to previously published PETases *Is*PETase and LCC, both enzymes differed largely in their structural features from known PETases and represent novel scaffolds. While the residues of the substrate active and binding sites are conserved in those PET-degrading enzymes, the enzymatic activities of PET93 and PET94 towards PET is much lower than that of the other mentioned PETases. This implies that the enzymatic activity towards polymers depends on a combination of different factors, such as surface hydrophobicity, position and accessibility of key residues, rather than only individual amino acids in the active site and binding pocket (Zhang et al., 2022).

Further they differed from the binding sites and lacked the typical porC-domain of the known PETases from the Flavobacteria (Zhang et al., 2022). Compared with these two bacteroidetal-PET esterases, PET93 and PET94 have several distinct characteristics. First, although type IX secretion system (T9SS) has been so far described as a Bacteroidota - specific secretion system and has been identified to play an important role in the transport of secreted enzymes (de Diego et al., 2016; Desvaux et al., 2009; Keiko et al., 2010; McBride, 2019), here PET93 and PET94 appeared to be secreted by the Sec/SPI system. The difference was observed for PET27 and PET30 which

showed a T9SS/PorC-like motif at the C-terminus (Zhang et al., 2022). Secondly, although they all belong to Bacteroidota phylum, PET93 and PET94 are present in the phylogenetic tree on a branch quite far away from PET27, PET30 and from other well-characterized enzymes. The phylogenetic analysis demonstrated that PET93 and PET94 originated from *Maribacter dokdonensis* UHH-5R5 and *Arenibacter palladensis* UHH-Hm9b genus of the Bacteroidota phylum, respectively, do not grouped within the subcluster with previously characterized PET-active enzymes as well as other enzymes from Bacteroidota. These findings suggests that Bacteroidota harbors a distinct class of PET-degrading enzymes that may contribute to environmental PET degradation.

Notably, homologs of bacteroidetal enzymes PET93 and PET94 were found globally in genome data sets covering a wide range of climate zones (Figure 4). It is likely due to the ability of Bacteroidota to decompose a wide range of biopolymers, including cellulose, algal polysaccharide (e.g. laminarin, alginate, xylan) and other complex carbohydrates (Dutschei et al., 2023; Kabisch et al., 2014; Tang et al., 2017). Similar to other Bacteroidotal-enzymes PET27 and PET30 (Zhang et al., 2022), our enzymes demonstrated PET-hydrolyzing activity even at 4°C, suggesting a potential role in slow, long-term degradation of PET microparticles in cold environments. While these data do not prove that PET93 and PET94 are active in nature, it is likely that they are secreted and will be involved in enzymatic PET degradation. Recently we showed that in *Vibrio gazogenes* a PETase (PET6) was expressed constitutively at a low but significant level under various growth conditions (Preuß et al., 2025). Assuming that in Maribacter and Arenibacter similar regulatory pathways may exist, it is likely that PET93 and 94 are also expressed at low levels under biofilm and planktonic growth conditions. Homologs of PET-degrading enzymes are found across diverse climates, likely due to the ability of Bacteroidota to decompose a range of biopolymers, including

cellulose, polysaccharide and algal cell walls (Thomas et al., 2011; Foley et al., 2016; Church, 2008).

Although the catalytic efficiency of PET93 and PET94 towards PET do not meet the level of industrial applications, their ecological significance should not be underestimated as they are derived from globally occurring microorganisms. Their global presence highlights that these microbes may play an important but not yet fully understood role in natural bioremediation of marine plastic pollution. Thus, future work will have to exploit the role of the secreted DLHs PET93 and PET94 in their native environment.

4.4 Iron as a potential regulatory factor in PET degradation pathway?

Genome analysis of UHH-Hm9b strains revealed a regulatory element *Fur-like Transcriptional regulator* located adjacent to the PET94 gene (Figure 10), suggesting that iron availability could modulate PET94 expression. Indeed, our study demonstrated that iron supplementation enhanced BHET degradation in UHH-Hm9b strain, as evidenced by larger halo formation in plate assays and a 9-fold increase in MHET release in liquid cultures. However, transcriptome analysis showed extremely low PET94 expression in both iron-supplemented and control conditions.

The results suggest that iron may enhance polyesterase activity in UHH-Hm9b primarily through post-transcriptional or post-translational mechanisms, such as iron functioning as a cofactor, stabilizing the enzyme structure, improving folding, or enhancing secretion and translation efficiency, rather than direct transcriptional regulation. Similar post-transcriptional effects have been reported for oxidative enzymes such as catalases and peroxidases, where iron influences enzyme maturation, stability, and catalytic efficiency without necessarily altering gene expression. (Galaris et al., 2019; Lei et al., 2016; Rouault & Klausner, 1996).

In addition, substrate concentration may also play a critical role in gene regulation. The BHET concentration used for RNA-seq (1mM) was considerably lower than the 10mM applied in the degradation assay, likely providing insufficient metabolic pressure to trigger strong transcriptional response of PET94. Transcriptomic regulation is often dose-dependent, and previous study has shown that increasing BHET concentrations modulate transcriptional regulation through interconnected regulatory pathways, including quorum sensing (QS), the cAMP-CRP system, and c-di-GMP signaling, with significantly upregulation of polyesterase-related genes only at higher substrate levels. For example, expression of *pet6* gene is markedly lower at 0.5 mM BHET compared to higher concentrations (Preuss et al.).

Finally, the absence of PET94 expression in our RNA-seq analysis raises the possibility that other, as yet uncharacterized, genes in UHH-Hm9b genome could contribute to BHET degradation. These enzymes may be annotated as “hypothetical proteins” which are not yet experimentally characterized and may encode for BHETases. Future studies should prioritize the cloning and expression of candidate upregulated hypothetical proteins identified in this dataset, as well as proteomic analyses, to uncover and characterize these alternative polyesterases.

4.5 Considerations and future perspectives

Despite the successful isolation of different Bacteroidetes strains from marine environment and characterization of two novel strains capable of forming biofilms on PET and expressing putative-PET degrading enzymes, we cannot exclude some limitations of this study.

Firstly, we have only small sample size, only 9 novel Bacteroidota strains were sent for whole genome sequencing and only two isolates were deeply analysed so far. Although the other strains were not chosen for further investigation, it does not mean

that they do not habor putative PET-degrading enzymes. Secondly, the degradation assays were conducted using PET foil under laboratory conditions, however in marine environment there are many different factors that might affect to the degradation process remains unknown. Thirdly, the transcriptomic data are just preliminary results. We aimed to investigate the effect of iron supplementation on PET-degrading gene expression. However, the transcriptomic data did not show clear induction of PET-related genes under tested condition. To better understand this potential regulation, further transcriptomic experiments should be conducted using broader range of iron and BHET concentrations. Also, to gain a deeper understanding of the iron regulatory mechanism involved in PET degradation, future work should include experiments to test whether *Fur-like Transcriptional regulator* binds directly to the PET94 promoter (e.g. electrophoretic mobility shift assay or chromatin immunoprecipitation), and transcriptomics under a broader range of iron and substrate concentrations to determine whether the gene becomes inducible. Such studies may reconcile why PET94 shows no/low mRNA expression yet measurable PET-degrading activity when iron is supplemented.

Finally, potential PET degradation in the natural environment is likely carried out by microbial consortia rather than individual strains. Biofilms on PET surfaces are typically composed of multi species communities, and the specific role of Bacteroidota within such natural consortia was not fully explored in this study. Understanding the interactions and contributions of Bacteroidota in a multi-species context will be critical for accessing their ecological relevance in PET degradation.

5. CONCLUSION

5 CONCLUSION

Dienelactone hydrolase (DLHs) have not previously been recognized as common or well-established enzyme for PET degradation. This study reported the first DLHs from Bacteroidota and expanded our knowdege of the biodiversity of PET-degrading enzymes by identifying and characterizing two novel enzymes, PET93 and PET94. The occurrence of homologs of these PET-active enzymes across diverse climate zones helps to understand the ecological role of the Bacteroidota in the degradation of marine PET nanoparticles. These enzymes were discovered through genome mining of a genena *Maribacter* sp. and *Arenibacter sp.*, sampled from marine aquaculture in Büsum, Germany, and exhibit low but measurable activity on PET.

Given that synthetic plastics like PET have only existed for a few decades, it is unlikely that many microorganisms evolved enzymes specifically to degrade them. This suggests that PET93 and PET94 may not have evolved for PET degradation as their primary function but instead accidentally interact with this synthetic polymer as a side reaction of their natural function. PET40 is an example of such an enzyme, which exhibits hydrolytic activity towards various substrates and revealing its promiscuous nature (Zhang et al., 2024).

Here *Maribacter sp*. and *Arenibacter sp.* show their ability to form biofilms on plastics surface and release detectable degradation products. The corresponding enzymes were successfully expressed in *E. coli*, and their hydrolytic activity was confirmed against a broad range of substrates which were reinforced through molecular docking experiments. Microscopic analysis showed that these Bacteroidota strains are able to colonize surfaces of PET films within a few days. However, the exact mechanisms underlying this microbial attachment to PET remain poorly understood and should be further investigated.

A visual comparison of halo formation on indicator plates revealed distinct differences between iron-supplemented and iron-free conditions, with larger halos observed in the presence of iron for strain UHH-Hm9b. UHPLC analysis supported these observations, which showed that after 3 days of incubation, MHET concentration increased approximately 9-fold in UHH-Hm9b cultures supplemented with 0.5 mM and 1 mM iron compared to iron-free controls. Interestingly, transcriptome analysis revealed that PET94 gene was not expressed under the tested condition. This suggests that the iron concentrations were likely below the threshold required for transcriptional activation. Further the observed enhancement is probably due to posttranslational effects, such as cofactor binding or altered enzyme stability, rather than increased transcription.

Although the efficiency of these genena *Maribacter* sp. and *Arenibacter sp.* towards PET degradation may not reach the level for industrial application, these bacterial species however may nonetheless play an important role in the natural bioremediation of marine plastic pollution. Future work will have to explore the role of the secreted DLHs PET93 and PET94 in their native environment.

6. REFERENCES

6 REFERENCES

Agostini, L., Moreira, J. C. F., Bendia, A. G., Kmit, M. C. P., Waters, L. G., Santana, M. F. M., Sumida, P. Y. G., Turra, A., & Pellizari, V. H. (2021). Deep-sea plastisphere: Long-term colonization by plastic-associated bacterial and archaeal communities in the Southwest Atlantic Ocean. *Science of The Total Environment*, *793*, 148335.

Ahmad, M., Li, J.-L., Wang, P.-D., Hozzein, W. N., & Li, W.-J. (2020). Environmental perspectives of microplastic pollution in the aquatic environment: a review. *Marine Life Science & Technology*, *2*(4), 414-430.

Alejandre-Colomo, C., Francis, B., Viver, T., Harder, J., Fuchs, B. M., Rossello-Mora, R., & Amann, R. (2021). Cultivable Winogradskyella species are genomically distinct from the sympatric abundant candidate species. *ISME Communications*, *1*(1).

Almagro Armenteros, J. J., Tsirigos, K. D., Sønderby, C. K., Petersen, T. N., Winther, O., Brunak, S., von Heijne, G., & Nielsen, H. (2019). SignalP 5.0 improves signal peptide predictions using deep neural networks. *Nature Biotechnology*, *37*(4), 420-423.

Alonso, C., Warnecke, F., Amann, R., & Pernthaler, J. (2007). High local and global diversity of Flavobacteria in marine plankton. *Environmental Microbiololy*, *9*(5), 1253-1266.

Amaral-Zettler, L. A., Zettler, E. R., & Mincer, T. J. (2020). Ecology of the plastisphere. *Nature Reviews Microbiology*, *18*(3), 139-151.

ASEZ. (2024). *Plastic Smog*. Retrieved July 4 from https://asez.org/plastic-smog/

Avcı, B., Krüger, K., Fuchs, B. M., Teeling, H., & Amann, R. I. (2020). Polysaccharide niche partitioning of distinct Polaribacter clades during North Sea spring algal blooms. *Isme j*, *14*(6), 1369-1383.

Bakunina, I., Nedashkovskaya, O., Balabanova, L., Zvyagintseva, T., Rasskasov, V., & Mikhailov, V. (2013). Comparative analysis of glycoside hydrolases activities from phylogenetically diverse marine bacteria of the genus Arenibacter. *Marine Drugs*, *11*(6), 1977-1998.

Bankevich, A., Nurk, S., Antipov, D., Gurevich, A. A., Dvorkin, M., Kulikov, A. S., Lesin, V. M., Nikolenko, S. I., Pham, S., Prjibelski, A. D., Pyshkin, A. V., Sirotkin, A. V., Vyahhi, N., Tesler, G., Alekseyev, M. A., & Pevzner, P. A. (2012). SPAdes: a new genome assembly algorithm and its applications to single-cell sequencing. *Journal of Computional Biology*, *19*(5), 455-477.

Bell, E. L., Smithson, R., Kilbride, S., Foster, J., Hardy, F. J., Ramachandran, S., Tedstone, A. A., Haigh, S. J., Garforth, A. A., Day, P. J. R., Levy, C., Shaver, M. P., & Green, A. P. (2022). Directed evolution of an efficient and thermostable PET depolymerase. *Nature Catalysis*, *5*(8), 673-681.

Berman, H. M., Westbrook, J., Feng, Z., Gilliland, G., Bhat, T. N., Weissig, H., Shindyalov, I. N., & Bourne, P. E. (2000). The Protein Data Bank. *Nucleic Acids Research*, *28*(1), 235-242.

Bertani, G. (1951). Studies on lysogenesis. I. The mode of phage liberation by lysogenic Escherichia coli. *Journal of Bacteriology*, *62*(3), 293-300.

Biundo, A., Ribitsch, D., & Guebitz, G. M. (2018). Surface engineering of polyester-degrading enzymes to improve efficiency and tune specificity. *Applied Microbiology and Biotechnology*, *102*(8), 3551-3559.

Bollinger, A., Thies, S., Knieps-Grünhagen, E., Gertzen, C., Kobus, S., Höppner, A., Ferrer, M., Gohlke, H., Smits, S. H. J., & Jaeger, K.-E. (2020). A Novel Polyester Hydrolase

From the Marine Bacterium Pseudomonas aestusnigri – Structural and Functional Insights [Original Research]. *Frontiers in Microbiology*, *Volume 11 - 2020*.

Bornscheuer, U. T. (2016). Feeding on plastic. *Science*, *351*(6278), 1154-1155.

Buchholz, P. C. F., Feuerriegel, G., Zhang, H., Perez-Garcia, P., Nover, L. L., Chow, J., Streit, W. R., & Pleiss, J. (2022). Plastics degradation by hydrolytic enzymes: The plastics-active enzymes database-PAZy. *Proteins*, *90*(7), 1443-1456.

Campanale, C., Massarelli, C., Savino, I., Locaputo, V., & Uricchio, V. F. (2020). A Detailed Review Study on Potential Effects of Microplastics and Additives of Concern on Human Health. *International Journal of Environmental Research and Public Health*, *17*(4), 1212.

Carniel, A., Valoni, É., Nicomedes, J., Gomes, A. d. C., & Castro, A. M. d. (2017). Lipase from Candida antarctica (CALB) and cutinase from Humicola insolens act synergistically for PET hydrolysis to terephthalic acid. *Process Biochemistry*, *59*, 84-90.

Carr, C. M., Clarke, D. J., & Dobson, A. D. W. (2020). Microbial Polyethylene Terephthalate Hydrolases: Current and Future Perspectives [Review]. *Frontiers in Microbiology*, *Volume 11 - 2020*.

Carr, C. M., Keller, M. B., Paul, B., Schubert, S. W., Clausen, K. S. R., Jensen, K., Clarke, D. J., Westh, P., & Dobson, A. D. W. (2023). Purification and biochemical characterization of SM14est, a PET-hydrolyzing enzyme from the marine sponge-derived Streptomyces sp. SM14 [Original Research]. *Frontiers in Microbiology*, *Volume 14 - 2023*.

Chen, H. L., Selvam, S. B., Ting, K. N., & Gibbins, C. N. (2021). Microplastic pollution in freshwater systems in Southeast Asia: contamination levels, sources, and ecological impacts. *Environmental Science and Pollution Research*, *28*(39), 54222-54237.

Chen, I.-M. A., Chu, K., Palaniappan, K., Ratner, A., Huang, J., Huntemann, M., Hajek, P., Ritter, Stephan J., Webb, C., Wu, D., Varghese, Neha J., Reddy, T. B. K., Mukherjee, S., Ovchinnikova, G., Nolan, M., Seshadri, R., Roux, S., Visel, A., Woyke, T.,…Ivanova, Natalia N. (2022). The IMG/M data management and analysis system v.7: content updates and new features. *Nucleic Acids Research*, *51*(D1), D723-D732.

Chiappone, M., Dienes, H., Swanson, D. W., & Miller, S. L. (2005). Impacts of lost fishing gear on coral reef sessile invertebrates in the Florida Keys National Marine Sanctuary. *Biological Conservation*, *121*(2), 221-230.

Chow, J., Perez-Garcia, P., Dierkes, R., & Streit, W. R. (2023). Microbial enzymes will offer limited solutions to the global plastic pollution crisis. *Microbial Biotechnology*, *16*(2), 195-217.

Cózar, A., Echevarría, F., González-Gordillo, J. I., Irigoien, X., Úbeda, B., Hernández-León, S., Palma, Á. T., Navarro, S., García-de-Lomas, J., Ruiz, A., Fernández-de-Puelles, M. L., & Duarte, C. M. (2014). Plastic debris in the open ocean. *Proceedings of the National Academy of Sciences*, *111*(28), 10239-10244.

Cui, Y., Chen, Y., Liu, X., Dong, S., Tian, Y. e., Qiao, Y., Mitra, R., Han, J., Li, C., Han, X., Liu, W., Chen, Q., Wei, W., Wang, X., Du, W., Tang, S., Xiang, H., Liu, H., Liang, Y.,…Wu, B. (2021). Computational Redesign of a PETase for Plastic Biodegradation under Ambient Condition by the GRAPE Strategy. *ACS Catalysis*, *11*(3), 1340-1350.

Danso, D., Chow, J., & Streit, W. R. (2019). Plastics: Environmental and Biotechnological Perspectives on Microbial Degradation. *Applied and Environmental Microbiology*, *85*(19), e01095-01019.

Danso, D., Schmeisser, C., Chow, J., Zimmermann, W., Wei, R., Leggewie, C., Li, X., Hazen, T., & Streit, W. R. (2018). New Insights into the Function and Global Distribution of Polyethylene Terephthalate (PET)-Degrading Bacteria and Enzymes in Marine and

Terrestrial Metagenomes. *Applied and Environmental Microbiology*, *84*(8), e02773-02717.

De Diego, I., Ksiazek, M., Mizgalska, D., Koneru, L., Golik, P., Szmigielski, B., Nowak, M., Nowakowska, Z., Potempa, B., Houston, J. A., Enghild, J. J., Thøgersen, I. B., Gao, J., Kwan, A. H., Trewhella, J., Dubin, G., Gomis-Rüth, F. X., Nguyen, K.-A., & Potempa, J. (2016). The outer-membrane export signal of Porphyromonas gingivalis type IX secretion system (T9SS) is a conserved C-terminal β-sandwich domain. *Scientific Reports*, *6*(1), 23123.

Debroas, D., Mone, A., & Ter Halle, A. (2017). Plastics in the North Atlantic garbage patch: A boat-microbe for hitchhikers and plastic degraders. *Science of The Total Environment*, *599-600*, 1222-1232.

Delacuvellerie, A., Cyriaque, V., Gobert, S., Benali, S., & Wattiez, R. (2019). The plastisphere in marine ecosystem hosts potential specific microbial degraders including Alcanivorax borkumensis as a key player for the low-density polyethylene degradation. *Journal of Hazardous Materials*, *380*, 120899.

Desvaux, M., Hébraud, M., Talon, R., & Henderson, I. R. (2009). Outer membrane translocation: numerical protein secretion nomenclature in question in mycobacteria. *Trends in Microbiology*, *17*(8), 338-340.

Dharmaraj, S. (2010). Marine Streptomyces as a novel source of bioactive substances. *World Journal of Microbiology and Biotechnology*, *26*(12), 2123-2139. =

Dierkes, R. F., Wypych, A., Pérez-García, P., Danso, D., Chow, J., & Streit, W. R. (2023). An Ultra-Sensitive Comamonas thiooxidans Biosensor for the Rapid Detection of Enzymatic Polyethylene Terephthalate (PET) Degradation. *Applied and Environmental Microbiology*, *89*(1), e01603-01622.

Dierkes Robert, F., Wypych, A., Pérez-García, P., Danso, D., Chow, J., & Streit Wolfgang, R. (2022). An Ultra-Sensitive Comamonas thiooxidans Biosensor for the Rapid Detection of Enzymatic Polyethylene Terephthalate (PET) Degradation. *Applied and Environmental Microbiology*, *89*(1), e01603-01622.

Dodd, D., Mackie, R. I., & Cann, I. K. (2011). Xylan degradation, a metabolic property shared by rumen and human colonic Bacteroidetes. *Molecular Microbiology*, *79*(2), 292-304.

Du, Y., Liu, X., Dong, X., & Yin, Z. (2022). A review on marine plastisphere: biodiversity, formation, and role in degradation. *Computational and Structural Biotechnology Journal*, *20*, 975-988.

Dudek, K. L., Cruz, B. N., Polidoro, B., & Neuer, S. (2020). Microbial colonization of microplastics in the Caribbean Sea. *Limnology and Oceanography Letters*, *5*(1), 5-17.

Dutschei, T., Beidler, I., Bartosik, D., Seeßelberg, J.-M., Teune, M., Bäumgen, M., Ferreira, S. Q., Heldmann, J., Nagel, F., Krull, J., Berndt, L., Methling, K., Hein, M., Becher, D., Langer, P., Delcea, M., Lalk, M., Lammers, M., Höhne, M.,…Bornscheuer, U. T. (2023). Marine Bacteroidetes enzymatically digest xylans from terrestrial plants. *Environmental Microbiology*, *25*(9), 1713-1727.

Enache, A. C., Grecu, I., & Samoila, P. (2024). Polyethylene Terephthalate (PET) Recycled by Catalytic Glycolysis: A Bridge toward Circular Economy Principles. *Materials (Basel)*, *17*(12).

Enyoh, C. E., Verla, A. W., Verla, E. N., Ibe, F. C., & Amaobi, C. E. (2019). Airborne microplastics: a review study on method for analysis, occurrence, movement and risks. *Environmental Monitoring and Assessment*, *191*(11), 668.

Eriksen, M., Lebreton, L. C. M., Carson, H. S., Thiel, M., Moore, C. J., Borerro, J. C., Galgani, F., Ryan, P. G., & Reisser, J. (2014). Plastic Pollution in the World's Oceans: More than

5 Trillion Plastic Pieces Weighing over 250,000 Tons Afloat at Sea. *PLOS ONE*, *9*(12), e111913.

Fagerburg, D. R., & Clauberg, H. (2004). Photodegradation of Poly(Ethylene Terephthalate) and Poly(Ethylene/1,4-Cyclohexylenedimethylene Terephthalate). In *Modern Polyesters: Chemistry and Technology of Polyesters and Copolyesters* (pp. 609-641).

Fecker, T., Galaz-Davison, P., Engelberger, F., Narui, Y., Sotomayor, M., Parra, L. P., & Ramírez-Sarmiento, C. A. (2018). Active Site Flexibility as a Hallmark for Efficient PET Degradation by I. sakaiensis PETase. *Biophysical Journal*, *114*(6), 1302-1312.

Flemming, H.-C., Wingender, J., Szewzyk, U., Steinberg, P., Rice, S. A., & Kjelleberg, S. (2016). Biofilms: an emergent form of bacterial life. *Nature Reviews Microbiology*, *14*(9), 563-575.

Frank Jeremy, A., Reich Claudia, I., Sharma, S., Weisbaum Jon, S., Wilson Brenda, A., & Olsen Gary, J. (2008). Critical Evaluation of Two Primers Commonly Used for Amplification of Bacterial 16S rRNA Genes. *Applied and Environmental Microbiology*, *74*(8), 2461-2470.

Gabbott, S., Key, S., Russell, C., Yonan, Y., & Zalasiewicz, J. (2020). Chapter 3 - The geography and geology of plastics: their environmental distribution and fate. In T. M. Letcher (Ed.), *Plastic Waste and Recycling* (pp. 33-63). Academic Press.

Galaris, D., Barbouti, A., & Pantopoulos, K. (2019). Iron homeostasis and oxidative stress: An intimate relationship. *Biochimica et Biophysica Acta (BBA) - Molecular Cell Research*, *1866*(12), 118535.

Gao, J.-W., Ying, J.-J., Dong, H., Liu, W.-J., He, D.-Y., Xu, L., & Sun, C. (2023). Characterization of Maribacter polysaccharolyticus sp. nov., Maribacter huludaoensis sp. nov., and Maribacter zhoushanensis sp. nov. and illumination of the distinct adaptative strategies of the genus Maribacter [Original Research]. *Frontiers in Marine Science*, *Volume 10 - 2023*.

Gao, M., Chen, L., Yang, J., Dong, S., Cao, Q., Cui, Z., Dong, Y., Liu, H., Shen, Y., Yang, H., Hao, Z., Zhang, L., Li, W., Tie, J. K., & Shen, G. (2024). Multimodal mechanisms of pathogenic variants in the signal peptide of FIX leading to hemophilia B. *Blood Advances*, *8*(15), 3893-3905.

Garcia Simão, R. d. C., Rocha, P. M. C., Martins, J. T. K., Turkiewicz, M., Plewka, J., da-Conceição Silva, J. L., Maller, A., Kadowaki, M. K., & Costa-Júnior, Á. P. S. (2024). Exploring biodegradable alternatives: microorganism-mediated plastic degradation and environmental policies for sustainable plastic management. *Archives of Microbiology*, *206*(12), 457.

Geyer, R., Jambeck, J. R., & Law, K. L. (2017). Production, use, and fate of all plastics ever made. *Science Advances*, *3*(7), e1700782.

Gross, R. A., & Kalra, B. (2002). Biodegradable Polymers for the Environment. *Science*, *297*(5582), 803-807.

Guo, W., Duan, J., Shi, Z., Yu, X., & Shao, Z. (2023). Biodegradation of PET by the membrane-anchored PET esterase from the marine bacterium Rhodococcus pyridinivorans P23. *Communications Biology*, *6*(1), 1090.

Gutierrez, T., Whitman, W. B., Huntemann, M., Copeland, A., Chen, A., Kyrpides, N., Markowitz, V., Pillay, M., Ivanova, N., Mikhailova, N., Ovchinnikova, G., Andersen, E., Pati, A., Stamatis, D., Reddy, T. B., Ngan, C. Y., Chovatia, M., Daum, C., Shapiro, N.,…Woyke, T. (2016). Genome Sequence of Arenibacter algicola Strain TG409, a

Hydrocarbon-Degrading Bacterium Associated with Marine Eukaryotic Phytoplankton. *Genome Announcements*, *4*(4).

Hopewell, J., Dvorak, R., & Kosior, E. (2009). Plastics recycling: challenges and opportunities. *Philosophical Transactions of the Royal Society B: Biological Sciences*, *364*(1526), 2115-2126.

Huang, Y., Qing, X., Wang, W., Han, G., & Wang, J. (2020). Mini-review on current studies of airborne microplastics: Analytical methods, occurrence, sources, fate and potential risk to human beings. *Trends in Analytical Chemistry*, *125*, 115821.

Hurley, R., Horton, A., Lusher, A., & Nizzetto, L. (2020). Chapter 7 - Plastic waste in the terrestrial environment. In T. M. Letcher (Ed.), *Plastic Waste and Recycling* (pp. 163-193). Academic Press.

Jaiswal, S., Sharma, B., & Shukla, P. (2020). Integrated approaches in microbial degradation of plastics. *Environmental Technology & Innovation*, *17*, 100567.

Jambeck, J. R., Geyer, R., Wilcox, C., Siegler, T. R., Perryman, M., Andrady, A., Narayan, R., & Law, K. L. (2015). Marine pollution. Plastic waste inputs from land into the ocean. *Science*, *347*(6223), 768-771.

Jiang, P., Zhao, S., Zhu, L., & Li, D. (2018). Microplastic-associated bacterial assemblages in the intertidal zone of the Yangtze Estuary. *Science of The Total Environment*, *624*, 48-54.

Jomrit, J., Suhardi, S., & Summpunn, P. (2023). Effects of Signal Peptide and Chaperone Co-Expression on Heterologous Protein Production in Escherichia coli. *Molecules*, *28*(14).

Jumper, J., Evans, R., Pritzel, A., Green, T., Figurnov, M., Ronneberger, O., Tunyasuvunakool, K., Bates, R., Žídek, A., Potapenko, A., Bridgland, A., Meyer, C., Kohl, S. A. A., Ballard, A. J., Cowie, A., Romera-Paredes, B., Nikolov, S., Jain, R., Adler, J.,…Hassabis, D. (2021). Highly accurate protein structure prediction with AlphaFold. *Nature*, *596*(7873), 583-589.

Juretschko, S., Timmermann, G., Schmid, M., Schleifer, K.-H., Pommerening-Röser, A., Koops, H.-P., & Wagner, M. (1998). Combined Molecular and Conventional Analyses of Nitrifying Bacterium Diversity in Activated Sludge: Nitrosococcus mobilis and Nitrospira-Like Bacteria as Dominant Populations. *Applied and Environmental Microbiology*, *64*(8), 3042-3051.

Kaandorp, M. L. A., Lobelle, D., Kehl, C., Dijkstra, H. A., & van Sebille, E. (2023). Global mass of buoyant marine plastics dominated by large long-lived debris. *Nature Geoscience*, *16*(8), 689-694.

Kabisch, A., Otto, A., König, S., Becher, D., Albrecht, D., Schüler, M., Teeling, H., Amann, R. I., & Schweder, T. (2014). Functional characterization of polysaccharide utilization loci in the marine Bacteroidetes 'Gramella forsetii' KT0803. *International Society for Microbial Ecology, 8*(7), 1492-1502.

Kalenborn, S., Zühlke, D., Reintjes, G., Riedel, K., Amann, R. I., & Harder, J. (2024). Genes for laminarin degradation are dispersed in the genomes of particle-associated Maribacter species [Original Research]. *Frontiers in Microbiology*, *Volume 15 - 2024*.

Kanta, P., Ghosh, T., Kaur, A., & Muthukumarappa, T. (2021). An innovative and cost-effective way to estimate alkaline phosphatase activity in in vitro cellular model systems. *International Journal of Biochemistry and Molecular Biology*, *12*(1), 1-7.

Kaushik, S., He, H., & Dalbey, R. E. (2022). Bacterial Signal Peptides- Navigating the Journey of Proteins [Review]. *Frontiers in Physiology*, *Volume 13 - 2022*.

Kawai, F., Kawabata, T., & Oda, M. (2019). Current knowledge on enzymatic PET degradation and its possible application to waste stream management and other fields. *Applied Microbiology and Biotechnology*, *103*(11), 4253-4268.

Keiko, S., Mariko, N., Hideharu, Y., Hideki, H., Mikio, S., Mark, J. M., Ryan, G. R., & Koji, N. (2010). A protein secretion system linked to bacteroidete gliding motility and pathogenesis. *Proceedings of the National Academy of Sciences*, *107*(1), 276-281.

Khan, S. A., Jeong, S. E., Baek, J. H., & Jeon, C. O. (2020). Maribacter algicola sp. nov., isolated from a marine red alga, Porphyridium marinum, and transfer of Maripseudobacter aurantiacus Chen et al. 2017 to the genus Maribacter as Maribacter aurantiacus comb. nov. *International Journal of Systematic and Evolutionary Microbiology*, *70*(2), 797-804.

Kirstein, I. V., Wichels, A., Gullans, E., Krohne, G., & Gerdts, G. (2019). The Plastisphere - Uncovering tightly attached plastic "specific" microorganisms. *PLOS ONE*, *14*(4), e0215859.

Kolton, M., Sela, N., Elad, Y., & Cytryn, E. (2014). Correction: Comparative Genomic Analysis Indicates that Niche Adaptation of Terrestrial Flavobacteria Is Strongly Linked to Plant Glycan Metabolism. *PLOS ONE*, *9*(1), 10.1371/annotation/1373eafbdc1379-1374a-1447a-1852b-1377a64503b64508ccb.

Koshti, R., Mehta, L., & Samarth, N. (2018). Biological Recycling of Polyethylene Terephthalate: A Mini-Review. *Journal of Polymers and the Environment*, *26*(8), 3520-3529.

Kovach, M. E., Elzer, P. H., Hill, D. S., Robertson, G. T., Farris, M. A., Roop, R. M., 2nd, & Peterson, K. M. (1995). Four new derivatives of the broad-host-range cloning vector pBBR1MCS, carrying different antibiotic-resistance cassettes. *Gene*, *166*(1), 175-176.

Kumar, S., Stecher, G., Li, M., Knyaz, C., & Tamura, K. (2018). MEGA X: Molecular Evolutionary Genetics Analysis across Computing Platforms. *Molecular Biology and Evolution*, *35*(6), 1547-1549.

Lapébie, P., Lombard, V., Drula, E., Terrapon, N., & Henrissat, B. (2019). Bacteroidetes use thousands of enzyme combinations to break down glycans. *Nature Communications*, *10*(1), 2043.

Larsbrink, J., & McKee, L. S. (2020). Chapter Two - Bacteroidetes bacteria in the soil: Glycan acquisition, enzyme secretion, and gliding motility. In G. M. Gadd & S. Sariaslani (Eds.), *Advances in Applied Microbiology* (Vol. 110, pp. 63-98). Academic Press.

Lei, X. G., Zhu, J. H., Cheng, W. H., Bao, Y., Ho, Y. S., Reddi, A. R., Holmgren, A., & Arnér, E. S. (2016). Paradoxical Roles of Antioxidant Enzymes: Basic Mechanisms and Health Implications. *Physiol Rev*, *96*(1), 307-364.

Lee CE, Lee SJ, Lee DG, Lee SH. (2016) Isolation of a New Agar Degrading Bacterium, Maribacter sp. SH-1 and Characterization of its Agarase. *Microbioly and Biotechnolgy*. Lett 2016;44:156-162.

Lian, X.-D., Guan, Y., Jiang, Y., Kwak, D.-H., Lee, M.-K., & Li, Z. (2025). Discovery of two novel Flavobacterium species with potential for complex polysaccharide degradation. *Scientific Reports*, *15*(1), 3494.

López-Sánchez, R., Rebollar, E. A., Gutiérrez-Ríos, R. M., Garciarrubio, A., Juarez, K., & Segovia, L. (2024). Metagenomic analysis of carbohydrate-active enzymes and their contribution to marine sediment biodiversity. *World Journal of Microbiology and Biotechnology*, *40*(3), 95.

Lu, D.-C., Wang, F.-Q., Amann, R. I., Teeling, H., & Du, Z.-J. (2023). Epiphytic common core bacteria in the microbiomes of co-located green (Ulva), brown (Saccharina) and red (Grateloupia, Gelidium) macroalgae. *Microbiome*, *11*(1), 126.

Lu, Z., Jiang, H., Hamouda, H.I., Wang, T., Dong, Y., and Mao, X. (2022). Biochemical Characterization of a Cold-Adapted λ-Carrageenase OUC-CglA from Maribacter vaceletii: An Efficient Tool for λ-Carrageenan Degradation. *Journal of Agricultural and Food Chemistry* 70(38)**,** 12135-12142.

Maitlo, G., Ali, I., Maitlo, H. A., Ali, S., Unar, I. N., Ahmad, M. B., Bhutto, D. K., Karmani, R. K., Naich, S. u. R., Sajjad, R. U., Ali, S., & Afridi, M. N. (2022). Plastic Waste Recycling, Applications, and Future Prospects for a Sustainable Environment. *Sustainability*, *14*(18), 11637.

Mann Alexander, J., Hahnke Richard, L., Huang, S., Werner, J., Xing, P., Barbeyron, T., Huettel, B., Stüber, K., Reinhardt, R., Harder, J., Glöckner Frank, O., Amann Rudolf, I., & Teeling, H. (2013). The Genome of the Alga-Associated Marine Flavobacterium Formosa agariphila KMM 3901T Reveals a Broad Potential for Degradation of Algal Polysaccharides. *Applied and Environmental Microbiology*, *79*(21), 6813-6822.

Marchler-Bauer, A., & Bryant, S. H. (2004). CD-Search: protein domain annotations on the fly. *Nucleic Acids Research*, *32*, W327-331.

Marques, J., Ares, A., Costa, J., Marques, M. P. M., de Carvalho, L. A. E. B., & Bessa, F. (2023). Plastisphere assemblages differ from the surrounding bacterial communities in transitional coastal environments. *Science of The Total Environment*, *869*, 161703.

McBride, M. J. (2019). Bacteroidetes Gliding Motility and the Type IX Secretion System. *Microbiology Spectrum*, *7*(1).

McKee, L. S., La Rosa, S. L., Westereng, B., Eijsink, V. G., Pope, P. B., & Larsbrink, J. (2021). Polysaccharide degradation by the Bacteroidetes: mechanisms and nomenclature. *Environmental Microbiology Reports*, *13*(5), 559-581.

Mergaert, J., & Swings, J. (1996). Biodiversity of microorganisms that degrade bacterial and synthetic polyesters. *Journal of Industrial Microbiology and Biotechnology*, *17*(5-6), 463-469.

Mueller, R.-J. (2006). Biological degradation of synthetic polyesters—Enzymes as potential catalysts for polyester recycling. *Process Biochemistry*, *41*(10), 2124-2128.

Mukherjee, S., Stamatis, D., Li, Cindy T., Ovchinnikova, G., Bertsch, J., Sundaramurthi, Jagadish C., Kandimalla, M., Nicolopoulos, Paul A., Favognano, A., Chen, I.-Min A., Kyrpides, Nikos C., & Reddy, T. B. K. (2022). Twenty-five years of Genomes OnLine Database (GOLD): data updates and new features in v.9. *Nucleic Acids Research*, *51*(D1), D957-D963.

Müller, R.-J., Kleeberg, I., & Deckwer, W.-D. (2001). Biodegradation of polyesters containing aromatic constituents. *Journal of Biotechnology*, *86*(2), 87-95.

Müller, R.-J., Schrader, H., Profe, J., Dresler, K., & Deckwer, W.-D. (2005). Enzymatic Degradation of Poly(ethylene terephthalate): Rapid Hydrolyse using a Hydrolase from T. fusca. *Macromolecular Rapid Communications*, *26*(17), 1400-1405.

Muringayil Joseph, T., Azat, S., Ahmadi, Z., Moini Jazani, O., Esmaeili, A., Kianfar, E., Haponiuk, J., & Thomas, S. (2024). Polyethylene terephthalate (PET) recycling: A review. *Case Studies in Chemical and Environmental Engineering*, *9*, 100673.

Nauendorf, A., Krause, S., Bigalke, N. K., Gorb, E. V., Gorb, S. N., Haeckel, M., Wahl, M., & Treude, T. (2016). Microbial colonization and degradation of polyethylene and biodegradable plastic bags in temperate fine-grained organic-rich marine sediments. *Mar Pollut Bull*, *103*(1-2), 168-178.

Nayanathara Thathsarani Pilapitiya, P. G. C., & Ratnayake, A. S. (2024). The world of plastic waste: A review. *Cleaner Materials*, *11*, 100220.

Nisticò, R. (2020). Polyethylene terephthalate (PET) in the packaging industry. *Polymer Testing*, *90*, 106707.

Oberbeckmann, S., Kreikemeyer, B., & Labrenz, M. (2018). Environmental Factors Support the Formation of Specific Bacterial Assemblages on Microplastics [Original Research]. *Frontiers in Microbiology*, *Volume 8 - 2017*.

Oberbeckmann, S., Osborn, A. M., & Duhaime, M. B. (2016). Microbes on a Bottle: Substrate, Season and Geography Influence Community Composition of Microbes Colonizing Marine Plastic Debris. *PLOS ONE*, *11*(8), e0159289.

OECD. (2022). Global Plastics Outlook: Policy Scenarios to 2060. *OECD Publishing, Paris*.

Olaniyan, O. T., & Adetunji, C. O. (2021). Biological, Biochemical, and Biodiversity of Biomolecules from Marine-Based Beneficial Microorganisms: Industrial Perspective. In C. O. Adetunji, D. G. Panpatte, & Y. K. Jhala (Eds.), *Microbial Rejuvenation of Polluted Environment: Volume 3* (pp. 57-81). Springer Singapore.

Oliveira, A. R., Sardinha-Silva, A., Andrews, P. L. R., Green, D., Cooke, G. M., Hall, S., Blackburn, K., & Sykes, A. V. (2020). Microplastics presence in cultured and wild-caught cuttlefish, Sepia officinalis. *Marine Pollution Bulletin*, *160*, 111553.

Orr, I. G., Hadar, Y., & Sivan, A. (2004). Colonization, biofilm formation and biodegradation of polyethylene by a strain of Rhodococcus ruber. *Applied Microbiology and Biotechnology*, *65*(1), 97-104.

Osman, A. I., Hosny, M., Eltaweil, A. S., Omar, S., Elgarahy, A. M., Farghali, M., Yap, P. S., Wu, Y. S., Nagandran, S., Batumalaie, K., Gopinath, S. C. B., John, O. D., Sekar, M., Saikia, T., Karunanithi, P., Hatta, M. H. M., & Akinyede, K. A. (2023). Microplastic sources, formation, toxicity and remediation: a review. *Environmental Chemistry Letters*, 1-41.

Palm, G. J., Reisky, L., Böttcher, D., Müller, H., Michels, E. A. P., Walczak, M. C., Berndt, L., Weiss, M. S., Bornscheuer, U. T., & Weber, G. (2019). Structure of the plastic-degrading Ideonella sakaiensis MHETase bound to a substrate. *Nature Communications*, *10*(1), 1717.

Pan, X., Raaijmakers, J. M., & Carrión, V. J. (2023). Importance of Bacteroidetes in host–microbe interactions and ecosystem functioning. *Trends in Microbiology*, *31*(9), 959-971.

Panda, A. K., Singh, R. K., & Mishra, D. K. (2010). Thermolysis of waste plastics to liquid fuel: A suitable method for plastic waste management and manufacture of value added products—A world prospective. *Renewable and Sustainable Energy Reviews*, *14*(1), 233-248.

Pawar, P., Shirgaonkar, S., & affiliations, R. (2016). Plastic marine debris: Sources, distribution and impacts on coastal and ocean biodiversity. *PENCIL Publication of Biological Sciences (OCEANOGRAPHY). 3(1): 40-54. (ISSN: 2408-5561). 3*, 40-54.

Pettersen, E. F., Goddard, T. D., Huang, C. C., Meng, E. C., Couch, G. S., Croll, T. I., Morris, J. H., & Ferrin, T. E. (2021). UCSF ChimeraX: Structure visualization for researchers, educators, and developers. *Protein Science*, *30*(1), 70-82.

Pinto, M., Langer, T. M., Hüffer, T., Hofmann, T., & Herndl, G. J. (2019). The composition of bacterial communities associated with plastic biofilms differs between different polymers and stages of biofilm succession. *PLOS ONE*, *14*(6), e0217165.

, T. M., Harrison, J., Simon, M., Varela, M. M., & Herndl, G. J. (2020). Putative degraders of low-density polyethylene-derived compounds are ubiquitous members of plastic-

associated bacterial communities in the marine environment. *Environmental Microbiology*, *22*(11), 4779-4793.

Plastic Europe. (2023). *Plastics—The Fast Facts*.

Preuß, L., Alawi, M., Dumnitch, A., Trinh, L., Maison, W., Burmeister, N., Poehlein, A., Daniel, R., Vollstedt, C., & Streit, W. (2025). Polyethylene terephthalate (PET) primary degradation products affect c-di-GMP-, cAMP-signaling, and quorum sensing (QS) in Vibrio gazogenes DSM 21264. *Microbiology Spectrum*, *13*, e0018125.

Pudack, C., Stepanski, M., & Fässler, P. (2020). PET Recycling – Contributions of Crystallization to Sustainability. *Chemie Ingenieur Technik*, *92*(4), 452-458.

Qian, Y., Huang, L., Yan, P., Wang, X., & Luo, Y. (2024). Biofilms on Plastic Debris and the Microbiome. *Microorganisms*, *12*(7).

Rafey, A., & and Siddiqui, F. Z. (2023). A review of plastic waste management in India – challenges and opportunities. *International Journal of Environmental Analytical Chemistry*, *103*(16), 3971-3987.

Ronkvist, Å. M., Xie, W., Lu, W., & Gross, R. A. (2009). Cutinase-Catalyzed Hydrolysis of Poly(ethylene terephthalate). *Macromolecules*, *42*(14), 5128-5138.

Rouault, T. A., & Klausner, R. D. (1996). Post-transcriptional regulation of genes of iron metabolism in mammalian cells. *JBIC Journal of Biological Inorganic Chemistry*, *1*(6), 494-499.

Sardon, H., & Dove, A. P. (2018). Plastics recycling with a difference. *Science*, *360*(6387), 380-381.

Satta, A., Zampieri, G., Loprete, G., Campanaro, S., Treu, L., & Bergantino, E. (2024). Metabolic and enzymatic engineering strategies for polyethylene terephthalate degradation and valorization. *Reviews in Environmental Science and Bio/Technology*, *23*(2), 351-383.

Seemann, T. (2014). Prokka: rapid prokaryotic genome annotation. *Bioinformatics*, *30*(14), 2068-2069.

Sharma, I., Sandeep, Jagota, N., Sharma, A., Bala, R., Sharma, S., & Sharma, A. (2025). Microbial Colonization and Degradation of Microplastics. In K. Khanna, S. Kaur Kohli, & R. Bhardwaj (Eds.), *Microplastics and Soil Microbiome: Recent trends and Future Prospects* (pp. 15-40). Springer Nature Singapore.

Shirke, A. N., White, C., Englaender, J. A., Zwarycz, A., Butterfoss, G. L., Linhardt, R. J., & Gross, R. A. (2018). Stabilizing Leaf and Branch Compost Cutinase (LCC) with Glycosylation: Mechanism and Effect on PET Hydrolysis. *Biochemistry*, *57*(7), 1190-1200.

Sin, L. T., & Tueen, B. S. (2023). 1 - Plastics and environmental sustainability issues. In L. T. Sin & B. S. Tueen (Eds.), *Plastics and Sustainability* (pp. 1-43). Elsevier.

Sokolova, T., Krishna, A., & Döring, T. (2023). Paper Meets Plastic: The Perceived Environmental Friendliness of Product Packaging. *Journal of Consumer Research*, *50*(3), 468-491.

Son, H. F., Cho, I. J., Joo, S., Seo, H., Sagong, H.-Y., Choi, S. Y., Lee, S. Y., & Kim, K.-J. (2019). Rational Protein Engineering of Thermo-Stable PETase from Ideonella sakaiensis for Highly Efficient PET Degradation. *ACS Catalysis*, *9*(4), 3519-3526.

Soong, Y.-H. V., Sobkowicz, M. J., & Xie, D. (2022). Recent Advances in Biological Recycling of Polyethylene Terephthalate (PET) Plastic Wastes. *Bioengineering*, *9*(3), 98.

Statista. (2023). *Statista Research Department Production Forecast of Thermoplastics Worldwide from 2025 to 2050*.

Sulaiman, S., Yamato, S., Kanaya, E., Kim, J.-J., Koga, Y., Takano, K., & Kanaya, S. (2012). Isolation of a Novel Cutinase Homolog with Polyethylene Terephthalate-Degrading Activity from Leaf-Branch Compost by Using a Metagenomic Approach. *Applied and Environmental Microbiology*, *78*(5), 1556-1562.

Sulaiman, S., Yamato, S., Kanaya, E., Kim, J. J., Koga, Y., Takano, K., & Kanaya, S. (2012). Isolation of a novel cutinase homolog with polyethylene terephthalate-degrading activity from leaf-branch compost by using a metagenomic approach. *Applied and Environmental Microbiology*, *78*(5), 1556-1562.

Sun, C., Zhao, W., Yue, W., Cheng, H., Long, A., Yin, J., Sun, F., & Wang, Y. (2025). Degradation of polymeric carbohydrates coupled with cellular motility driving microbial niche separation in the Pearl River Estuary surface sediment. *Journal of Environmental Sciences*.

Tang, K., Lin, Y., Han, Y., & Jiao, N. (2017). Characterization of Potential Polysaccharide Utilization Systems in the Marine Bacteroidetes Gramella Flava JLT2011 Using a Multi-Omics Approach [Original Research]. *Frontiers in Microbiology*, *Volume 8 - 2017*.

Taniguchi, I., Yoshida, S., Hiraga, K., Miyamoto, K., Kimura, Y., & Oda, K. (2019). Biodegradation of PET: Current Status and Application Aspects. *ACS Catalysis*, *9*(5), 4089-4105.

Thomas, F., Hehemann, J.-H., Rebuffet, E., Czjzek, M., & Michel, G. (2011). Environmental and Gut Bacteroidetes: The Food Connection [Review]. *Frontiers in Microbiology*, *volume 2 - 2011*.

Thushari, G. G. N., & Senevirathna, J. D. M. (2020). Plastic pollution in the marine environment. *Heliyon*, *6*(8).

Tournier, V., Duquesne, S., Guillamot, F., Cramail, H., Taton, D., Marty, A., & André, I. (2023). Enzymes' Power for Plastics Degradation. *Chemical Reviews*, *123*(9), 5612-5701.

Tribedi, P., & Sil, A. K. (2014). Cell surface hydrophobicity: a key component in the degradation of polyethylene succinate by Pseudomonas sp. AKS2. *Journal of Applied Microbiology*, *116*(2), 295-303.

Trincone, A. (2010). Potential biocatalysts originating from sea environments. *Journal of Molecular Catalysis B-enzymatic - J MOL CATAL B-ENZYM*, *66*, 241-256.

Umarov, R. K., & Solovyev, V. V. (2017). Recognition of prokaryotic and eukaryotic promoters using convolutional deep learning neural networks. *PLOS ONE*, *12*(2), e0171410.

Urbanek, A. K., Mirończuk, A. M., García-Martín, A., Saborido, A., de la Mata, I., & Arroyo, M. (2020). Biochemical properties and biotechnological applications of microbial enzymes involved in the degradation of polyester-type plastics. *Biochimica et Biophysica Acta (BBA) - Proteins and Proteomics*, *1868*(2), 140315.

Vaksmaa, A., Egger, M., Lüke, C., Martins, P. D., Rosselli, R., Asbun, A. A., & Niemann, H. (2022). Microbial communities on plastic particles in surface waters differ from subsurface waters of the North Pacific Subtropical Gyre. *Marine Pollution Bulletin*, *182*, 113949.

Vaksmaa, A., Hernando-Morales, V., Zeghal, E., & Niemann, H. (2021). Microbial Degradation of Marine Plastics: Current State and Future Prospects. In S. J. Joshi, A. Deshmukh, & H. Sarma (Eds.), *Biotechnology for Sustainable Environment* (pp. 111-154). Springer Singapore.

Vaksmaa, A., Knittel, K., Abdala Asbun, A., Goudriaan, M., Ellrott, A., Witte, H. J., Vollmer, I., Meirer, F., Lott, C., Weber, M., Engelmann, J. C., & Niemann, H. (2021). Microbial Communities on Plastic Polymers in the Mediterranean Sea [Original Research]. *Frontiers in Microbiology*, *12*.

van Sebille, E., Wilcox, C., Lebreton, L., Maximenko, N., Hardesty, B. D., van Franeker, J. A., Eriksen, M., Siegel, D., Galgani, F., & Law, K. L. (2015). A global inventory of small floating plastic debris. *Environmental Research Letters*, *10*(12), 124006.

Vidal, P., Robles-Martín, A., Fernandez-Lopez, L., Gonzalez-Alfonso, J. L., Almendral, D., Muñoz-Tafalla, R., Plou, F. J., Guallar, V., & Ferrer, M. (2024). Unlocking a Key Residue in a Lipase for Efficient Polyethylene Terephthalate (PET) Hydrolysis and Influencing Depolymerization Product Profiles. *ChemCatChem*, *16*(23), e202400765.

Walker, T. R., Baechler, B. R., Markley, L., Grünzner, M., Akuoko, I. S. G., Bowyer, C., Menzel, C., Muntaha, S. T., Macdonald, A., Allen, D., & Cowan, E. (2023). Plastic Pulse of the Public: A review of survey-based research on how people use plastic. *Cambridge Prisms: Plastics*, *1*, e8, Article e8.

Wang, Y., & Qian, H. (2021). Phthalates and Their Impacts on Human Health. *Healthcare*, *9*(5), 603.

Wawer, J., Panuszko, A., Kozłowski, D., Juniewicz, J., Szymikowski, J., & Brodnicka, E. (2025). Sustainable Management of Microplastic Pollutions from PET Bottles: Overview and Mitigation Strategies. *Applied Sciences*, *15*(10), 5322.

Webb, H. K., Arnott, J., Crawford, R. J., & Ivanova, E. P. (2013). Plastic Degradation and Its Environmental Implications with Special Reference to Poly(ethylene terephthalate). *Polymers*, *5*(1), 1-18.

Wei, R., Breite, D., Song, C., Gräsing, D., Ploss, T., Hille, P., Schwerdtfeger, R., Matysik, J., Schulze, A., & Zimmermann, W. (2019). Biocatalytic Degradation Efficiency of Postconsumer Polyethylene Terephthalate Packaging Determined by Their Polymer Microstructures. *Advanced Science*, *6*(14), 1900491.

Wei, R., & Zimmermann, W. (2017). Microbial enzymes for the recycling of recalcitrant petroleum-based plastics: how far are we? *Microbial Biotechnology*, *10*(6), 1308-1322.

Wilkes, R. A., & Aristilde, L. (2017). Degradation and metabolism of synthetic plastics and associated products by Pseudomonas sp.: capabilities and challenges. *Journal of Applied Microbiology*, *123*(3), 582-593.

Wolter, L. A., Mitulla, M., Kalem, J., Daniel, R., Simon, M., & Wietz, M. (2021a). CAZymes in Maribacter dokdonensis 62–1 From the Patagonian Shelf: Genomics and Physiology Compared to Related Flavobacteria and a Co-occurring Alteromonas Strain [Original Research]. *Frontiers in Microbiology*, *12*.

Wolter, L. A., Mitulla, M., Kalem, J., Daniel, R., Simon, M., & Wietz, M. (2021b). CAZymes in Maribacter dokdonensis 62–1 From the Patagonian Shelf: Genomics and Physiology Compared to Related Flavobacteria and a Co-occurring Alteromonas Strain [Original Research]. *Frontiers in Microbiology*, *Volume 12 - 2021*.

Wright, R. J., Bosch, R., Gibson, M. I., & Christie-Oleza, J. A. (2020). Plasticizer Degradation by Marine Bacterial Isolates: A Proteogenomic and Metabolomic Characterization. *Environmental Science & Technology*, *54*(4), 2244-2256.

Wright, R. J., Langille, M. G. I., & Walker, T. R. (2020). Food or just a free ride? A meta-analysis reveals the global diversity of the Plastisphere. *International Society for Microbial Ecology Journal*, *15*(3), 789-806.

Yan, Z.-F., Feng, C.-Q., Zhou, J.-Q., Huang, Q.-S., Chen, X.-Q., Xia, W., & Wu, J. (2024). Complete degradation of PET waste using a thermophilic microbe-enzyme system. *International Journal of Biological Macromolecules*, *260*, 129538.

Yang, Y., Liu, W., Zhang, Z., Grossart, H.-P., & Gadd, G. M. (2020). Microplastics provide new microbial niches in aquatic environments. *Applied Microbiology and Biotechnology*, *104*(15), 6501-6511.

Yoon, B.-J., & Oh, D.-C. (2012). Spongiibacterium flavum gen. nov., sp. nov., a member of the family Flavobacteriaceae isolated from the marine sponge Halichondria oshoro, and emended descriptions of the genera Croceitalea and Flagellimonas. *International Journal of Systematic and Evolutionary Microbiology*, *62*(Pt_5), 1158-1164.

Yoshida, S., Hiraga, K., Takehana, T., Taniguchi, I., Yamaji, H., Maeda, Y., Toyohara, K., Miyamoto, K., Kimura, Y., & Oda, K. (2016). A bacterium that degrades and assimilates poly(ethylene terephthalate). *Science*, *351*(6278), 1196-1199.

Zettler, E. R., Mincer, T. J., & Amaral-Zettler, L. A. (2013). Life in the “Plastisphere”: Microbial Communities on Plastic Marine Debris. *Environmental Science & Technology*, *47*(13), 7137-7146.

Zhai, X., Zhang, X. H., & Yu, M. (2023). Microbial colonization and degradation of marine microplastics in the plastisphere: A review. *Frontier Microbiology*, *14*, 1127308.

Zhan, P., Tang, K., Chen, X., & Yu, L. (2017). Complete genome sequence of Maribacter sp. T28, a polysaccharide-degrading marine flavobacteria. *Journal of Biotechnology*, *259*, 1-5.

Zhang, H., Dierkes, R. F., Perez-Garcia, P., Costanzi, E., Dittrich, J., Cea, P. A., Gurschke, M., Applegate, V., Partus, K., Schmeisser, C., Pfleger, C., Gohlke, H., Smits, S. H. J., Chow, J., & Streit, W. R. (2024). The metagenome-derived esterase PET40 is highly promiscuous and hydrolyses polyethylene terephthalate (PET). *Febs Journal*, *291*(1), 70-91.

Zhang, H., Perez-Garcia, P., Dierkes, R. F., Applegate, V., Schumacher, J., Chibani, C. M., Sternagel, S., Preuss, L., Weigert, S., Schmeisser, C., Danso, D., Pleiss, J., Almeida, A., Höcker, B., Hallam, S. J., Schmitz, R. A., Smits, S. H. J., Chow, J., & Streit, W. R. (2022). The Bacteroidetes Aequorivita sp. and Kaistella jeonii Produce Promiscuous Esterases With PET-Hydrolyzing Activity [Original Research]. *Frontiers in Microbiology*, *12*.

Zhao, S., Wang, T., Zhu, L., Xu, P., Wang, X., Gao, L., & Li, D. (2019). Analysis of suspended microplastics in the Changjiang Estuary: Implications for riverine plastic load to the ocean. *Water Research*, *161*, 560-569.

7. SUPPLEMENTARY DATA

7. SUPPLEMENTARY DATA

Amino acid sequence of PET93 and PET94 from *Maribacter dokdonensis* and *Arenibacter palladensis*

>WKW63607.1 dienelactone hydrolase [*Maribacter dokdonensis*]

MKFRALLFSASLIAILFNGLTINTVNAQTNDFLYGDQLPDAPELSSRGEYKVGVKTVNLVNPN
QVDILNSKEGNDPTYDRPITIEVWYPANVGDDAKTVVYDEVMGTRGDSLRPLTPFTFKGRA
YRDATPKTGNKFPLVVVSHGYVGSRYLMTYLTENLASKGYIVAAIDHTDSTFKDANAFQSTL
LNRPKDIRFVINEMEKMGAKGSKNNLEGVVDANNTAIIGYSMGGYGVLNVGGAGYSAGLAQ
FFTGMTGGSTAISVHTAGNAAYEKMIDARIKAIVAFAPWGMERGVWDAEGLKGLKTPTFFIA
GSQDDISGYEKGIKAIYEGAVNADRYLLTYMNARHNVAPNPPPAEALAPGLHIDEYYRYAEP
SWDQRKMNNINQHFVTAFIGKHLKNQDSTKFLEVQEDSNEKDWTGFKPRSSTGMELLHAQ
PAN

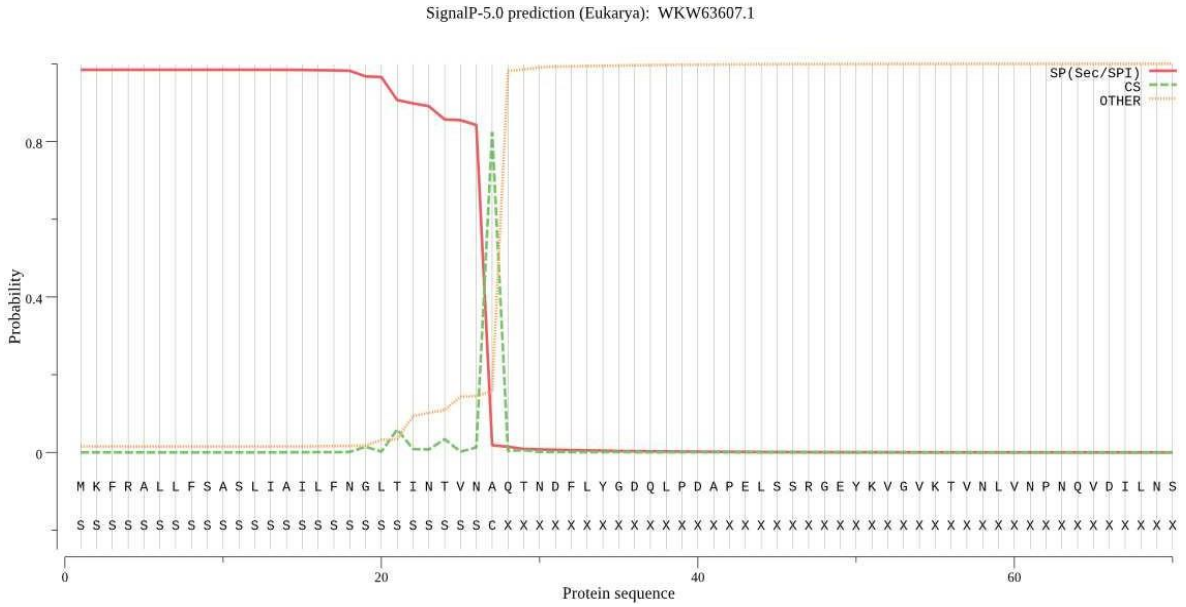

Figure S1. *Signal peptide prediction for* protein PET93 *using SignalP-5.0 (Eukarya setting). The plot shows the predicted presence of a signal peptide at the N-terminus of the protein sequence. The red line (SP) indicates the probability that a given amino acid position is part of a signal peptide (Sec/SPI). The green dashed line (CS) marks the predicted cleavage site for the signal peptide. The yellow-orange line (OTHER) shows the probability of the sequence being non-secretory.*

>WKW63608.1 dienelactone hydrolase [*Arenibacter palladensis]*

MPILNRFAHFQLILCFLISNLVLNAQTGSFVYGDALPDAPELSARGSYAVGVRTLDFVNKGQA
DVLNSKNGIDPIYDRPLKVEVWYPAQLAEGAKETVVYDEVMGTAHDSLRPLTPITFKGRASR
DAAPLTTDGSFPLLVVAHGYVGSRYLMTYLTENLASKGYVVVAIDHTDSTFRDASPFASTLV
NRAKDISFVLNQTVNLGKAADNNFLAGLVDSENIGIIGYSMGGYGVLNVAGAGYSDGLVGFF
SGMTGGSKAIVDLAMSNPDFPKVDPRIKAVVAFAPWGMERGIWDAEGLKGLKVPTFFIAGS
QDDISGYEKGIKAIYTGAVNADRYLLTYENARHNVAPNPPPAESFEPGLHIDEYYRYAEPSW
DERKINNVNQHFITAFLGIHLKQKDYSKFLELQENSNEKDWTGFKARSSTGMELLHDKPAP

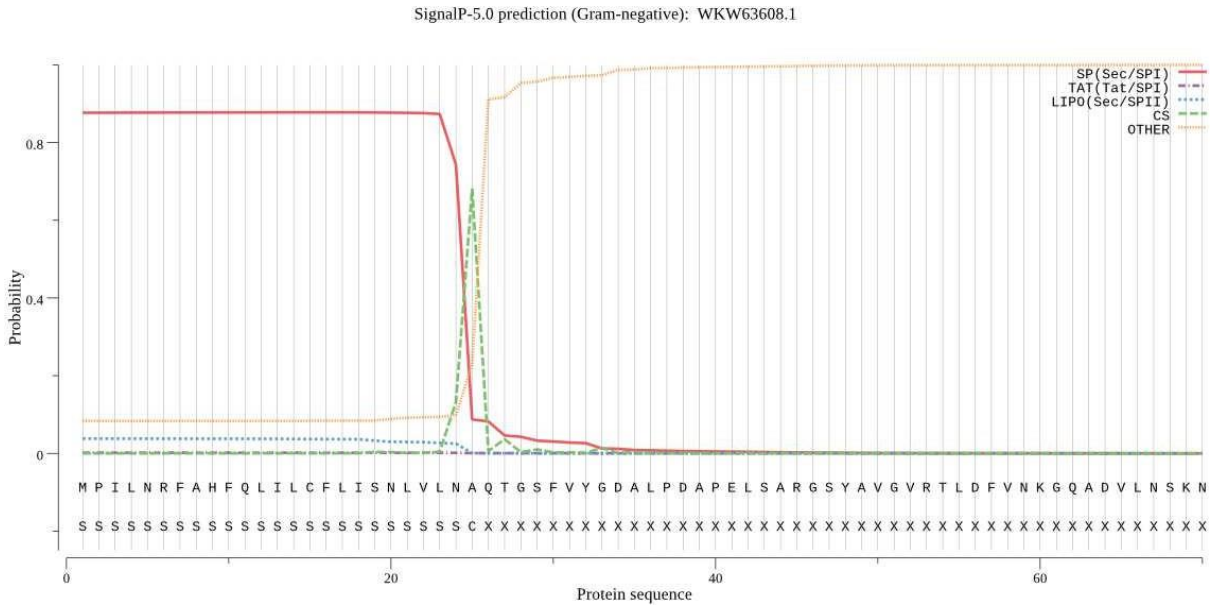

Figure S2. *Signal peptide prediction for protein PET94 using SignalP-5.0 (Eukarya setting). The plot shows the predicted presence of a signal peptide at the N-terminus of the protein sequence. The red line (SP) indicates the probability that a given amino acid position is part of a signal peptide (Sec/SPI). The green dashed line (CS) marks the predicted cleavage site for the signal peptide. The yellow-orange line (OTHER) shows the probability of the sequence being non-secretory.*

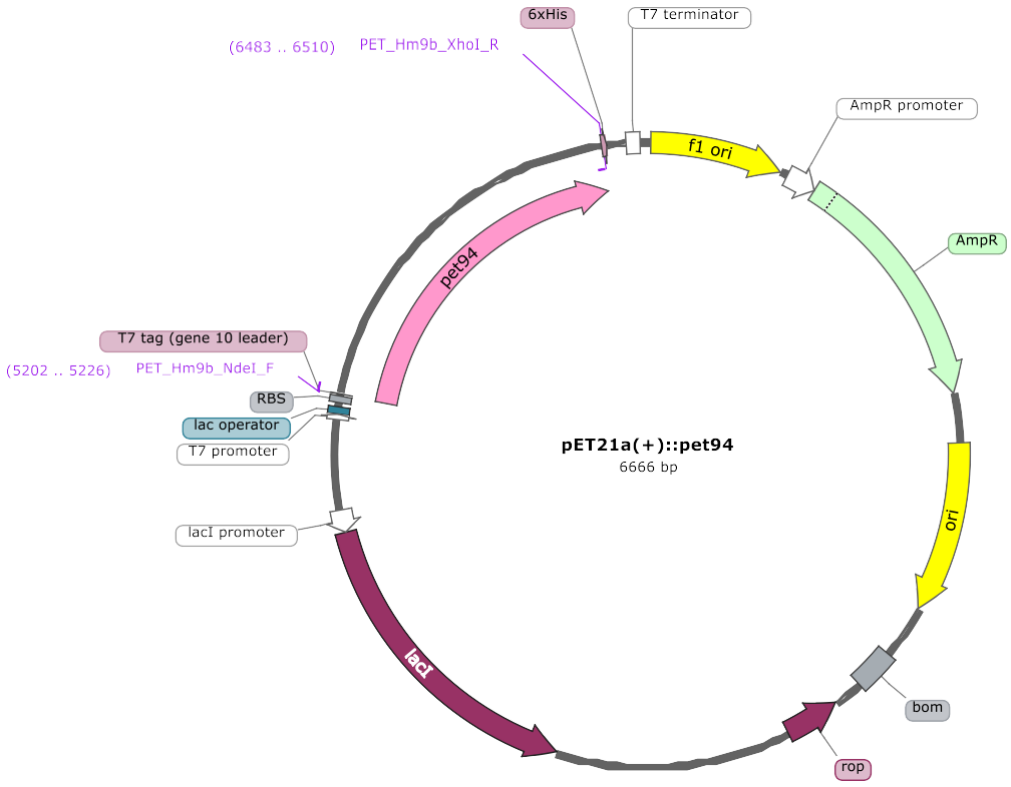

Figure S3. *Plasmid map of recombinant expression vector carrying the PET93 gene*

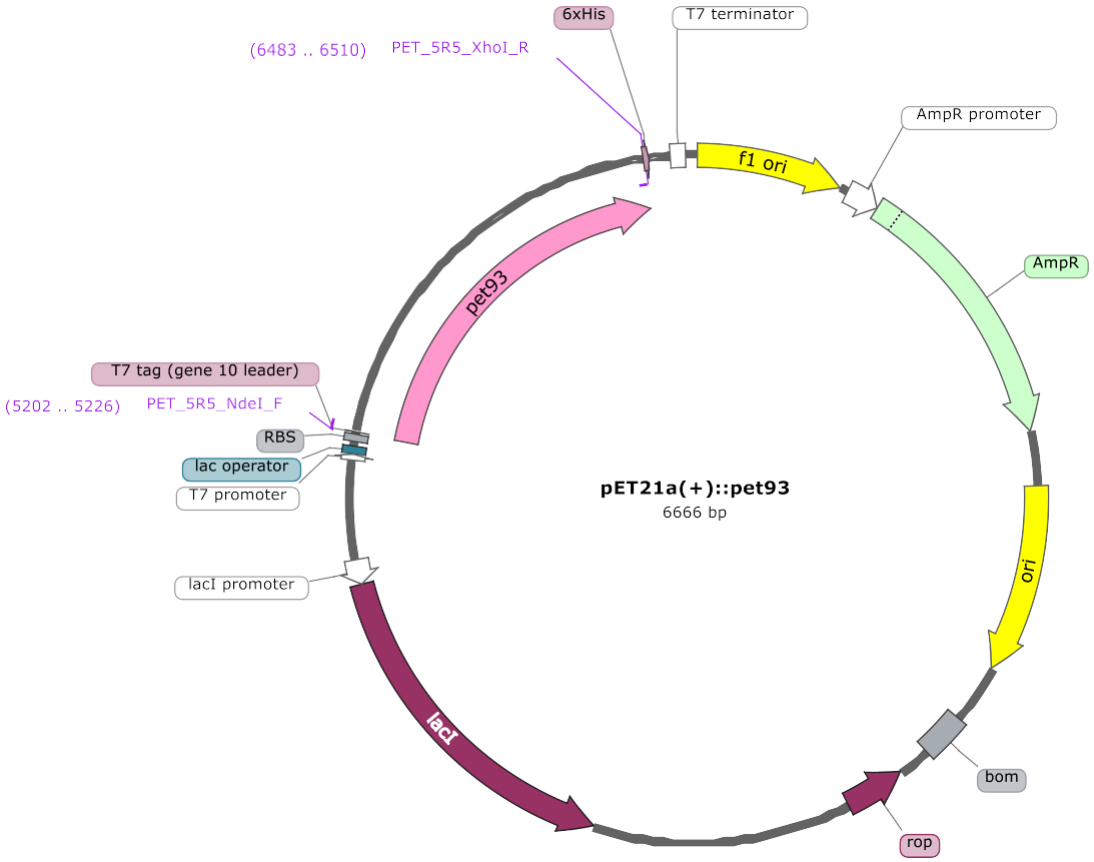

Figure S4. *Plasmid map of recombinant expression vector carrying the PET94 gene*

Table S1. *Quantitative analysis of biofilm morphology formed by the Bacteroidota isolates UHH-5R5 and UHH-Hm9b on PET foil over a 7-day incubation period using BiofilmQ. Representative data of n = 3 independent biofilms for each treatment are presented.*

File name	Biofilm HeighttoLength (a.u.)	Biofilm HeightToWidth (a.u.)	Biofilm LengthToWidth (a.u.)	Biofilm_Height (µm)	Biofilm_Length (µm)	Biofilm_MeanThickness (µm)	Biofilm_Volume (µm³)	Biofilm_Width (µm)
UHH-Hm9b								
Day 2_1	0.149	0.148	0.995	17.970	120.492	9.641	516.638	121.111
Day 2_2	0.138	0.123	0.886	17.445	126.046	7.846	2180.643	142.210
Day 2_3	0.159	0.126	0.797	17.588	110.796	7.811	895.251	139.082
Day 3_1	0.179	0.192	1.072	23.766	132.779	14.158	3952.286	123.923
Day 3_2	0.207	0.220	1.059	26.950	129.891	8.250	686.550	122.704
Day 3_3	0.185	0.234	1.265	27.631	149.093	13.594	7164.869	117.871
Day 6_1	0.227	0.201	0.884	27.500	120.993	13.847	4001.465	136.920
Day 6_2	0.138	0.139	1.010	17.562	127.373	11.973	1690.761	126.103
Day 6_3	0.220	0.162	0.740	25.210	114.850	14.458	3133.971	155.285
Day 7_1	0.208	0.225	1.083	27.701	133.384	13.814	2955.924	123.141
Day 7_2	0.247	0.222	0.901	27.756	112.514	12.820	168.790	124.934
Day 7_3	0.236	0.224	0.950	27.649	117.053	18.754	989.514	123.256
UHH-5R5								
Day 2_1	0.095	0.078	0.827	10.218	107.691	6.822	2308.372	130.280
Day 2_2	0.045	0.031	0.682	4.830	107.507	4.638	535.207	157.634
Day 2_3	0.057	0.079	1.389	7.876	139.261	6.318	693.113	100.298

Day 3_1	0.103	0.093	0.902	12.255	118.500	5.743	4800.371	131.320
Day 3_2	0.106	0.086	0.814	12.490	118.239	5.362	4166.769	145.258
Day 3_3	0.164	0.146	0.892	19.327	118.140	9.191	915.154	132.372
Day 6_1	0.218	0.210	0.960	27.540	126.147	16.111	8821.380	131.399
Day 6_2	0.183	0.225	1.225	27.256	148.627	15.079	10738.695	121.354
Day 6_3	0.182	0.214	1.176	25.552	140.453	12.470	643.019	119.436
Day 7_1	0.148	0.252	1.708	27.694	187.544	10.714	5502.643	109.809
Day 7_2	0.171	0.209	1.223	23.544	137.758	8.479	2288.972	112.649
Day 7_3	0.199	0.223	1.123	27.118	136.300	14.975	10349.788	121.350

Table S2. *Homologs of PET93 hydrolases from Bacteroidota isolates UHH-5R5 and UHH-Hm9b. Data were retrieved from the publicly available IMG/MER database, applying thresholds of ≥50% sequence identity and ≥80% sequence coverage.*

Gene ID	Locus Tag	Genome name	Isolation Country	Latitude	Longitude
UHH-5R5 homologs					
2546243389	ADICYQ_2709	*Cyclobacterium qasimii* M12-11B	Norway	79.00105	11.66625
2890793592	Ga0443375_01_526053_527357	*Cyclobacterium qasimii* NBRC 106168	Norway	79.00105	11.66625
2515733714	B156DRAFT_01776	*Spirosoma luteum* DSM 19990	Norway	78.2122	15.8
2515842746	B157DRAFT_06708	*Spirosoma spitsbergense* DSM 19989	Norway	78.21	15.8
2774668436	Ga0226569_114770	*Arenibacter algicola* SMS7	Sweden	58.8734	11.07782
2595693039	LX87DRAFT_00794	*Larkinella arboricola* DSM 21851	Russia	55.75	37.62
2585370157	FG20DRAFT_3328	*Zobellia amurskyensis* MAR_2009_138	Germany	55.0255	8.4567
2592972043	GQ41DRAFT_0959	*Arenibacter algicola* MAR_2009_79	Germany	55.0255	8.4567
2676739754	Ga0040979_3239	*Maribacter sp.* MAR_2009_60	Germany	55.0255	8.4567
2667678916	Ga0040978_1313	*Maribacter dokdonensis* MAR_2009_71	Germany	55.0255	8.4567
2832368994	Ga0335984_1474	*Zobellia galactanivorans* OII3	Germany	54.67	9.94
2574425426	P177DRAFT_00341	*Maribacter forsetii* DSM 18668	Germany	54.1841	7.9
2558431147	P178DRAFT_1169	*Maribacter sp.* Hel_I _7	Germany	54.1841	7.9
8000209034	Ga0596861_0008_300124_301428	*Maribacter dokdonensis* AG-HH-5R5	Germany	54.1318	8.8753
2515427593	B036DRAFT_03034	*Neolewinella persica* DSM 23188	Ireland	53.27	-9.056
2504771602	Halhy_2235	*Haliscomenobacter hydrossis* O, DSM 1100	Netherlands	51.77	5.53
8065844926	Ga0487514_01_1236377_1237705	*Zobellia roscoffensis* Asnod2-B02-B	France	48.7266	-3.9897
3001348201	Ga0487513_01_1242554_1243882	*Zobellia nedashkovskayae* Asnod2-B07-B	France	48.7266	-3.9897
8065850772	Ga0487512_01_3324766_3326094	*Zobellia nedashkovskayae* Asnod3-E08-A	France	48.7266	-3.9897
3001333670	Ga0488450_01_1260666_1261994	*Zobellia roscoffensis* Asnod1-F08	France	48.7266	-3.9897
2881099053	Ga0442556_33_349623_350918	*Arundinibacter roseus* DMA-k-7a	Hungary	47.7	16.69997
8055965970	Ga0616553_11_1042874_1044202	*Zobellia barbeyronii* KMM 6746	Russia	47.51669	152.813
648160996	FB2170_02060	*Maribacter sp.* HTCC2170	USA	44.655	-124.064
644104643	Flav2ADRAFT_1526	*Flavobacteria bacterium* MS024-2A (unscreened)	USA	43.84978	-69.6266

8080698659	Ga0625472_07_32683_33957	*Portibacter lacus* YM8-076	Japan	43.27284	142.5722
2910289591	Ga0477856_036_38108_39436	*Zobellia amurskyensis* KMM 3526	Russia	43.14794	131.891
2890770580	Ga0441612_223_154750_156033	*Larkinella sp.* C7	China	43.1	119.37
8058070572	Ga0617454_01_1769634_1770962	*Zobellia alginiliquefaciens* LLG6346-3.1	France	42.76904	9.33353
2919024960	Ga0454494_10_5124_6437	*Arcicella sp.* BE51	USA	42.444	-76.5019
2919355278	Ga0454526_11_5124_6437	*Arcicella sp.* BE140	USA	42.444	-76.5019
2919350065	Ga0454525_11_5124_6437	*Arcicella sp.* BE139	USA	42.444	-76.5019
8048528387	Ga0616067_01_1951018_1952100	*Zobellia laminariae* AS94	USA	42.42	-70.907
3001341769	Ga0584015_08_147227_148549	*Zobellia uliginosa* C3R17	USA	42.25	-70.54
8074547076	Ga0580702_01_922024_923352	*Zobellia sp.* B3R18	USA	42.25	-70.54
8100324962	Ga0488656_01_1350439_1351743	*Maribacter sp.* 6B07	USA	42.25	-70.54
3001904140	Ga0580690_04_133467_134774	*Arenibacter algicola* E3M18	USA	42.25	-70.54
8074614719	Ga0580712_45_213521_214849	*Zobellia galactanivorans* A2M03	USA	42.25	-70.54
2890828893	Ga0441110_04_6487_7779	*Runella sp.* CRIBMP	USA	42.23591	-81.7859
2890197314	Ga0440108_02_155726_157030	*Emticicia sp.* CRIBPO	USA	42.23591	-81.7859
2808571772	Ga0321368_117257	*Spongiimicrobium salis* Da_B9	Spain	42.11444	3.168333
2721515523	Ga0175219_111860	*Maribacter sp.* 1_2014MBL_MicDiv	USA	41.52733	-70.6757
2884363254	Ga0442147_16_52030_53331	*Spirosoma sp.* 209	USA	40.70124	-74.0287
2890750500	Ga0441869_11_349676_350959	*Cyclobacterium roseum* SYSU L10180	China	40.50182	85.02692
2890710313	Ga0442907_13_418729_420021	*Cyclobacterium sp.* SYSU L10401	China	40.50182	85.02692
2890760553	Ga0440852_11_379535_380818	*Cyclobacterium sp.* SYSU L10167	China	40.50182	85.02692
646858067	Trad_2647	*Truepera radiovictrix* RQ-24, DSM 17093	Portugal	37.946	-25.49
2884494525	Ga0441408_01_1388066_1389361	*Maribacter algicola* PoM-212	South Korea	37.64039	126.5886
8001640529	Ga0594633_08_15931_17229	*Flagellimonas sp.* 389	China	37.55817	122.0907
8077179044	Ga0627981_45_82466_83773	*Muriicola sp.* Z0-33	China	37.5292	122.0108
8099929817	Ga0626244_078_5418_6725	*Arenibacter sp.* S6351L	China	37.51718	122.1552
8077281885	Ga0626238_127_136883_138184	*Arenibacter sp.* F20364	China	37.51118	122.1439
2897639915	Ga0441610_12_1042881_1044170	*Maribacter sp.* RZ26	China	37.51118	122.1439
8078693221	Ga0627007_04_12753_14045	*Lacihabitans sp.* CCS-44	South Korea	37.45573	129.1895

640617222	ALPR1_05630	*Algoriphagus machipongonensis* PR1	USA	37.42	-75.69
8071170371	Ga0581854_08_68151_69446	*Spirosoma sp.* RHs26	South Korea	37.37771	127.5979
2890815525	Ga0440155_36_295790_297082	*Cyclobacterium plantarum* GBPx2	Iran	37.27387	54.14993
2623579142	SB49_04750	*Sediminicola sp.* YIK13	South Korea	37.26667	126.4333
2517148360	RudluDRAFT_0983	*Rudanella lutea* DSM 19387	South Korea	37.263	127.028
2623582104	AAY42_03745	*Muricauda eckloniae* DOKDO 007	South Korea	37.23333	131.8667
2861801624	Ga0436359_050_168825_170123	*Cyclobacterium marinum* Atlantic-IS	North Atlantic Ocean	37.0567	-73.5113
2845821377	Ga0398781_01_3824902_3826197	*Flavobacteriaceae bacterium* F202Z8	South Korea	36.78109	126.2954
2834236294	Ga0337323_3415	*Maribacter litoralis* SDRB-Phe2	South Korea	36.66617	126.2106
2906824236	Ga0446167_12_10442_11746	*Flavobacterium sp.* ASW18X	China	36.44574	120.798
2920457388	Ga0481285_24_11737_13044	*Arenibacter arenosicollis* BSSL-BM3	South Korea	36.37273	126.586
2967498004	Ga0440713_44_196380_197681	*Lunatibacter salilacus* CUG 91308	China	36.33	100.37
2920068231	Ga0477952_12_16130_17458	*Limnovirga soli* KCS-6	South Korea	36.3	127.3
2832967971	Ga0393098_3166	*Muricauda aurantiaca* HME9304	South Korea	36.0759	120.4085
2890885683	Ga0440596_07_627843_629129	*Flagellimonas algicola* AsT0115	South Korea	36	126
8055114222	Ga0616906_03_99341_100636	*Spirosoma liriopis* RP8	South Korea	35.9078	127.7669
2774555809	Ga0198768_112759	*Deinococcus puniceus* DY1	South Korea	35.86056	127.7464
2571070915	Q371DRAFT_04942	*Deinococcus misasensis* DSM 22328	Japan	35.41927	133.8642
2790839146	Ga0304276_1007138	*Maribacter sp.* 4G9	Japan	35.16	139.61
3000161165	Ga0442852_02_374859_376166	*Cytophagaceae bacterium* SJW1-29	South Korea	35.08978	127.7449
8078051908	Ga0626623_09_414643_415917	*Flagellimonas sp.* 2012CJ39-3	South Korea	33.3846	126.5535
8064342266	Ga0559750_01_4033798_4035096	*Flagellimonas sp.* CMM7	South Korea	33	126
2890835923	Ga0444202_07_441737_443035	*Flagellimonas sp.* CMM7	South Korea	33	126
2509080589	DeipiDRAFT_00001900	*Deinococcus pimensis* KR-235, DSM 21231	USA	32.92784	-112.305
8002456163	Ga0594566_01_865258_866562	*Maribacter sp.* MMG018	USA	32.73299	-117.257
8124090958	Ga0674574_01_5119903_5121201	*Imperialibacter roseus* P4T	USA	31.2714	-102.68
8026246356	Ga0444592_04_28376_29677	*Bacteroidetes bacterium* AG-901-E05	Atlantic Ocean	31.07	-64.17
8026765874	Ga0447146_12_39013_40299	*Bacteroidetes bacterium* AG-892-D16	Atlantic Ocean	31.07	-64.17
2505793149	RunsI_3883	*Runella slithyformis* LSU4, DSM 19594	USA	30.417	-91.167

2832454624	Ga0337407_5034	*Runella aurantiaca* YX9	China	27.96722	112.8431
2506486384	Emtol_0927	*Emticicia oligotrophica* GPTSA100-15, DSM 17448	India	26.75602	94.20945
2832106458	Ga0336645_3811	*Fibrisoma montanum* HYT19	China	25.04244	113.7427
2914067816	Ga0442815_14_714997_716286	*Pareuzebyella sediminis* S2-4-21	China	24.85	118.67
2964275936	Ga0442816_07_673424_674713	*Pareuzebyella sediminis* MT2-5-19	China	24.85	118.67
8046923320	Ga0615507_11_371971_373236	*Portibacter marinus* 10MBP4-2-1	China	24.81823	118.6732
2700893107	Ga0137942_100379	*Cytophaga sp.* FL35	USA	24.56306	-81.4008
8063583800	Ga0607407_03_90615_91904	*Cytophaga sp.* FL35	USA	24.56306	-81.4008
2723494309	Ga0175042_111868	*Maribacter hydrothermalis* T28	Taiwan	24	121
2994701013	Ga0587408_078_152776_154110	*Lunatimonas salinarum* KCTC 42988	India	21.85524	72.32298
2548890299	GCKDRAFT_01856	*Croceivirga radicis* S86	Micronesia	11.523	151.494
2982560847	Ga0577150_01_1908993_1910297	*Maribacter sp.* 151	Australia	-38.3336	142.621
8002498218	Ga0594204_44_82137_83441	*Algoriphagus aquimarinus* ACAM 450	Antarctica	-68	78
2894866264	Ga0441611_037_63082_64380	*Maribacter sp.* ACAM166	Antarctica	-68	78
2792181821	Ga0309199_12455	*Arenibacter catalasegens* P308H10	Antarctica	-69	76
2739624306	Ga0196854_10569	*Algoriphagus antarcticus* DSM 15986 (v2) (version 2)	Antarctica	-69.385	76.37841
8002500727	Ga0559560_049_173548_174849	*Algoriphagus antarcticus* DSM 15986	Antarctica	-69.385	76.37841

Table S3. *Homologs of PET94 hydrolases from Bacteroidota isolates UHH-5R5 and UHH-Hm9b. Data were retrieved from the publicly available IMG/MER database, applying thresholds of ≥50% sequence identity and ≥80% sequence coverage.*

Hm9b homologs					
Gene ID	**Locus Tag**	**Genome Name**	**Isolation Country**	**Latitude**	**Longitude**
2546243389	ADICYQ_2709	*Cyclobacterium qasimii* M12-11B	Norway	79.00105	11.66625
2890793592	Ga0443375_01_526053_527357	*Cyclobacterium qasimii* NBRC 106168	Norway	79.00105	11.66625
2515733714	B156DRAFT_01776	*Spirosoma luteum* DSM 19990	Norway	78.2122	15.8
2515842746	B157DRAFT_06708	*Spirosoma spitsbergense* DSM 19989	Norway	78.21	15.8
2774668436	Ga0226569_114770	*Arenibacter algicola* SMS7	Sweden	58.87242	11.06366
2778165481	Ga0248407_161130	*Janthinobacterium psychrotolerans* S3-2	Denmark	56.1828	10.17629
2595693039	LX87DRAFT_00794	*Larkinella arboricola* DSM 21851	Russia	55.75	37.62
2667678916	Ga0040978_1313	*Maribacter dokdonensis* MAR_2009_71	Germany	55.0255	8.4567
2585370157	FG20DRAFT_3328	*Zobellia amurskyensis* MAR_2009_138	Germany	55.0255	8.4567
2592972043	GQ41DRAFT_0959	*Arenibacter algicola* MAR_2009_79	Germany	55.0255	8.4567
2676739754	Ga0040979_3239	*Maribacter sp.* MAR_2009_60	Germany	55.0255	8.4567
2832368994	Ga0335984_1474	*Zobellia galactanivorans* OII3	Germany	54.67	9.94
2558431147	P178DRAFT_1169	*Maribacter sp.* Hel_I _7	Germany	54.1841	7.9
2574425426	P177DRAFT_00341	*Maribacter forsetii* DSM 18668	Germany	54.1841	7.9
8000209034	Ga0596861_0008_300124_301428	*Maribacter dokdonensis* AG-HH-5R5	Germany	54.1318	8.8753
2515427593	B036DRAFT_03034	*Neolewinella persica* DSM 23188	Ireland	53.27	-9.056
8001908943	Ga0594730_11_249862_251190	*Zobellia russellii* KMM 3677	Russia	52.33419	36.60303
2910278776	Ga0477857_08_1217993_1219321	*Zobellia laminariae* KMM 3676	Russia	52.33419	36.60303
8065844926	Ga0487514_01_1236377_1237705	*Zobellia roscoffensis* Asnod2-B02-B	France	48.7266	-3.9897
3001333670	Ga0488450_01_1260666_1261994	*Zobellia roscoffensis* Asnod1-F08	France	48.7266	-3.9897
3001348201	Ga0487513_01_1242554_1243882	*Zobellia nedashkovskayae* Asnod2-B07-B	France	48.7266	-3.9897
8065850772	Ga0487512_01_3324766_3326094	*Zobellia nedashkovskayae* Asnod3-E08-A	France	48.7266	-3.9897
2620655879	Ga0039355_111800	*Zobellia galactanivorans* DsijT	France	48.14524	-4.35629

2881099053	Ga0442556_33_349623_350918	*Arundinibacter roseus* DMA-k-7a	Hungary	47.7	16.69997
8055965970	Ga0616553_11_1042874_1044202	*Zobellia barbeyronii* KMM 6746	Russia	47.52363	152.8107
648160996	FB2170_02060	*Maribacter sp.* HTCC2170	USA	44.655	-124.064
644104643	Flav2ADRAFT_1526	*Flavobacteria bacterium* MS024-2A (unscreened)	USA	43.84978	-69.6266
8080698659	Ga0625472_07_32683_33957	*Portibacter lacus* YM8-076	Japan	43.20081	142.5392
2910289591	Ga0477856_036_38108_39436	*Zobellia amurskyensis* KMM 3526	Russia	43.13641	131.8848
2890770580	Ga0441612_223_154750_156033	*Larkinella sp.* C7	China	43.1	119.37
8058070572	Ga0617454_01_1769634_1770962	*Zobellia alginiliquefaciens* LLG6346-3.1	France	42.76904	9.33353
8048528387	Ga0616067_01_1951018_1952100	*Zobellia laminariae* AS94	USA	42.42	-70.907
3001341769	Ga0584015_08_147227_148549	*Zobellia uliginosa* C3R17	USA	42.25	-70.54
8074547076	Ga0580702_01_922024_923352	*Zobellia sp.* B3R18	USA	42.25	-70.54
3001904140	Ga0580690_04_133467_134774	*Arenibacter algicola* E3M18	USA	42.25	-70.54
8100324962	Ga0488656_01_1350439_1351743	*Maribacter sp.* 6B07	USA	42.25	-70.54
8074614719	Ga0580712_45_213521_214849	*Zobellia galactanivorans* A2I 03	USA	42.25	-70.54
2890197314	Ga0440108_02_155726_157030	*Emticicia sp.* CRIBPO	USA	42.23591	-81.7859
2890828893	Ga0441110_04_6487_7779	*Runella sp.* CRIBMP	USA	42.23591	-81.7859
2808571772	Ga0321368_117257	*Spongiimicrobium salis* Da_B9	Spain	42.11444	3.168333
2721515523	Ga0175219_111860	*Maribacter sp.* 1_2014MBL_MicDiv	USA	41.52733	-70.6757
2890760553	Ga0440852_11_379535_380818	*Cyclobacterium sp.* SYSU L 0167	China	40.50182	85.02692
2890750500	Ga0441869_11_349676_350959	*Cyclobacterium roseum* SYSU L10180	China	40.4684	85.51032
2515907397	B153DRAFT_02476	*Spirosoma panaciterrae* DSM 21099	South Korea	37.91626	127.2038
2516421498	B154DRAFT_00033	*Segetibacter koreensis* DSM 18137	South Korea	37.91626	127.2038
2700210779	Ga0131097_3515	*Algoriphagus halophilus* DSM 15292	South Korea	37.71317	126.45
2897639915	Ga0441610_12_1042881_1044170	*Maribacter sp.* RZ26	China	37.55838	122.1533
8077179044	Ga0627981_45_82466_83773	*Muriicola sp.* Z0-33	China	37.5292	122.0108
8078693221	Ga0627007_04_12753_14045	*Lacihabitans sp.* CCS-44	South Korea	37.45246	129.1922
640617222	ALPR1_05630	*Algoriphagus machipongonensis* PR1	USA	37.42	-75.69
8071170371	Ga0581854_08_68151_69446	*Spirosoma sp.* RHs26	South Korea	37.38044	127.601
2890815525	Ga0440155_36_295790_297082	*Cyclobacterium plantarum* GBPx2	Iran	37.28586	54.12379

2623579142	SB49_04750	*Sediminicola sp.* YIK13	South Korea	37.26667	126.4333
2517148360	RudluDRAFT_0983	*Rudanella lutea* DSM 19387	South Korea	37.263	127.028
2623582104	AAY42_03745	*Muricauda eckloniae* DOKD 007	South Korea	37.23333	131.8667
2861801624	Ga0436359_050_168825_170123	*Cyclobacterium marinum* Atlantic-IS	USA	37.0567	-73.5113
2832426529	Ga0337346_2388	*Muricauda koreensis* ECD12	South Korea	36.79991	126.4363
2506468824	Cycma_3952	*Cyclobacterium marinum* Raj, DSM 745	USA	36.67702	-120.005
2906824236	Ga0446167_12_10442_11746	*Flavobacterium sp.* ASW18X	China	36.44574	120.798
2967498004	Ga0440713_44_196380_197681	*Lunatibacter salilacus* CUG 91308	China	36.33	100.37
2920068231	Ga0477952_12_16130_17458	*Limnovirga soli* KCS-6	South Korea	36.3	127.3
2832967971	Ga0393098_3166	*Muricauda aurantiaca* HME 9304	South Korea	36.0759	120.4085
2890885683	Ga0440596_07_627843_629129	*Flagellimonas algicola* AsT0 15	South Korea	36	126
8055114222	Ga0616906_03_99341_100636	*Spirosoma liriopis* RP8	South Korea	35.9078	127.7669
2790839146	Ga0304276_1007138	*Maribacter sp.* 4G9	Japan	35.16	139.61
8078690697	Ga0627006_023_48688_49980	*Lacihabitans sp.* CS3-21	South Korea	35.04876	128.9176
8078051908	Ga0626623_09_414643_415917	*Flagellimonas sp.* 2012CJ39-3	South Korea	33.3846	126.5535
2889832122	Ga0443539_12_800808_802112	*Croceivirga sp.* JEA036	South Korea	33.25849	126.6494
8064342266	Ga0559750_01_4033798_4035096	*Flagellimonas sp.* CMM7	South Korea	33	126
2890835923	Ga0444202_07_441737_443035	*Flagellimonas sp.* CMM7	South Korea	33	126
8002456163	Ga0594566_01_865258_866562	*Maribacter sp.* MMG018	USA	32.73288	-117.257
8099924753	Ga0626761_23_337354_338775	*Arenibacter sp.* N53	China	31.43939	122.2886
8124090958	Ga0674574_01_5119903_5121201	*Imperialibacter roseus* P4T	USA	31.2714	-102.68
8026765874	Ga0447146_12_39013_40299	*Bacteroidetes bacterium* AG-892-D16	Atlantic Ocean	31.07	-64.17
8026246356	Ga0444592_04_28376_29677	*Bacteroidetes bacterium* AG-901-E05	Atlantic Ocean	31.07	-64.17
2505793149	Runsl_3883	*Runella slithyformis* LSU4, DSM 19594	USA	30.417	-91.167
2789098472	Ga0303171_1004209	*Arsenicibacter rosenii* SM-1	China	29.6103	111.3468
2832454624	Ga0337407_5034	*Runella aurantiaca* YX9	China	27.96722	112.8431
2832544890	Ga0336335_3116	*Larkinella punicea* ZZJ9	China	27.83097	112.9381
2506486384	Emtol_0927	*Emticicia oligotrophica* GPTSA100-15, DSM 17448	India	26.75602	94.20945
2832106458	Ga0336645_3811	*Fibrisoma montanum* HYT19	China	25.04244	113.7427

2914067816	Ga0442815_14_714997_716286	*Pareuzebyella sediminis* S2-4-21	China	24.85	118.67
2964275936	Ga0442816_07_673424_674713	*Pareuzebyella sediminis* MT 2-5-19	China	24.85	118.67
8046923320	Ga0615507_11_371971_373236	*Portibacter marinus* 10MBP 4-2-1	China	24.81723	118.6649
2700893107	Ga0137942_100379	*Cytophaga sp.* FL35	USA	24.56306	-81.4008
8063583800	Ga0607407_03_90615_91904	*Cytophaga sp.* FL35	USA	24.56306	-81.4008
2723494309	Ga0175042_111868	*Maribacter hydrothermalis* T 28	Taiwan	24	121
8002489485	Ga0594444_49_42594_43904	*Algoriphagus pacificus* YJ13	China	23.81248	114.4554
2994701013	Ga0587408_078_152776_154110	*Lunatimonas salinarum* KC TC 42988	India	21.85524	72.32298
2789752970	Ga0303181_101167	*Croceivirga radicis* HSG9	China	19.7011	109.8361
2548890299	GCKDRAFT_01856	*Croceivirga radicis* S86	Micronesia	11.523	151.494
2881390997	Ga0440289_056_15317_16636	*Flavilitoribacter nigricans* DSM 23189	Nigeria	9.494648	7.879082
2982560847	Ga0577150_01_1908993_1910297	*Maribacter sp.* 151	Australia	-38.3336	142.621
8002498218	Ga0594204_44_82137_83441	*Algoriphagus aquimarinus* ACAM 450	Antarctica	-68	78
2894866264	Ga0441611_037_63082_64380	*Maribacter sp.* ACAM166	Antarctica	-68	78
2792181821	Ga0309199_12455	*Arenibacter catalasegens* P 308H10	Antarctica	-69	76
2739624306	Ga0196854_10569	*Algoriphagus antarcticus* DSM 15986 (v2) (version 2)	Antarctica	-69.385	76.37841
8002500727	Ga0559560_049_173548_174849	*Algoriphagus antarcticus* DSM 15986	Antarctica	-69.385	76.37841
8077281885	Ga0626238_127_136883_138184	*Arenibacter sp.* F20364	China	37.51118	122.1439

8. ACKNOWLEDGEMENT

Throughout my PhD journey, I have been fortunate to receive tremendous support, assistance and encouragement from many people, without whom this work would not have been possible.

At the end of 2019, I began my PhD journey while at the same time preparing to welcome my first child. I am deeply grateful to **Prof. Dr. Wolfgang Streit** for his exceptional support in making it possible for me to pursue my PhD in his group while also taking on the new role of being a mother. His understanding, encouragement, and flexibility enabled me to balance the challenges of research and family life, and for that I remain truly thankful. I also sincerely appreciate his valuable time, guidance, and constructive suggestions during the accomplishment of this study.

My heartfelt thanks go to **Dr. Ifey Alio and Dr. Christel Vollstedt,** for their endless support, patience, kindness, and insightful supervision from the very beginning. I am also thankful to **Dr. Pablo Pérez García** for his valuable guidance and to **Dr. Anja Poehlein** (University of Göttingen) for performing the transcriptome sequencing. Further, I truly appreciate **Inka, Petra, and Angela** for their generous assistance in the lab.

I would like to sincerely thank **International University, Vietnam National University, Ho Chi Minh City** for providing me with the opportunity to further advance my knowledge in Germany.

My thanks also go to my colleagues and friends for creating a friendly atmosphere and for always being there whenever I encounter challenges. Special thanks to **Sasi, Golo, Myllena, Raphael and Mingwei** for cheering me up during difficult times and sharing the ups and downs of this journey. Thank you, **Marno** and **Robert,** for your great help with UHPLC and Reporter strain. My gratitude also goes to all members of our research group. You all made my days in the lab truly enjoyable.

Finally, I must express my very profound gratitude to my family. To **my parents**, who have always believed in me, respected my choices, and provided unconditional love and support.

To my husband, **Duy Hoang**, who has always been my greatest supporter and “best friend”. To my daughter, **Vy Hoang**, who made my PhD journey more challenging but, at the same time, gave me the greatest motivation to persevere and complete this thesis. And to all my Vietnamese friends, who have been my home away from home during my life abroad.

Without all of you, this achievement would not have been possible.

Hamburg, 14/09/2025

Trinh, Thi Truc Ly